

MACHINE LEARNING APPROACHES TO PROVIDE SPATIO-TEMPORAL  
CHARACTERIZATION OF HUMAN BRAIN FUNCTIONAL ACTIVITIES

by

Nader Shahni Karamzadeh  
A Dissertation  
Submitted to the  
Graduate Faculty  
of  
George Mason University  
in Partial Fulfillment of  
The Requirements for the Degree  
of  
Doctor of Philosophy  
Computational Sciences and Informatics

Committee:

\_\_\_\_\_ Dr. Edward Wegman, Dissertation Director  
\_\_\_\_\_ Dr. Amir Gandjbakhche, Committee  
Member  
\_\_\_\_\_ Dr. James Gentle, Committee Member  
\_\_\_\_\_ Dr. James L. Olds, Committee Member  
\_\_\_\_\_ Dr. Kevin Curtin, Acting Department Chair  
\_\_\_\_\_ Dr. Donna M. Fox, Associate Dean, Office  
of Student Affairs & Special Programs,  
College of Science  
\_\_\_\_\_ Dr. Peggy Agouris, Dean, College of  
Science

Date: \_\_\_\_\_ Spring Semester 2016  
George Mason University  
Fairfax, VA

Machine Learning Approaches to Provide Spatio-Temporal Characterization of Human  
Brain Functional Activities

A Dissertation submitted in partial fulfillment of the requirements for the degree of  
Doctor of Philosophy at George Mason University

by

Nader Shahni Karamzadeh  
Master of Science  
George Mason University, 1987

Director: Edward Wegman, Professor  
Department of Computational Data Science and Informatics

Spring Semester 2016  
George Mason University  
Fairfax, VA



THIS WORK IS LICENSED UNDER A [CREATIVE COMMONS  
ATTRIBUTION-NONCOMMERICALS 3.0 UNPORTED LICENSE](https://creativecommons.org/licenses/by-nc/3.0/).

## **Dedication**

This dissertation is dedicated to 5 pillars of my life: My wife Atefeh, My dad Omid, my mom Parvin, my brother Nima, and my sister Negur.

## **Acknowledgements**

During the past several years of my life as a graduate student, I have had the privilege of getting to know and work with many inspiring people, from whom I've learned a great deal and have received invaluable knowledge. First and foremost, I would like to thank my 15 years friend/wife Atefeh for standing beside me through the ups and downs of this journey. I want to thank her for always believing in me, giving me wise advices, love, and support. I would like to thank Dr. Amir Gandjbakhche, my Ph.D. advisor at the National Institutes of Health, without whom this dissertation would not have been possible. I would also like to thank my advisor at GMU, Dr. Edward Wegman for his continuous support of my research. His guidance helped me through the process of research and writing this dissertation. I would also want to thank my parents for their unconditional support and encouragement. My dad's persistence, dedication, and passion for research have always been such an inspiration to me.

I would also like to thank Dr. James Olds and Dr. James Gentle for their encouragement and insightful comments. This thesis would not have been possible without the support of my coworkers at the National Institutes of Health. Finally, I would like to express my sincere gratitude to my MSc advisor Dr. Anthony Stefanidis.

## Table Of Contents

|  |      |
|--|------|
| Table Of Contents .....  | v    |
| List of Tables .....   | viii |
| List of Figures .....  | x    |
| Abstract .....   | xiii |
| 1. Introduction.....   | 1    |
| 1.1. Biomarker identification .....  | 1    |
| 1.2. Brain Functional Activity.....  | 2    |
| 1.2.1. Brain cerebral cortex .....   | 2    |
| 1.2.2. Functional Neuroimaging.....  | 4    |
| 1.2.3. Neuroimaging Modalities .....   | 5    |
| 1.3. Neuroimaging and Biomarker Detection .....                                    | 8    |
| 1.3.1. Electroencephalography (EEG).....   | 8    |
| 1.3.2. Functional Near Infrared Spectroscopy (fNIRS).....                          | 17   |
| fNIRS Hemodynamic Spatio-temporal Characteristics as Biomarker .....               | 18   |
| 1.4. Neuroimaging Feature Extraction Approach for Biomarker Identification .....   | 19   |
| 1.4.1 The General Problem of Feature Extraction.....                               | 20   |
| 1.4.2. EEG and fNIRS Feature Extraction Techniques .....                           | 22   |
| 1.5. Limitations of the Current Multivariate Feature Extraction Techniques .....   | 26   |
| 1.6 Organization.....  | 27   |
| 2. Cluster Analysis to Capture Functional Connectivity .....                       | 30   |
| 2.1 Functional Connectivity .....  | 30   |
| 2.2 Dynamic Time Warping (DTW).....  | 32   |
| 2.3 Quality Threshold (QT) Cluster Analysis .....                                  | 35   |
| 2.4 Summary of Chapter 2 .....   | 37   |
| 3. Capturing Dynamic Patterns of Task-Based Functional Connectivity with EEG ..... | 38   |

|  |    |
|--|----|
| 3.1. Dynamic Patterns of Functional Connectivity .....   | 38 |
| 3.2 Methodology .....  | 40 |
| 3.2.1 Experimental Paradigms and Data acquisition .....  | 40 |
| 3.2.2 EEG data acquisition and preprocessing .....   | 41 |
| 3.2.3 ERP Segmentation .....   | 42 |
| 3.2.4 Employing DTW and QT clustering .....  | 43 |
| 3.3 Clustering Performance Evaluation.....   | 46 |
| 3.4 Investigating the Identified Functionally Connected Regions .....  | 49 |
| 3.5 Summary of Chapter 3 .....   | 53 |
| 4. Relative Brain Signature (RBS):.....  | 55 |
| 4.1 RBS a Multichannel and Reference-based Feature Extraction Technique .....  | 55 |
| 4.2 Relative Brain Signature (RBS) .....   | 56 |
| 4.2.1 Population-Specific-Dataset (PSD) .....  | 56 |
| 4.2.2 Population-Specific-Subspace (PSS).....  | 57 |
| 4.2.3 Orthogonal Complement Projection.....  | 58 |
| 4.2.4 Quantifying the Relative Association to Classes.....   | 58 |
| 4.3 Summary of Chapter 4 .....   | 59 |
| 5. Functional Biomarker Identification Using RBS.....  | 61 |
| 5.1 EEG and Alcoholic Studies.....   | 61 |
| 5.2 Experimental Paradigms and Data Acquisition .....  | 63 |
| 5.3 ERP Feature Extraction Using RBS.....  | 64 |
| 5.4 Identifying Functionally Distinct Brain Regions of Alcoholic Subjects.....   | 67 |
| 6. Identifying Functional Biomarkers in Human Prefrontal Cortex for Individuals with<br>Traumatic Brain Injury (TBI) Using Functional Near-Infrared Spectroscopy (fNIRS) ... | 78 |
| 6.1 TBI and PFC .....  | 79 |
| 6.2 Functional Near infrared Spectroscopy and Traumatic Brain Injury .....   | 79 |
| 6.3.1 Participant.....   | 84 |
| 6.3.2 Experimental Design .....  | 85 |
| 6.3.3 Preprocessing.....   | 86 |
| 6.3.4 Feature extraction .....   | 88 |
| 6.3.5 Feature selection and pattern classification .....   | 91 |
| 6.3.6 Classification evaluation.....   | 92 |
| 6.4 Results .....  | 94 |

|   |     |
|---|-----|
| 6.4.1 Trial/Channel removal .....   | 94  |
| 6.4.2 Temporal Feature Extraction/Classification .....  | 95  |
| 6.4.3 Temporal feature extraction/classification without rejecting trials/channels .                  | 100 |
| 6.4.4 Spatio-temporal feature extraction .....  | 102 |
| 6.4.5 Task load effects (i.e. parametric effects) in distinguishing TBI from healthy population ..... | 106 |
| 6.5 Discussion .....  | 107 |
| 6.6 Summary of Chapter 6 .....  | 110 |
| 7. Summary and Future Work.....   | 112 |
| 7.1 Summary .....   | 112 |
| 7.2 Future work .....   | 117 |
| References.....   | 119 |

## List of Tables

|  |     |
|--|-----|
| Table 1-1 Comparison of neuroimaging modalities. Adopted from (Nicolas-Alonso and Gomez-Gil, 2012) and (Koike et al., 2013) .....  | 7   |
| Table 3-1 Average silhouette coefficient value corresponding to functionally connected regions of figure 3-3. Silhouette coefficient value varies between -1 and 1 whereas a positive silhouette coefficient value suggests that the ERP signal is more similar to its own cluster members as opposed to members of other clusters. Values closer to 1 correspond to improved performance for the clustering task. ....  | 49  |
| Table 5-1 Sets of EEG channels (RBS components) selected for the first 11 classification experiments across their 1000 sampling iterations. ....   | 73  |
| Table 6-1 Demographic and Clinical Characteristics of the Study Population .....   | 85  |
| Table 6-2 Accuracy, specificity (accuracy of classifying healthy subjects correctly), and sensitivity (accuracy of classifying TBI subject correctly) of the classification experiments for the feature space constructed using one feature element. The largest accuracy value is obtained for the feature space constructed by the left slope of the activity curve (CSL) variable. Overall, the accuracy of correctly identifying the TBI subjects (sensitivity) is larger than the accuracy of correctly detecting the healthy subjects for feature set of any size. ....  | 98  |
| Table 6-3 Classification performance obtained by using the optimum feature sets of sizes 2 to 11 is presented. The optimum feature sets are selected from all the potential feature combinations of a certain size. Among all the combinations of features for a certain size, the one with the highest accuracy value is selected as the optimum feature set. The optimum classification performance is obtained for the feature space constructed by the triple of 3 features of “activity curve slopes (CS)”, “HbO kurtosis (HK)“, and “activity starting time (CAS)” resulted in the best separation between the TBI and healthy subjects. Comparison between the specificity and sensitivity indicates that in all the cases, sensitivity has been superior to the specificity meaning TBI subjects have been classified with higher accuracy. .... | 98  |
| Table 6-4 Classifying TBI and healthy subjects by characterizing subjects in the features space defined by the identified optimal feature set [CA,HDFT,CF] using 3 different classifiers. Decision Tree classifier outperformed LDA and SVM classifiers. ....  | 100 |
| Table 6-5 Feature sets with the largest accuracy values were selected from all the potential feature combinations of different sizes. HbO and HbR signals have been  |     |

|   |     |
|---|-----|
| averaged across all the trials without applying the trial/channel rejection procedure on the signals. ....  | 101 |
| Table 6-6 Accuracy, specificity (accuracy of classifying healthy subjects correctly), and sensitivity (accuracy of classifying TBI subject correctly) for the spatio-temporal classification. Similar to the single feature temporal classification, HbO variance (HV) and activity curve's left slope (CSL) resulted in relatively larger classification accuracy. However, single variable spatio-temporal classification outperformed single variable temporal classification. Similar to temporal classification, the accuracy of correctly identifying the TBI subjects (sensitivity) is consistently larger than the accuracy of correctly detecting the healthy subjects. .... | 102 |
| Table 6-7 Comparison of the classification performance across tasks with different loads of complexity for the identified optimal feature set [CS, HK, CAS] using the Decision Tree classification .....  | 106 |

## List of Figures

|  |    |
|--|----|
| Figure 1-1 Four lobe of human brain .....  | 3  |
| Figure 1-2 EEG signals are recorded non-invasively by placing the electrodes on the scalp to record the electrical signals that cross the scalp, skull, and other layers. An electrode placed on the scalp records the summed signal from many cells. Adopted from9  |    |
| Figure 1-3 Visualizing a number of Event Related Potential Components (ERPs). ERPs consist of a series of elicited components (ERP components) which are time-locked events and reveal several sensory, cognitive and motor processes (Polich and Kok, 1995)   |    |
| .....  | 14 |
| Figure 1-4 The general diagram for a supervised machine learning classification. The neuroimaging signals from the subjects of different classes are used to train a classifier model. The trained classifier makes prediction for the neuroimaging signals collected from the subjects with unknown class affiliation. ....                             | 21 |
|  |    |
| Figure 2-1 Two hypothetical time series with an overall similar shape but not well aligned along the time axis. To find the optimal alignment between two time series, one point from the first time series may be compared against a number of points from the second time series, after (Keogh and Ratanamahatana, 2005). ....                         | 33 |
| Figure 2-2 Two time series, which have similar pattern of activity but are not aligned in the time domain. Matrix $C$ is the cost matrix in which the optimal warping path is shown as the sequence of solid squares (shown in red). ....  | 34 |
| Figure 2-3 Two hypothetical time series with an overall similar shape but not well aligned along the time axis. To find the optimal alignment between two time series, one point from the first time series may be compared against a number of points from the second time series and the best match is selected. ....                                  | 35 |
|  |    |
| Figure 3-1 (a) Target (b) non target frequent (c) and non-target infrequent stimuli.....   | 40 |
| Figure 3-4 3D maps of functionally connected regions obtained by two similarity techniques over the full length signal: (a) DTW and (b) cross-correlation. ....  | 52 |
|  |    |
| Figure 4-1 For the given neuroimaging time series from the two population of subject, first the two PSD are computed for each group of subjects (a). For every channel site of a population, its subspace and its orthogonal complement subspace is constructed. Then, every single time series of a subject is projected onto the orthogonal complement |    |

subspace of the population (Figure 4-1-b). Finally, subject's RBS feature vectors that reveal the level of association of a subject to a specific population are computed within the projected subspaces (Figure 4-1-c). ..... 60

Figure 5-1 RBS vectors for an alcoholic and a control subject are illustrated. Two RBS vectors for an alcoholic subject and a control subject are shown. The components of the RBS vectors, quantify the association of an ERP waveform and the alcoholic population (shown in blue) or to the control population (shown in red). A positive value closer to 1, for a component of the RBS vectors indicates a stronger association to a certain population whereas smaller positive values and the negative values suggest the corresponding ERP data is weakly associated to a population. In a, majority of Alcoholic-RBS component values are significantly associated to the alcoholic population while for the Control-RBS component values, majority of the ERPs were weakly associated to the control population. In b, Control-RBS component values illustrate a strong relation to the control population while Alcoholic-RBS demonstrates weak association to the alcoholic population. .... 67

Figure 5-2 Performance evaluation for LDA classification between alcoholics and control subjects. (a) The x-axis corresponds to different number of significant components used to generate the feature vectors and the y-axis denotes the accuracy. The dot-line corresponds to the average classification accuracy and the dash-lines represent the standard deviation for the computed accuracy. (b) The x-axis corresponds to different number of significant components used to generate the feature vectors. The red and blue dot-lines denote the average specificity and average sensitivity (respectively) for a certain number of significant components used to construct the feature vector..... 71

Figure 5- 3 Different views for the top 11 functionally distinct brain areas between alcoholic and control subject. The red area corresponds to the most significant component and the yellow strip around the red determines the boundary of that region. These areas, with respect to their spatial extent are frontal and anterior frontal, centro-parietal, parieto-occipital and occipital lobes. .... 72

Figure 5-4 Process of computing RBS vectors without projecting signal onto the orthogonal subspaces and vs. the proposed approach, for an alcoholic subject. (a) Subject's ERPs were not projected to the orthogonal subspaces and only similarity between subject's ERP and its corresponding ERP from Control-PSD and Alcoholic-PSD was computed. As demonstrated in a, very similar values of association to the alcoholic and control populations were obtained across all of the components of the Alcoholic- and Control-RBS. (b) The RBS vectors for the same subject were constructed by projecting the ERPs onto the orthogonal subspaces of the populations and then the similarity was computed. The computed similarity vectors in a were not able to characterize subjects with respect to its original population association in comparison to the RBS vectors illustrated in b. .... 76

Figure 6-1 Visualizing the HbO signal (in red), activity curve and a number of hemodynamic features extracted in this study. The activity curve is a positive deflection representing the activation embodied in the HbO signal. The activity curve is formed by oxygenation's increase and its returns to same level of oxygenation. .... 91

Figure 6-2 Channel distribution for the healthy and TBI populations after the channel/trial removal step is illustrated. For the TBI subjects, less number of subjects shares a common channel whereas for majority of the healthy subjects share similar channels are kept. In the TBI population, more than half of the subjects share only channel 16. However, in healthy population except for channel 16, all the other channels are shared among more than half of the subjects. .... 95

Figure 6-3 ROC curve for the classifying subjects into TBI and healthy groups, in the feature space constructed by the optimum feature set [CA, HDFT, CF]. Specificity and sensitivity values at each point of the graph are obtained by averaging the corresponding values across the 1000 run of the random subsampling procedure. Area under the curve of 0.85 is obtained for the constructed model, which signifies the high accuracy of the constructed classification model. .... 99

Figure 6-4 The average activity maps for the CSL and HV features for the healthy (a) and TBI (b) subjects are illustrated. The activity map for a spatio-temporal feature associated to a population is obtained by averaging every subjects' (from the corresponding population) spatio-temporal feature set. For the TBI population, the larger HV values are located at multiple locations with largest on the right hemisphere whereas for the healthy population the largest HV is concentrated on the left hemisphere of the Brodmann area 10 (BA 10). Furthermore, healthy subjects on average show larger HV values for the HbO signal that indicates oxygenation signal has shown higher variation in the healthy subjects. The HbO signal in response to the High Complexity task for the healthy subjects shows larger variation and is spatially less diffuse than for the TBI subjects. Larger CSL values correspond to faster rate of oxygenation consumption. Considering the activity map for healthy subjects, largest CSL values cover the left frontopolar of the BA 10. A comparison of healthy and TBI subjects' CSL activity map reveals that healthy subjects have shown higher oxygenation consumption rate in response to the High complexity task at all the sites of fNIRS data collection. .... 105

## **Abstract**

### **MACHINE LEARNING APPROACHES TO PROVIDE SPATIO-TEMPORAL CHARACTERIZATION OF HUMAN BRAIN FUNCTIONAL ACTIVITIES**

Nader Shahni Karamzadeh, PhD

George Mason University, 2016

Dissertation Director: Dr. Edward Wegman

Recently, the interest in pattern recognition approaches to the analysis of clinical neuroimaging data has increased substantially. A crucial advantage of multivariate pattern recognition algorithms in comparison to the traditional univariate approaches is that they provide predictions on the level of individual subjects. It is this multivariate nature of pattern recognition algorithms that results in increased sensitivity over univariate methods and has led to numerous applications in clinical research. Meanwhile, advances in neuroimaging technologies have improved our understanding of brain function in psychiatric and neurological disorders such as mood disorders, drug abuse and addiction, schizophrenia, Alzheimer's disease, traumatic brain injury,-. These promising advances in functional neuroimaging technology and multivariate pattern recognition's applications in neuroimaging data analysis motivated the work presented in this dissertation. Monitoring and evaluating of human brain performance during the execution of functional experiments have revealed evidence regarding distinctive pattern

of brain activity between healthy individuals and individuals with brain functional disorders. Except for certain cases, to date, the results of these studies have had minimal clinical impact and despite much interest in the use of brain scans for diagnostic and prognostic purposes, traditional and often ineffective diagnostic and prognostic approaches are the common practice for neurologists and psychiatrists.

There are a few limitations that restrict the clinical translations of identifying functional biomarkers to characterize certain brain functional disorders. Firstly, majority of the related studies are focused on group studies that attempt to signify differences between the groups of subjects and do not provide description at the individual level. Secondly, the common techniques for characterizing functional neuroimaging response at the individual level are traditional single-channel time series feature extraction techniques that do not necessarily fit into the neuroimaging multichannel time series frameworks. Finally, for the more recently developed modalities such as fNIRS very few studies have attempted to identify biomarkers in brain disorders through the data mining and machine learning approaches. Therefore, in this dissertation emphasis was placed on improving, developing, and extracting clinically adaptable neuroimaging features to enable translating the laboratory work into clinical environments. In particular, machine learning algorithms and data mining techniques were utilized to generate spatio-temporal features from the neuroimaging time series and were evaluated for diagnosis of certain brain activity disorders. The presented work in this dissertation offers novel approaches for neuroimaging feature extraction, effective dimensionality reduction, and has applications in non-invasive and early diagnosis of certain brain functional disorders.

# **1. Introduction**

## **1.1. Biomarker identification**

Advances in neuroimaging technologies have improved our understanding of brain function in psychiatric and neurological disorders such as mood disorders, drug abuse and addiction, schizophrenia, Alzheimer's disease, traumatic brain injury, etc. Monitoring and evaluating of human brain performance during the execution of functional experiments have revealed evidence regarding distinctive pattern of brain activity between healthy individuals and individuals with brain disorders. Except for certain cases, to date, the results of these studies have had minimal clinical impact and despite much interest in the use of brain scans for diagnostic and prognostic purposes, traditional and often ineffective diagnostic and prognostic approaches are the common practice for neurologists and psychiatrists.

One of the reasons for this hesitation in translating the laboratory work into clinical environments, is that major research for investigating the brain disorders using the neuroimaging modalities is focused on group studies where signifying a difference between the healthy population and a population with brain disorder is of interest rather than characterizing the individuals with brain disorder. The neuroimaging modalities will be useful in the clinical settings if decision making on the individual using their collected

data is possible at the level of the individual. To be able to explicate the functional basis of the brain disorders, a data analytics framework is required that can signify the set of potential biomarkers in the individuals from the group with brain disorder and their differences with the individual from the healthy individuals. However, fully identifying the potential functional biomarkers encompassed in the collected spatio-temporal brain activity from the individuals with brain disorder is a challenging problem as each of the neuroimaging modalities have their own inherent spatial and temporal limitation. In this dissertation, problem of identifying the functional biomarkers for brain disorders is addressed through utilizing through Machine learning (ML) (Bishop, 2006) algorithms. ML algorithms are employed to improve, develop, and explore the functional biomarkers for the functional neuroimaging data collected from the human cerebral cortex (Hagmann et al., 2008).

## 1.2. Brain Functional Activity

### 1.2.1. Brain cerebral cortex

There are about 100 billion neurons in human brain. Neurons send and receive electro-chemical signals to and from the brain and nervous system. Neurons are connected with an average of 1000 other neurons. The local interconnections between neurons construct structural segregated and functionally specialized regions of the human cerebral cortex(Hagmann et al., 2008). Brain's cerebral cortex covers the outermost layer of the brain and consists of nerve cell bodies made up of gray matter. As shown in Figure 1-1, cerebral cortex is divided into four different lobes with distinct location and

functionality: frontal lobe, occipital lobe, parietal lobe, and temporal lobe (Hagmann et al., 2008).

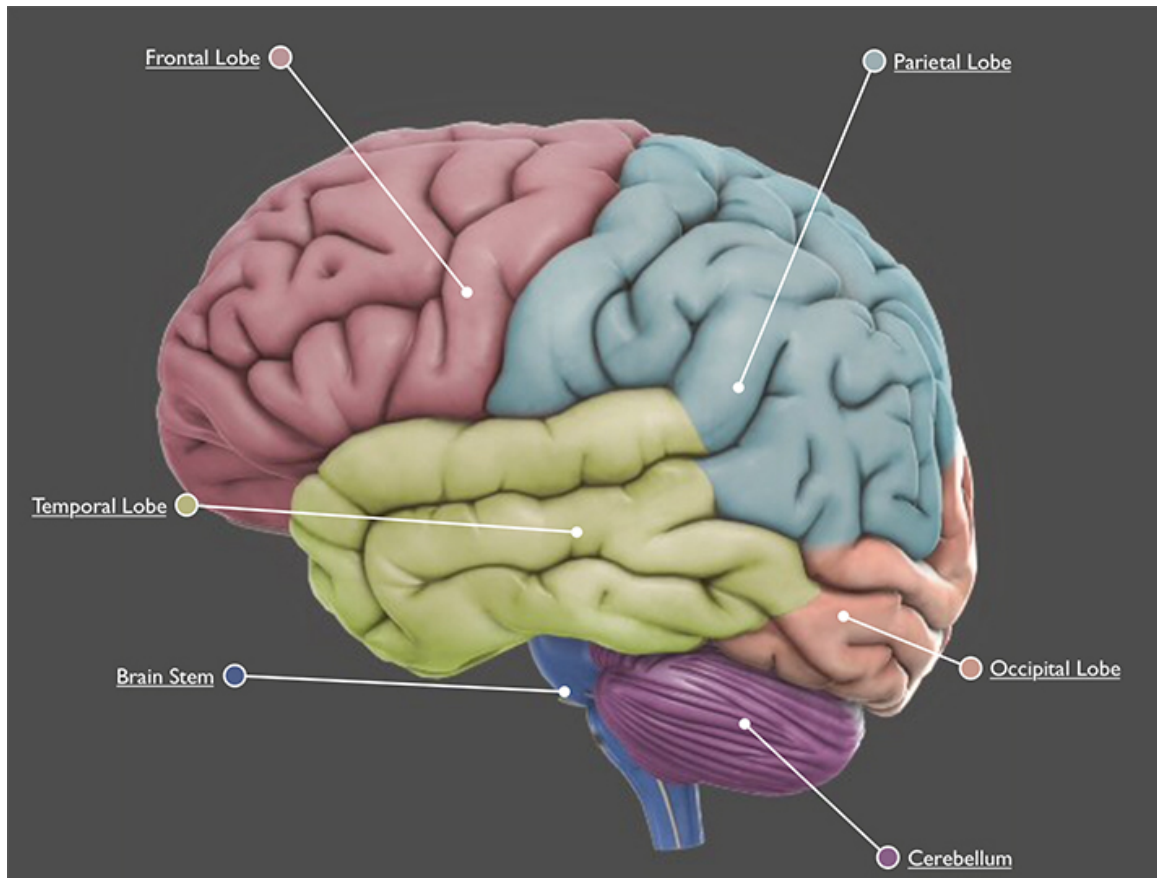


**Figure 1-1 Four lobe of human brain**

Brain frontal lobe, which is positioned at the most anterior region of the brain, is involved in higher-level cognitive functions like reasoning and judgment, decision-making, problem solving, attention, short-term memory tasks, motivation and planning.

The parietal lobe is immediately posterior to frontal lobe and is anterior to the occipital lobe. The parietal lobes is involved in sensation and perception as well as integrating sensory input, primarily with visual system.

Temporal lobe is located anterior to the occipital lobe. Temporal lobe manages sensory input, auditory perception, language and speech production, as well as memory association and formation. It is also involved in semantics, or word meaning.

Finally, occipital lobe, which is positioned at the most posterior regions of the brain, is primary visual processing center of the brain. Movement and color recognition and visual-spatial processing are interpreted within the occipital lobe.

Overall, cerebral cortex is responsible for sensing and interpreting input from various sources and providing cognitive function. In other words, most of the information processing in the brain takes place in the cerebral cortex.

### 1.2.2. Functional Neuroimaging

Assessment of brain activity with the purpose of characterizing its spatio-temporal activity is performed through designing an experimental paradigm. The components of an experimental design are a number of participants, associated to one or more groups, a functional task to be executed by the participants, and one or more functional neuroimaging modalities to collected individuals' brain response during the experiment.

The functional experiments designs are divided into two categories with respect to presence or absence of in-situ stimulus: (a) experiments in which subjects perform a well-defined task, e.g., making a decision or task-based experiments and (b) experiments in

which the brain activity is captured in the absence of a task, i.e. when the subject is in a state of wakeful rest and mind-wandering.

### 1.2.3. Neuroimaging Modalities

Functional neuroimaging modalities enable determining when and where neural activity occurs, in two different ways: (a) through capturing hemodynamic variations and (b) capturing electric impulses generated due to neuron communications.

The hemodynamic response is the process in which blood provides glucose to the neurons corresponding to the activated regions at a greater rate than the neurons of the inactive areas. Increase in metabolic demand upturn cerebral blood flow (CBF) to the activated area of the brain results in an excess of oxyhemoglobin in the veins of the active area, and in a change of the local ratio of oxyhemoglobin to deoxyhemoglobin with respect to the inactive areas (Villringer and Dirnagl, 1994). A number of modalities are designed to quantify these changes with different spatial and temporal resolutions. Imaging modalities such as functional Magnetic Resonance (fMRI) (Huettel et al., 2004) imaging and functional Near Infrared Spectroscopy (fNIRS) (Villringer et al., 1993) are able to quantify the hemodynamic variations. The collected data using the aforementioned imaging is an indirect, with low temporal resolution (because blood flows slowly), of neural activity.

On the other hand, neurons' communication takes place through an electrochemical process, by electro-chemical transmitters exchanging information between neurons. As a result of this process, neurons release ionic currents that flow within and across neuronal

assemblies. Imaging modalities such as electroencephalography (EEG) (Niedermeyer and da Silva, 2005; Teplan, 2002) or magnetoencephalography (MEG) (Hämäläinen et al., 1993) are capable of measuring changes in electrical activity as group of neurons become active. Imaging modalities of this category provide a direct measurement for neuronal activity and offer higher temporal resolution relative to the modalities that belong to the other category.

A summary for a number of commonly used neuroimaging modalities is illustrated in Table 1-1. As it can be seen in Table 1-1, every modality, offers its own advantages and disadvantages with respect to spatial and temporal resolution, portability, head movement restraint, etc. Generally, the imaging modality of choice is determined by the purpose of the study. The functional brain activity for this dissertation has been collected by EEG and fNIRS modalities. Therefore, in the following sections common approaches to identify biomarkers for EEG and fNIRS modalities will be reviewed.

Table 1-1 Comparison of neuroimaging modalities. Adopted from (Nicolas-Alonso and Gomez-Gil, 2012) and (Koike et al., 2013)

|                                     | <b>fNIRS</b>                | <b>fMRI</b>                          | <b>PET</b>   | <b>EEG</b>                 | <b>MEG</b>  |
|-------------------------------------|-----------------------------|--------------------------------------|--|----------------------------|---|
| <b>Measure of neuronal activity</b> | <b>Indirect</b>             | <b>Indirect</b>                      | <b>Indirect</b>                                    | <b>Direct</b>              | <b>Direct</b>   |
| <b>Activity Measured</b>            | <b>Hemodynamic response</b> | <b>Hemodynamic response</b>          | <b>Hemodynamic response</b>                        | <b>Electrical activity</b> | <b>Magnetic fields generated by neuronal activity</b> |
| <b>Measurement area</b>             | <b>Cerebral cortex</b>      | <b>Whole brain</b>                   | <b>Whole brain</b>                                 | <b>Cerebral cortex</b>     | <b>Cerebral cortex</b>                                |
| <b>Temporal resolution (ms)</b>     | $\geq 500$                  | $2 \times 10^3$<br>– $3 \times 10^3$ | $\geq 10^4$  | $\geq 0.5$                 | $\geq 0.5$  |
| <b>Spatial resolution (mm)</b>      | <b>20</b>                   | $\geq 1$                             | $\geq 10$  | <b>20</b>                  | $\geq 5$  |
| <b>Invasiveness</b>                 | <b>No</b>                   | <b>No</b>                            | <b>Intravenous injection of radioactive ligand</b> | <b>No</b>                  | <b>No</b>   |
| <b>Body movement</b>                | <b>Tolerable</b>            | <b>No</b>                            | <b>No</b>  | <b>No</b>                  | <b>No</b>   |
| <b>Head restraint</b>               | <b>No</b>                   | <b>Yes</b>                           | <b>Yes</b>   | <b>No</b>                  | <b>Yes</b>  |
| <b>Size, Movable</b>                | <b>Small, movable</b>       | <b>Large, fix</b>                    | <b>Large, fix</b>                                  | <b>Small, movable</b>      | <b>Large, fix</b>                                     |
| <b>Portability</b>                  | <b>Yes</b>                  | <b>No</b>                            | <b>No</b>  | <b>Yes</b>                 | <b>No</b>   |

### 1.3. Neuroimaging and Biomarker Detection

Studies of brain function aiming to identify spatio-temporal biomarkers in different brain disorders have received increased attention over the past few years.

The functional data is measured at equally spaced time intervals to trace fast-paced neuronal activity during a period. Therefore, the collected brain activity data is typically translated into tractable signals formatted as time series, which is an ordered sequence of values. Identifying biomarkers from the collected neuroimaging data for a specific brain disorder refers to detecting the spatio-temporal characteristics encompassed in the time series of the individuals with the brain disorder.

#### 1.3.1. Electroencephalography (EEG)

As discussed in the previous section, EEG is capable of measuring the electric brain activity caused by the flow of the electric currents during synaptic excitations, Figure 1-2. EEG signals are recorded non-invasively by placing the electrodes on the scalp to record the electrical signals that cross the scalp, skull, and other layers. An electrode placed on the scalp records the summed signal from many cells.

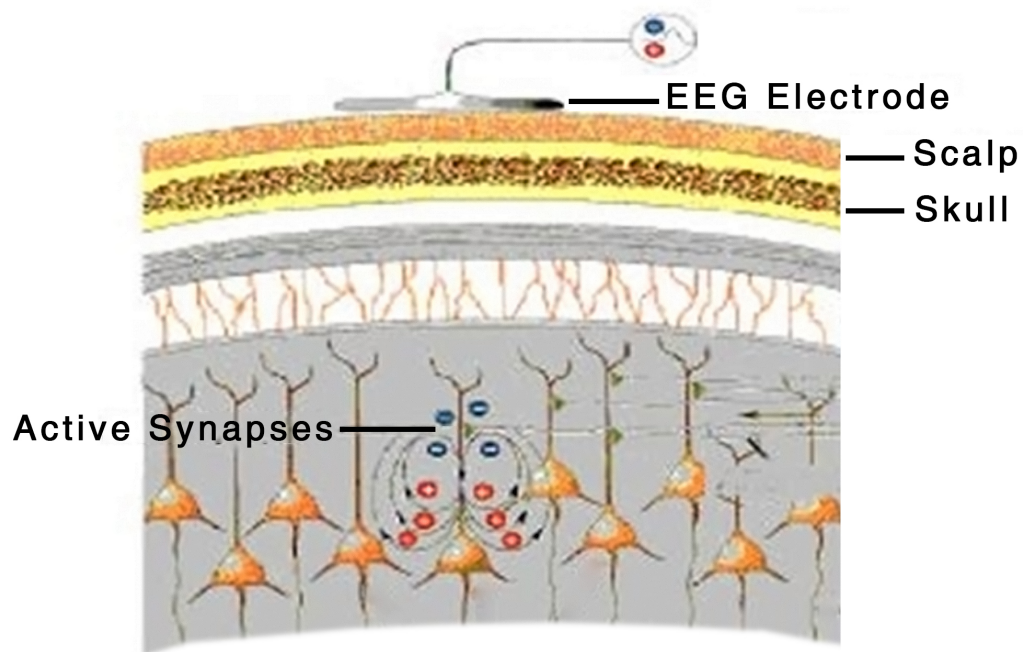


**Figure 1-2 EEG signals are recorded non-invasively by placing the electrodes on the scalp to record the electrical signals that cross the scalp, skull, and other layers. An electrode placed on the scalp records the summed signal from many cells. Adopted from**

EEG signals' amplitude ranges from 0.5 to 100  $\mu\text{V}$  where measurements are made over millisecond intervals (Teplan, 2002). These signals in the time domain may be converted to signals in frequency domain by means of Fourier transform (Bracewell, 1965) where contribution of sine waves with different frequencies are visible. The EEG consists of the activity of an ensemble of generators producing rhythmic activity in several frequency ranges. To minimize the random behavior of the EEG response, sensory stimulation (i.e. task-based experiments) is employed to make these generators act more in a more correlated way. EEG's stimulus-elicited responses are short-lasting events that give rise to "evoked" rhythms. These evoked rhythms in the frequency domain, signify ensembles

of millions of neuron activity suggesting the transition from a disordered to an ordered state (Basar et al., 2012) while in the time domain the so called event-related potentials (ERPs) manifest these transient variations after a stimulus is presented. Below, several works related to employing frequency rhythms and ERPs in studying individuals with brain disorders is reviewed.

### EEG Frequency Rhythms as Biomarkers

In the first recording of human EEG, Berger (Haas, 2003), had mentioned the presence of two rhythms in the collected time series corresponding to certain frequency ranges of 7.5-12.5 (alpha rhythms) and 12.5-30 (beta rhythms) Hz. Following this finding, researchers identified a number of such signals that are be classified according to their frequencies. These well-known frequency ranges have been defined as theta (4-7 Hz), delta (<4 Hz), and gamma (30-100 Hz) rhythms with respect to their distribution over the scalp or biological significance.

EEG oscillations have been associated with different states of brain functioning (Başar et al., 1999; Klimesch, 1999; Moretti et al., 2004) while in the physiological sense, power of these oscillations denotes the synchronized activity corresponding to a number of neurons (Klimesch, 1999). Variations in EEG frequency bands' magnitude have been employed as biomarker for many of the neurodevelopmental, neuropsychological, neurodegenerative, and psychiatric disorders (Van Deursen et al., 2008).

Alpha rhythms is known to appear in normal adults during wakefulness, best observed when subjects' eye are closed and are known to be detected mostly in the posterior region of the head (Niedermeyer, 2005). Evidence regarding alpha rhythm's association to

cognitive and memory performance has been presented in (Başar et al., 1999; Niedermeyer, 2005). Decrease in alpha wave activity is historically linked to early diagnosis of Alzheimer disease (Gordon and Sim, 1967; Letemendia and Pampiglione, 1958). Furthermore, decrease in the alpha and beta wave activity has been reported in individuals with mild Alzheimer (Hogan et al., 2003; Moretti et al., 2004)

Beta waves are dominant during normal state of wakefulness with open eyes and are majorly distributed in the frontal and central part of the scalp (Teplan, 2002). Beta rhythm is considered as an index of cortical arousal and has been reported to be related to attention, perception, and cognition (Coyle et al., 2004).

Spatial distribution of the beta power as well as variations in its magnitude has been studied as biomarkers in various studies. For instance, in the study by (Rangaswamy et al., 2002) increase in Beta's (absolute) power was observed in alcohol-dependent subjects, uniformly distributed across the scalp where significant increase was observed in the central region. They concluded that Beta power is potentially an electrophysiological biomarker that signifies the imbalance in the excitation–inhibition homeostasis in the cortex.

Relative changes in beta/delta power from the temporal lobes sites has been used as biomarkers in a work by (Merica and Gaillard, 1992). They examined if the rate of change in the spectral characteristics of EEG in beta/delta power may differentiate patients with insomnia from normal sleepers (control). To validate the effectiveness of their proposed biomarkers in categorizing subjects, a classification attempt was made on

a sample of 23 insomniac and 12 control subjects where classification accuracy of 75% was achieved.

Theta band is present in drowsiness or meditation and its power has been associated with the condition of the sleep (Torsvall, 1987). Its magnitude has also been used as biomarker for predicting the treatment outcome for the subjects with major depressive disorder (MDD) in (Iosifescu et al., 2009). A number of studies have attempted to use theta band as biomarker in the ADHD studies. In particular, magnitude variations of the theta band have been examined for the subjects with different range of age (children, teenagers, and adults with and without ADHD). (Snyder and Hall, 2006) have conducted a meta-analysis of these studies and have reported a consistent increase in theta power during a resting state in subjects with ADHD.

Delta waves are present in healthy adults and are the main characteristics of the deep sleep (Harmony et al., 1996). Delta wave's magnitude has been reported to decrease in subjects with depression (Borbély et al., 1984), AD (Basar et al., 2012) and increases in schizophrenic subjects (Flor-Henry et al., 2004; Mientus et al., 2002).

Gamma activity oscillations occur in the high frequency range of the temporal spectrum of the EEG. It is known to reflect perceptual and cognitive processes (Basar et al., 2012; Tiitinen et al., 1993), therefore has typically been examined in association with cognitive impairment and dementia related disorders (Scheibel et al., 2003; Van Deursen et al., 2008). In (Van Deursen et al., 2008), authors attempted to investigate the gamma band power as diagnostic biomarker for subjects with AD. Among three groups of subjects from AD (15 subjects), mild cognitive disorder (20 subjects), and 20 healthy control

subjects, increase in gamma band power was observed for subjects with AD in comparison with MCI and controls.

#### EEG ERPs as Biomarkers

The alteration of the ongoing EEG in response to stimuli is named an event related potential (ERP). ERPs consist of a series of elicited components (ERP components) which are time-locked events and reveal several sensory, cognitive and motor processes (Polich and Kok, 1995). Amplitudes of the ERPs are very low in comparison to the EEG time series. ERP components embedded in EEG signals can be extracted from the EEG signal by means of EEG signal averaging techniques over a number of trials. By including numerous task-related trials in the averaging process, the averaged signal reveals more of the ERP component and the non-stimulus related EEG activity is minimized (Friedman and Johnson, 2000). In Figure 1-3 a number of ERP components are visualized.

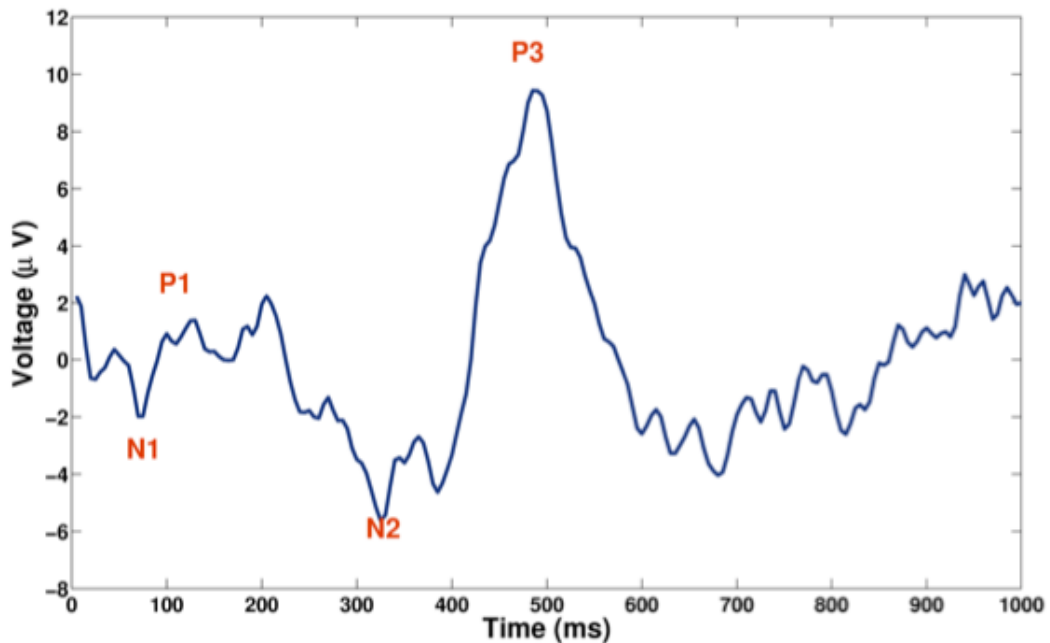


Figure 1-3 Visualizing a number of Event Related Potential Components (ERPs). ERPs consist of a series of elicited components (ERP components) which are time-locked events and reveal several sensory, cognitive and motor processes (Polich and Kok, 1995)

Amplitude, latency (the points in time at which the peak occurs), and scalp's (spatial) distribution are three common features that are considered from the ERP components (Johnson and Rosenfeld, 1992). Component amplitude denotes the extent of neural activation while component latency shows the timing of this activation. The spatial distribution for the components' activation provides a map for the components' pattern of activity (Friedman and Johnson, 2000).

ERP components are traditionally labeled by their polarity (i.e. P for positive going signal and N for negative going signal) as well as a value (in ms) that denotes the expected latency for the appearance of the wave's peak. P100, N100, N200, and P300, with the

occurrence expected latency windows of [50–190], [50–190], [150–300], [250–500] ms, respectively are four well-studied components that have been employed as biomarkers in studies involving populations with neurodevelopmental, neuropsychological, neurodegenerative disorders(Luck et al., 2011; Stahl et al., 2012; Taylor et al., 2014)

The following discussion regarding employing ERP components as biomarkers is limited to P100, N100, and P300 components that potentially can cover two broad categories of disorders. P100 and N100 components have been associated with processing of different stages of human attention procedure and P300 component has been associated to brain's cognitive procedure.

Two common sensory stimuli to evoke N100 and P100 components are auditory and visual stimuli. Generally, it is well established that N100 and P100 are elicited in response to exogenous processes, which are modulated by physical stimulus attributes. These components are generated in temporal or visual cortex in response to an auditory or visual stimulus, respectively. Visual and auditory P100 and N100 amplitude have been reported to be modulated by attention(Hillyard and Anllo-Vento, 1998) (Luck et al., 1990). Therefore, these components have been studied as potential biomarkers in disorders pertaining to attention deficit such as ADHD (Nazari et al., 2010)

In (Nazari et al., 2010), authors attempted to determine whether visual P100 latency and amplitude could be considered as potential biomarkers for ADHD. They collected the P100 ERP components from 15 children with ADHD and 15 children from normal control population. Delayed in latency and lower amplitude for P100 in ADHD population in comparison to the normal population was observed.

P300 component is known to reflect the fundamental cognitive events involving stimulus evaluation and immediate memory in normal populations in (Johnson and Rosenfeld, 1992; Nazari et al., 2010; Polich and Kok, 1995). It is usually elicited in response to the psychological tasks when subjects attend and discriminate stimuli that differ from one another on some dimension(Polich and Kok, 1995). It is relatively large in amplitude (10-20 V) and was first reported 30 years ago (Sutton et al., 1965). P300 scalp distribution typically increases in magnitude from the frontal to parietal electrodes (Polich and Kok, 1995) while its P300 is also believed to reflect an information-processing cascade when attentional and memory mechanisms are engaged (Polich, 2007; Portin et al., 2000).

P300 power as potential biomarker to differentiate populations with cognitive dysfunction such as MCI and AD has been investigated in several studies (Frodl et al., 2002; Polich et al., 1990). In an attempt to investigate P300 potential to be used as biomarker for diagnosis of AD in its early stages (Polich, 1989) concluded that P300 amplitude was smaller and peak latency longer for the Alzheimer patients compared to control subjects.

P300 has also been employed to characterize schizophrenia disorder. Initially, (Roth and Cannon, 1972) reported smaller P300 in schizophrenic subjects in comparison to normal control. Later, P300 amplitude was adopted to be studied as a potential biomarker in schizophrenic individuals by more researchers (Duncan, 1988; Ford, 1999; Friedman and Squires-Wheeler, 1994);(McCarley et al., 1991). In (Jeon and Polich, 2003), authors conducted a meta-analysis by working on a collection of 104 articles

pertaining to employing P300 as biomarker to characterize the schizophrenic subjects by identifying the underlying P300 deficits in the schizophrenic population in comparison to the normal control. They concluded that P300 was smaller in amplitude and showed a longer in latency in schizophrenic patients compared to normal controls.

### 1.3.2. Functional Near Infrared Spectroscopy (fNIRS)

As discussed in section 1.1, fNIRS is a non-invasive neuroimaging modality that is able to measure brain activity through quantifying the concentration changes of oxy-hemoglobin (HbO) and deoxy-hemoglobin (HbR).

Typically, an fNIRS device is comprised of a light source that is coupled to the participant's head via a light-emitting diodes (LEDs) and a light detector. The emitting diode sends the Infrared light through the skull to a depth of approximately 1–3 cm below its surface. The intensity of the reflected light is measured by the receiving detector and enables quantifying the changes in the concentration of the HbR and HbO.

The early ages of the fNIRS data analysis was focused on discriminating the signal that represents brain activity from the noise (Germon et al., 1994; Hoshi et al., 2001; Kleinschmidt et al., 1996). As a result, taking the average values of the hemodynamic signals during the task period and performing a statistical test to identify the task-relevant hemodynamic response became a popular technique (Tak and Ye, 2014). However, this approach does not utilize the time and shape dependent characteristics of the HbO and HbR signals. To address this limitation, (Schroeter et al., 2004) utilized the well-known general linear model (GLM)(Schroeter et al., 2004) that linearly unmixes the data into several task-related and non-task related sources . GLM

was later employed by several other researchers for fNIRS data analysis (Custo et al., 2010; Koh et al., 2007; Minagawa-Kawai et al., 2010; Shimada and Hiraki, 2006; Singh and Dan, 2006).

### fNIRS Hemodynamic Spatio-temporal Characteristics as Biomarker

Majority of fNIRS studies aiming to investigate the significance of difference between the healthy control group and the group with the neurological disorder, extract hemodynamic features from the HbO signal. It is due to the fact that HbO has higher sensitivity to the changes in cerebral blood flow than the HbR (Hoshi et al., 2001). fNIRS first use in clinical application dates back to 1994 in a study by (Okada et al., 1994). In this study, hemodynamic signals were from 38 healthy and 38 chronic schizophrenic subjects from the forebrain area of the both hemisphere were collected. To investigate the differences in the patterns of hemodynamic changes between the two populations in response to the mirror-drawing task, median, maximum and minimum values of the hemodynamic signals for every subject were extracted. For every variable, statistical test was employed to investigate the significance of difference between the populations. Authors reported that half of the schizophrenic subjects had deregulated patterns between the two hemispheres in the forebrain area where as the normal subjects showed distinct and well-integrated patterns of hemodynamic changes.

(Monden et al., 2015) attempted to explore a method that enables characterizing individuals with ADHD to accurately distinguish individuals with ADHD from the healthy individuals. The hemodynamic was collected in response to the go/no-go task (Jodo and Kayama, 1992) from 30 ADHD and 30 typical developing control children.

Authors employed compared HbO amplitude across certain regions of the brain and reported that subjects were classified to the ADHD and typical groups with high accuracy.

#### 1.4. Neuroimaging Feature Extraction Approach for Biomarker Identification

As discussed in the previous sections, several attempts using the standard univariate analysis have been made to identify possible biomarkers from the neuroimaging data, which could be used for early diagnosis, treatment planning and monitoring of disease progression in individuals with certain brain function disorder. The proposed approaches have revealed a host of functional and structural alterations between subjects with wide range of brain function disorders and healthy control subjects. Although the commonly used univariate analysis is a valid methodology for comparing the brain activity between the two groups of subjects, but it does not fully exploit all the potential biomarkers that may play role in distinguishing the subjects. In addition, while it is capable of signifying differences between subjects with distinctive brain activity at a group level, it is incapable of providing a general model to satisfactory discriminate a patient from the healthy control subjects.

Over the past few years, supervised and unsupervised Machine learning (ML) (Bishop, 2006) multivariate methods have been employed to address these limitations. In particular, supervised ML methods have been vastly used to differentiate task-specific or resting-state brain activity in brain-computer interface (BCI) (Lotte et al., 2007b) applications and infrequently to classify healthy subjects from individuals with a neurological disorders (Ahmadlou et al., 2010; Bosl et al., 2011; Rizk-Jackson et al.,

2011; Stahl et al., 2012; Woon et al., 2007). Figure 1-4 illustrates the general problem that the supervised ML attempts to address.

The advantage of employing multivariate ML algorithms for analyzing neuroimaging data is that unlike the traditional univariate group studies allows characterization at the level of the individual level, therefore yielding result with a potentially high clinical translation. Furthermore, the multivariate ML methods are sensitive to spatial distribution and subtle effects in the brain that would be undetectable using the univariate group analysis methods as the focus in these methods is on gross differences at group level.

In the general supervised ML framework aiming to classify subjects to a group of healthy/typical and a group with brain disorder using the neuroimaging modalities, the algorithm receives a set of observation regarding the subjects (the neuroimaging data and class labels for subjects). A subset of the input data is used as “training” data to build a predictive model that can be applied to make to associate new subjects to one of the classes with respects to its collected data by a neuroimaging modality (Guyon and Elisseeff, 2006).

#### 1.4.1 The General Problem of Feature Extraction

As discussed above, the supervised ML approach has infrequently been utilized to automatically distinguish subjects with neurological disorder from the healthy subjects. The assumption underlying this approach is that anomalous brain activity is present in the neuroimaging data collected from the subjects with neurological disorder. The anomalous

activities are identified through informative feature extraction and the classification algorithm. Informative features are a number of characteristics extracted from the individuals' neuroimaging signals that reflect similarities to a certain class of individuals as well as differences from the other class.

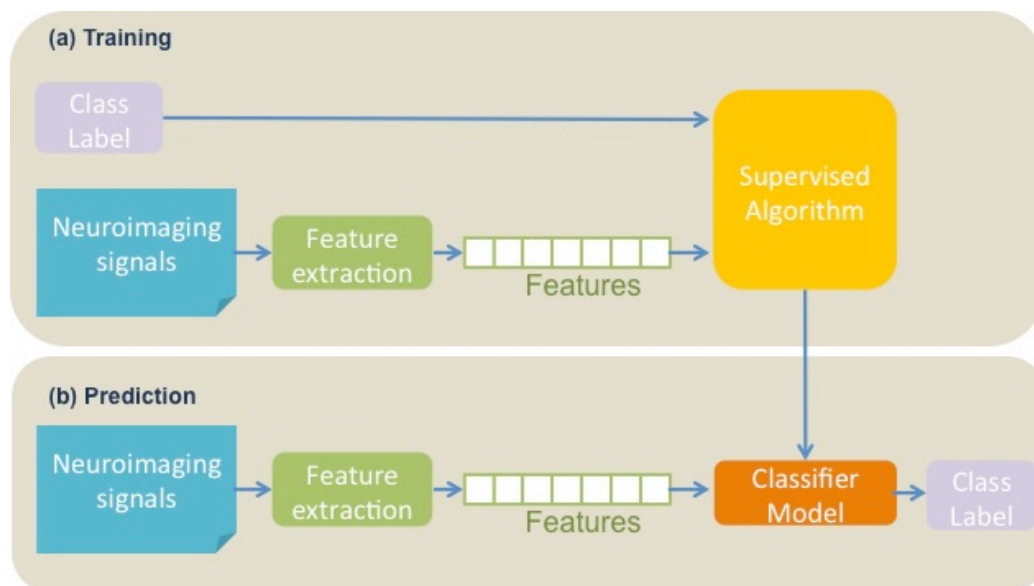


**Figure 1-4** The general diagram for a supervised machine learning classification. The neuroimaging signals from the subjects of different classes are used to train a classifier model. The trained classifier makes prediction for the neuroimaging signals collected from the subjects with unknown class affiliation.

Significance of feature extractions from the EEG and fNIRS signals is twofold.

- *Reducing Artifacts.* In the context of functional imaging of task related activity, artifacts are the captured activities that are evoked by a phenomenon other than the experimental manipulation. EEG signals are known to be highly susceptible to the contamination caused by eye movements, blinks, cardiac signals, and

muscle activities whereas fNIRS hemodynamic signals are prone to combination of “spontaneous” hemodynamics (reflecting ongoing brain activity), various sources of physiological activity, and measurement noise. These artifacts present significant challenges for analysis and interpretation of the signals. Feature extraction as a mean of mining informative components of the signals, improves the performance of the aforementioned supervised ML approach.

- *Dimensionality Reduction.* A major challenge in employing ML algorithms for EEG and fNIRS data analysis is their high dimensionality. The high dimensionality of the data is a natural consequence of the high temporal resolution of these modalities. The high dimensionality of the data adds more complexity, increases the computational time, and complicates the application of the ML procedures on the data due to the phenomenon called “curse of dimensionality” (Lotte et al., 2007b). In the supervised ML procedure, the curse-of-dimensionality occurs if the number of training data is small (here, number of individuals data) compared to the size of the input data and results in poor performance for the employed algorithm (Lotte et al., 2007a).

In the following section, most commonly used feature extraction techniques for EEG and fNIRS studies are reviewed.

#### 1.4.2. EEG and fNIRS Feature Extraction Techniques

Mathematically, feature extraction is the process of extracting features from the raw data through a functional mapping. In other words, let  $x$  be the neuroimaging time series of dimension  $n$ ,  $x = (x(1), x(2) \dots x(n))$ ,  $x(i) \in \mathbb{R}$ . The components  $x(i)$  of

this time series are the original features. A new set of features

$y = (y(1), y(2), \dots, y(m))$  ( $m < n$ ) are extracted by a mapping function  $F$ ,

$$y(i) = F_i(x(1), x(2), \dots, x(n)).$$

In multivariate EEG feature extraction approach, features may be obtained in time domain or frequency domain. The autoregressive model (AR) (Gersch and Yonemoto, 1977) and discrete wavelet transform (DWT) are the most commonly used feature extraction techniques to investigate various neurological disorders using EEG in time domain and frequency domain, respectively.

Early paper on AR method was published in 1977 by (Gersch and Yonemoto, 1977). The authors described that AR models can be used to describe an EEG time series for the purpose of feature extraction. In an AR model, it is assumed that the value of the current sample,  $x_t$ , can be estimated as a linearly weighted sum of the previous samples,  $x(1), x(2), \dots, x(n-p)$ , where  $p$  is the model order and is generally chosen to be smaller than the number of time series samples. The AR model of a signal  $x$  for in discrete time  $t$  is defined as follows:

$$\widehat{x(t)} = \sum_{i=1}^p a_i x(t-i) + \varepsilon(t) \quad (1.1)$$

where,  $\widehat{x(t)}$  indicates the predicted value of  $x(t)$  and  $a_1, a_2, \dots, a_p$ , denote the weight coefficient of the  $p$ th-order model. The AR model parameters have been used in classifying patients with epilepsy (Chisci et al., 2010; Mousavi et al., 2008), patients with cognitive impairment (Li et al., 2014), patients with ADHD (Sadatnezhad et al., 2011) and sleep stages (Estrada et al., 2004).

The wavelet transform is an effective EEG feature extraction technique due to its attractive properties such as time–frequency localization (obtaining a signal at particular time and frequency, etc.) (Adeli et al., 2003). EEG analysis using Discrete Wavelet Transform (DWT) the original signal is decomposed into a several successive frequencies bands by utilizing a scaling and a wavelet function, associated with low-pass and high-pass filters.

The original EEG signal,  $x$ , is first passed through a half-band high-pass filter  $h[.]$ , and a low-pass filter  $l[.]$  (Rioul and Vetterli, 1991). The filtering followed by sub-sampling is one level of the successive decomposition procedure (this procedure is commonly referred to as sub-band coding). The following formulation describes the first step of this procedure:

$$d_{1k} = \sum_n x(n) \cdot l(2k - n),$$

$$a_{1k} = \sum_n x(n) \cdot h(2k - n),$$

where  $d_{1k}$  and  $a_{1k}$  are level 1 detail and approximation coefficients at translation  $k$  ( see (Shensa, 1992) , respectively. The second level of the wavelet transform is applied on the approximation coefficients of the first level,  $a_{1k}$  and  $a_{2k}$  and  $d_{2k}$  are obtained. This process may be repeated until no more subsampling is possible. The output at each level of this successive decomposition, called sub band, is a signal with a certain frequency range. Researchers either use the original sub band signals (or a subset of them) as feature elements or attempt to extract features from these signals to classify individuals with brain function disorder. For instance, the former has been employed in a study by

(Polikar et al., 1997) where the goal has been to develop a highly accurate diagnosis technique for AD. The sub bands were considered as feature vectors and fed to the classification algorithm to classify individuals with AD. The latter approach was employed in (Ahmadlou et al., 2010) where the goal was to accurately classify children with autism. In this study, the fractile dimensions (Higuchi, 1988) of every sub band (obtained from a 3 level decomposition) were computed and used as feature vectors for classifying children with autism.

Although fNIRS has been available for several years but it has not achieved significant clinical use with respect to its availability and potential benefits. The research literatures published to date regarding potential fNIRS clinical use has mostly focused on applicability and reliable of the modality. The multivariate feature extraction approaches for fNIRS have been majorly developed for the BCI applications. The commonly used features from the fNIRS HbO signal are the signal's maximum peak amplitude (Bennett et al., 2014; Ehlis et al., 2008; Kurz et al., 2014), mean value (Doi et al., 2013; Ehlis et al., 2008; Plenger et al., 2015), variance (Gottemukkula and Derakhshani, 2011) , slope (Hai et al., 2013), skewness and kurtosis (Holper and Wolf, 2011) . A number of researchers have attempted to employ the constructed BCI systems as a communication means for patients with motor disorders such as amyotrophic lateral sclerosis (ALS) (Naito et al., 2007) , or Duchenne muscular dystrophy (DMD) (Power and Chau, 2013). (Power and Chau, 2013) fitted a regression lines to the HbO and HbR signals and considered the slope of the lines as the features to classify a mental arithmetic task from a natural baseline state in an individual with DMD. Authors reported overall classification

accuracy of 71.1% and suggested that their findings demonstrate the potential of fNIRS-BCI to be used by individual with DMD.

### 1.5. Limitations of the Current Multivariate Feature Extraction Techniques

It is very well established that brain functional and structural alterations due to a set of brain disease. These alterations expand over a widely distributed network of brain regions (Grady et al., 2001; Kennedy and Courchesne, 2008; Yu-Feng et al., 2007; Zhang et al., 2011). It signifies the importance of the spatial characterization in the process of biomarker identification thorough the feature extraction technique. Nevertheless, as discussed in section 1.3, the commonly used multichannel feature extraction techniques for EEG and fNIRS are essentially time series analysis techniques, which are not designed to incorporate the spatial information into their analysis. This highlights the need to develop higher level of feature extraction techniques that not only are capable of detecting information and discarding the noise but also considers the potential spatial connection between the collected signals.

Furthermore, the typical EEG and fNIRS feature extraction techniques obtain discriminative information from individuals' signals by treating signals from different channels independently and do not to consider the potential relation and correlation among the signals. To overcome this limitation, multivariate time series feature extraction techniques that attempt to identify features from multiple time series by treating multichannel data jointly need to be developed.

## 1.6 Organization

In this dissertation, the supervised and unsupervised ML algorithms are employed to improve, develop, and explore the spatio-temporal characteristics of the EEG and fNIRS neuroimaging data.

In Chapter 2, a new approach to trace the dynamic patterns of task-based functional connectivity, by combining dynamic time warping (DTW), and Quality Threshold (QT) clustering techniques, is presented. To capture the patterns of functional connectivity, DTW is employed to measure the functional similarities among channels. Unlike commonly used temporal similarity measures, such as cross correlation, DTW compares time series by taking into consideration that their alignment properties may vary in time. QT clustering analysis is then used to automatically identify the functionally connected regions in the brain.

In chapter 3, the proposed approach in chapter 2 is evaluated on the EEG signals recorded from 5 healthy subjects as they performed an auditory oddball and a visual modified oddball tasks. As discussed in chapter 2, the stimulus-elicited brain responses are short-lasting events (John, 1990; John and Harmony, 1990; Koenig et al., 2005; Lehmann et al., 2005; Lehmann et al., 1998). Identifying the temporal windows corresponding to these events would be critical in studying task-based functional

connectivity. Ignoring these variations can lead to dismissing the dynamic interactions of the brain regions (Kang et al., 2011a). In the context of EEG, ERPs consisting of a series of elicited components (ERP components) manifest these transient variations after a stimulus is presented. The ERP components are time-locked events that reveal several sensory, cognitive and motor processes (Alexander et al., 1995). Hence, part of my proposed method of identifying functionally connected regions during the execution of the task, is concerned with exploring EEG signals within the expected temporal windows of a number of previously studied ERP components.

In chapter 4, a novel neuroimaging time series feature extraction technique, relative brain signature (RBS) is developed. This technique uses orthogonal subspace projection to transform a set of time series associated to data point (e.g. set of EEG time series corresponding to a subject) into a new coordinate system. The proposed technique provides effective dimensionality reduction, which is crucial for neuroimaging data such as EEG with high temporal resolution. The proposed technique was named relative brain signature as the values in the transformed space quantify the relative association of every single time series to a class. Another unique characteristics of this technique is that it relies on the a priori information corresponding to a class, therefore, is feasible for clinical studies where databases corresponding to a class of certain disorder are available.

In Chapter 5, the developed method in chapter 4 is applied on an EEG data set of abstinent alcoholics and control subjects. To characterize subjects' relationship to the alcoholic and control populations, one RBS vector with respect to the alcoholic and one with respect to the control population is constructed. The applicability of the extracted

RBS vectors in identifying functional biomarkers over the brain of alcoholics is evaluated. To achieve this goal, a classification algorithm is used to categorize subjects into alcoholics and controls classes using the RBS feature extraction technique.

In chapter 6, an approach for exploring potential hemodynamic functional biomarkers within the prefrontal cortex (PFC) that characterize subjects with Traumatic Brain Injury (TBI) is explained. To achieve this goal, a task-related hemodynamic response detection followed by a heuristic search for optimum set of hemodynamic features is introduced. To identify the hemodynamic signals that show task-related hemodynamic activity, trials with negatively correlated oxygenated hemoglobin (HbO) and deoxygenated hemoglobin (HbR) and HbO larger than HbR were considered for analysis. For identifying the optimum hemodynamic features, unlike common single feature analysis for studying TBI and healthy subjects, all the possible combinations of multiple hemodynamic features to compare the TBI and healthy populations were evaluated. Eleven hemodynamic features were extracted from HbO to determine the optimum set of biomarkers. I investigated the effectiveness of the extracted features in separating TBI and healthy subjects by utilizing a machine learning classification algorithm to score all the possible combinations of features according to their predictive power.

In chapter 7, findings and contribution of this dissertation are reviewed.

## **2. Cluster Analysis to Capture Functional Connectivity**

In Chapter 2, a new approach to trace the dynamic patterns of task-based functional connectivity, by combining dynamic time warping (DTW), and Quality Threshold (QT) clustering techniques, is presented. To capture the patterns of functional connectivity, DTW is employed to measure the functional similarities among channels. Unlike commonly used temporal similarity measures, such as cross correlation, DTW compares time series by taking into consideration that their alignment properties may vary in time. QT clustering analysis is then used to automatically identify the functionally connected regions in the brain.

### **2.1 Functional Connectivity**

It is well established that brain is composed of functionally segregated regions. However, in contrast to such local specialization, brain activity is globally integrated at many levels ranging from the neuron to overall behavioral output (Tononi et al., 1994). Functional connectivity (FC) (Fingelkurts et al., 2005) is the approach of investigating the integration between these functionally segregated regions. Studies of resting state and task-based FC aiming to provide a biomarker through the potential connection between these spatially distinct regions have received increased attention over the past few years. Aside from healthy populations, different patient groups, including patients with autism (Kleinhans et al., 2008; Koshino et al., 2005; Pollonini et al., 2010), traumatic brain

injury (TBI) (Kasahara et al., 2010; Mayer et al., 2011), Alzheimer (Dauwels et al., 2010; Uhlhaas and Singer, 2006), and depression (Greicius et al., 2007; Sheline et al., 2010), have been the subject of FC studies. These studies have identified altered connectivity networks in patient groups compared to the healthy group.

However, It has been shown that the interactions between brain regions during the execution of a task are temporally dynamic (Kang et al., 2011b; Kelly et al., 2008; Liu et al., 1999). These interactions generally happen within milliseconds intervals. EEG by providing high temporal resolution can therefore, be employed to capture these short-lasting events (Bhattacharya and Petsche, 2005; Koenig et al., 2002; Lehmann et al., 2012).

Assessing functional connectivity requires employing an appropriate measure of functional coupling among brain regions. Accordingly, several measures for detecting functional connectivity in either time domain or frequency domain have been proposed (Bhattacharya and Petsche, 2005; Jalili and Knyazeva, 2011; Pijnenburg et al., 2008). However, considering the short-lasting nature of the neurons' commutations, to be able to trace the dynamic patterns of functional similarity among cortical regions, analysis in the time domain would be appropriate. Furthermore, the dynamic time warping (DTW) algorithm was employed to measure similarity among signals within each segment. DTW is a common practice in the field of speech processing (Sakoe and Chiba, 1978) and is used to compare time series by taking into consideration that their alignment properties may vary in time. In other words, DTW measures similarity between two signals by compressing/expanding them and looking for their best nonlinear temporal alignment.

With respect to the well-documented non-stationary behavior of the EEG signals, employing DTW is more appropriate in comparison to the conventionally used methods such as cross-correlation which generally requires the assumption of stationary.

## 2.2 Dynamic Time Warping (DTW)

As previously stated, the majority of the functional connectivity studies performed in the time domain use cross-correlation to analyze the similarities among signals. The major limitation of this technique is that it fails to capture the similarities if the alignment properties of the signals vary in time. To address this issue and to assess brain functional connectivity during the execution of a task more accurately, employing the dynamic time warping technique is proposed.

DTW technique finds the optimal alignment between two time series through a non-linear compression and extension of the time axes (as depicted in Figure 2-1). In fact, the basic problem that DTW attempts to solve is how to align the two time series in order to generate the most representative distance measure of their overall difference. Figure 2-2 illustrates how the analysis is done. Suppose, we are interested in computing the DTW distance between two EEG signals  $\mathbf{d}=(d_1, d_2, \dots, d_N)$  and  $\mathbf{e}=(e_1, e_2, \dots, e_N)$  of length  $N$ . The first step is to calculate the distance between each point in signal  $\mathbf{d}$  and all the points in signal  $\mathbf{e}$ . Euclidean distance metric can be used for such distance computation. Therefore, for every point in signal  $\mathbf{d}$ ,  $N$  measured distance values are obtained, resulting in an  $N \times N$  matrix (cost matrix)  $\mathbf{C} \in \mathbb{R}^{N \times N}$  (Figure 2-3). The signals are associated to this matrix such that the bottom-left and top-right corners of the matrix represent the distance between their beginning and the ending points, respectively.

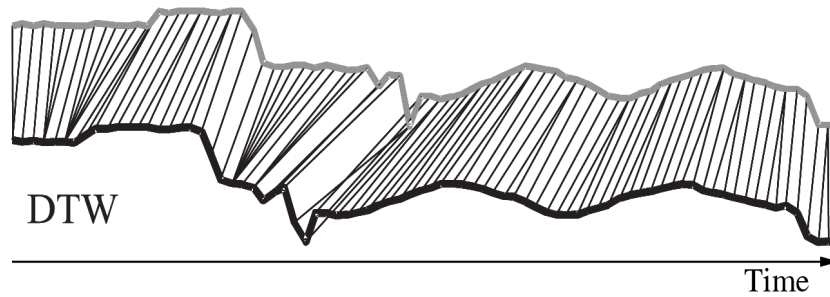


**Figure 2-1 Two hypothetical time series with an overall similar shape but not well aligned along the time axis. To find the optimal alignment between two time series, one point from the first time series may be compared against a number of points from the second time series, after (Keogh and Ratanamahatana, 2005).**

Once the cost matrix is formed, the second step is to find the best alignment between signals  $\mathbf{d}$  and  $\mathbf{e}$ . This alignment may be sought in a form of a warping path,  $\mathbf{p}$ , consisting of a set of elements taken from matrix  $\mathbf{C}$  ( $\mathbf{p}=[p_1 \dots p_L]$ , where  $N \leq L \leq 2N-1$ ).

A number of conditions can be enforced on this search, to reasonably limit the number of potential path candidates. For the analysis, only the paths satisfying the following conditions were considered:

- Boundary condition: start and end points of the warping path have to be the very first and last points of the given time signals, respectively
- Monotonicity condition: For any two consecutive points of the path,  $p_k = c_{i,j}$  and  $p_{k-1} = c_{m,n}$ , ( $c_{i,j}$  and  $c_{m,n} \in \mathbf{C}$ ), the following condition should be satisfied:  $i-m \geq 0$ ,  $j-n \geq 0$ . This condition guarantees that the path will not turn back on itself.
- Step size condition: restricts the path to advance only one step at a time

The optimal warping path (optimal alignment) is the one having the minimal total cost among all possible warping paths. Mathematically the optimal warping path ( $d_{DTW}$ ) can be formulated as

$$d_{DTW} = \min \left( \frac{\sum_{L=1}^L p_L}{L} \right).$$

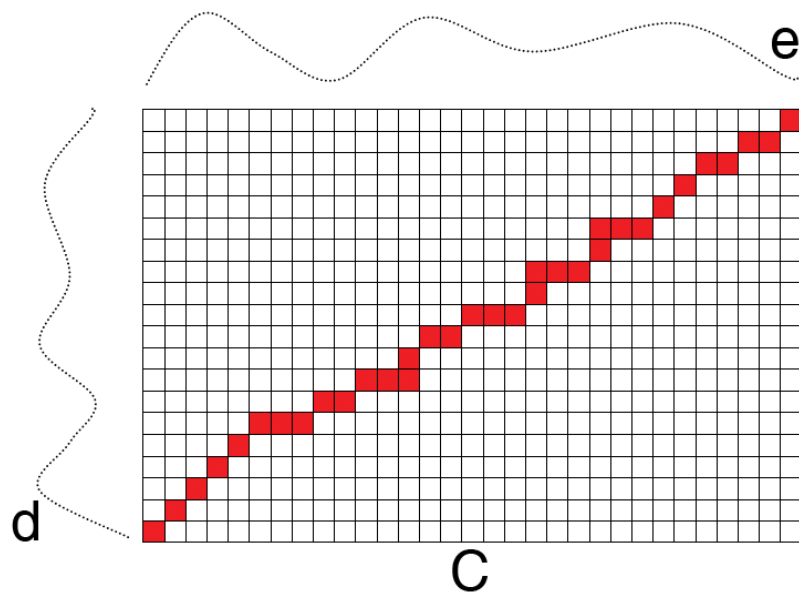


**Figure 2-2** Two time series, which have similar pattern of activity but are not aligned in the time domain. Matrix C is the cost matrix in which the optimal warping path is shown as the sequence of solid squares (shown in red).

Advantage of employing DTW technique in comparison to the common time series similarity measurement techniques that compute the point-to-point distance between two signals is visualized in Figure 2-3. Two hypothetical time series with an overall similar shape but not well aligned along the time axis (shown as **a** and **b** in the figure). To find the optimal alignment between two time series, DTW attempts to compare one point from the first time series against a number of points from the second

time series and selects the best match. The difference in the point selection for comparison between DTW (red dashed line) and other common point-to-point selection techniques (solid blue line) is also illustrated in Figure 2-3. As depicted in this figure, DTW's selection represents more of the similarity in the pattern of the signals in comparison to the other approaches.

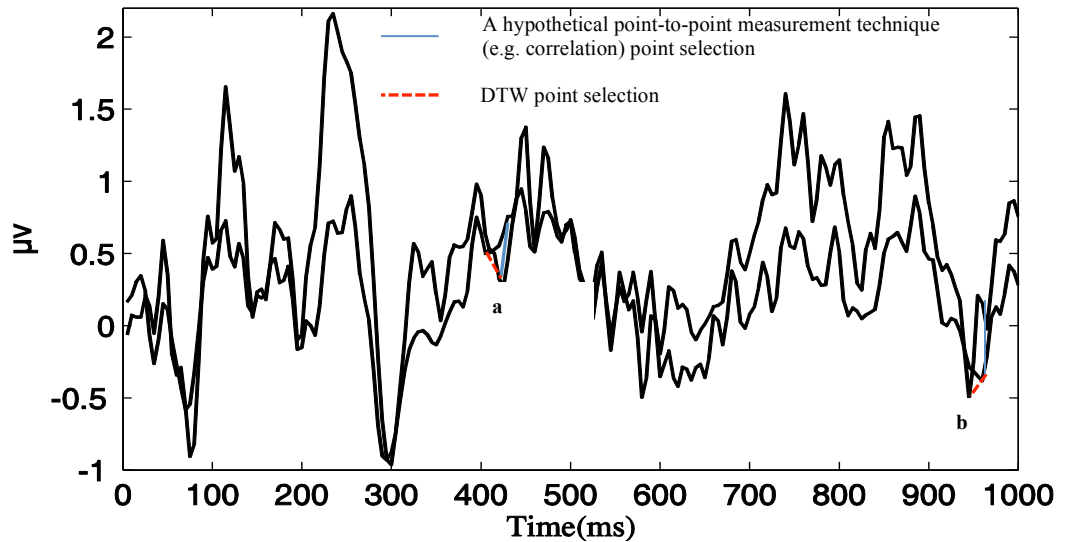


**Figure 2-3** Two hypothetical time series with an overall similar shape but not well aligned along the time axis. To find the optimal alignment between two time series, one point from the first time series may be compared against a number of points from the second time series and the best match is selected.

### 2.3 Quality Threshold (QT) Cluster Analysis

The Quality threshold (QT) clustering is a partitioning clustering algorithm (Boley et al., 1999) originally developed for the analysis of gene expression data (Heyer et al., 1999). One of the advantages of using QT over other clustering methods such as k-

means (Hartigan and Wong, 1979) is that it does not require specifying the number of clusters apriori. Moreover, the outcome of the algorithm is not dependent on the order of the points to be clustered, and it always returns the same cluster outcomes. Since the number of functionally connected regions in the brain in response to a functional task is not known in advance and needs to be determined, QT seems a feasible choice to tackle this problem.

Let  $X = \{x_1, x_2, \dots, x_n\}$  be the set of EEG signals, which are collected from different sites of the scalp and  $Y = \{y_1, y_2, \dots, y_n\}$  be the  $n$   $m$ -dimensional feature vectors corresponding to  $\{x_1, x_2, \dots, x_n\}$ . Here  $y_j$  is the feature vector extracted from  $x_j$ .

QT clustering approach is employed to identify the functionally connected regions in the brain from the set of EEG signals. Clusters are the functionally connected regions and the data points are the  $n$  feature vectors.

The basic idea of QT clustering for a given set of data points,  $Y$ , and a threshold value,  $d$ , is as follows: Form a candidate cluster,  $C_i$ , by starting with a random data point  $y_i$  and iteratively add other points  $y_j \in (Y - C_i)$ , with each iteration adding the point that  $\min_j (\text{diameter}(C_i \cup y_j))$

where the diameter of a cluster (or quality of a cluster) is:

$$\text{diameter}(C) = \min_{m,n \in C} (D_{y_m y_n})$$

where  $D_{y_m y_n}$  is the DTW distance between  $y_m$  and  $y_n$ .

The process continues until no point can be added without surpassing the diameter threshold,  $d$ . If surpassing the threshold occurs, a second candidate cluster is formed by

starting with another point,  $y_k$  ( $k \neq j$ ). In order to achieve reasonable clustering quality, already assigned points are available for forming another candidate cluster. Once a candidate cluster corresponding to every data point is constructed, QT selects the candidate cluster with largest number of data points, removes the points, which belong to the cluster from consideration, and repeats the procedure on the remaining set of data.

## 2.4 Summary of Chapter 2

In this chapter, a novel approach for detecting the functionally connected regions in the brain, which is a well-established high-order functional biomarker for many brain disorders, is proposed. The first novelty of this approach lies in using a cluster analysis, QT, approach for automatically grouping the signals that have similar patterns of behavior. Advantages of employing QT to identify functionally connected regions are twofold. Firstly, it enables exploring all the possible clusters that indicate similar neural activity. Secondly, the algorithm determines the number of functionally connected regions and it should not be specified a priori. The second novelty of the proposed approach corresponds to utilizing the DTW dissimilarity measure that unlike the commonly used methods considers the potential misalignment of the EEG signals through a non-linear compression and extension of the time axes.

### **3. Capturing Dynamic Patterns of Task-Based Functional Connectivity with EEG**

#### 3.1. Dynamic Patterns of Functional Connectivity

In the previous chapter, a method to identify the functionally connected regions was proposed. In this chapter, the proposed method is evaluated on the EEG signals recorded from 5 healthy subjects as they performed an auditory oddball and a visual modified oddball tasks. As discussed in chapter 2, the stimulus-elicited brain responses are short-lasting events (John, 1990; John and Harmony, 1990; Koenig et al., 2005; Lehmann et al., 2005; Lehmann et al., 1998). Identifying the temporal windows corresponding to these events would be critical in studying task-based functional connectivity. Ignoring these variations can lead to dismissing the dynamic interactions of the brain regions (Kang et al., 2011a). In the context of EEG, ERPs consisting of a series of elicited components (ERP components) manifest these transient variations after a stimulus is presented. The ERP components are time-locked events that reveal several sensory, cognitive and motor processes (Alexander et al., 1995). Hence, part of my proposed method of identifying functionally connected regions during the execution of the task, is concerned with exploring EEG signals within the expected temporal windows of a number of previously studied ERP components.

In the present study, I attempted to establish a dynamic pattern for task-based functional connectivity, which will enable tracing functionally connected regions during the execution of the tasks. To achieve this goal, first, EEG signals are divided into several segments. The temporal windows for EEG segmentation are set the same as the time intervals, where the occurrence of ERP components is expected. Second, DTW algorithm was utilized to measure similarity among signals within each segment that resulted in a similarity matrix. Finally, the similarity matrix is used as an input to the QT clustering algorithm. For each task, the proposed approach was able to establish a unique sequence of dynamic pattern (observed in all 5 subjects) for brain functional connectivity.

The rest of the chapter is organized as follows. First, experimental paradigms, data acquisition process, and analysis techniques are described. Next, results are presented and discussed.

## 3.2 Methodology

### 3.2.1 Experimental Paradigms and Data acquisition

Five right-handed subjects (aged  $27.2 \pm 5.1$  years) participated in this study. All subjects provided written informed consents approved by the Georgetown University Institutional Review Board prior to the experiments. They had self-reported normal hearing and normal vision (corrected in one case).

For each participant, both tasks were completed in one session lasting about two hours. Two versions of the oddball paradigm, a modified visual (Wang et al., 1999) and an auditory (IRAGUI et al., 1993) were used. For the visual task, sequences of three different stimuli (shown in Figure 3-1) were presented. Each stimulus was presented for 50 ms, with inter-trial interval (ITI) of 1000-2000 ms. The plus sign image (Figure 3-1-a) was designated as a target stimulus with the appearance probability of 15%. Two other images appeared as frequent (Figure 3-1-b) and infrequent (Figure 3-1-c) non-target stimuli with the probability of 60% and 25%, respectively. Overall, 45 target and 250 non-target stimuli were presented. Subjects were asked to press a button when a target stimulus appeared on the screen.

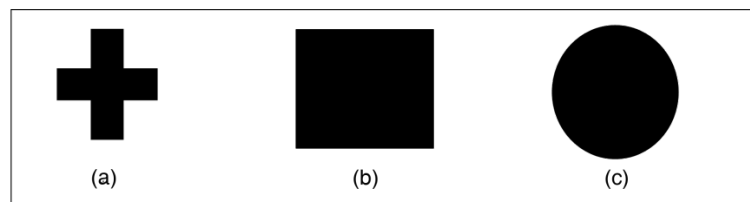


**Figure 3-1 (a) Target (b) non target frequent (c) and non-target infrequent stimuli**

For the auditory oddball task, the auditory stimuli were presented for 50 ms in duration with an ITI of [1000-2000] ms. The stimuli were pure tones of 1000 Hz (non-target) and 2000 Hz (target) in frequency. The target stimulus was presented with probability of 15% with an overall of 45% targets versus 250 non-target stimuli.

### 3.2.2 EEG data acquisition and preprocessing

Brain potentials were recorded using 128-channel EEG system (Electrical Geodesic, Inc., Eugene, OR). The signals recorded from each channel were first visually examined for motion artifacts. Single trials impacted by motion were identified and removed from further analysis. The signal quality in few channels was found to be poor (possibly due to the dryness of the sensors during the recording). These channels were replaced by the average of their neighboring channels. For every participant, average ERP waveforms for target stimuli-related trials of both tasks (visual/auditory) were computed. To filter the physiological artifacts, the signals were high pass filtered at 1 Hz. Other major artifacts related to eye blink or muscle activities were then removed by employing the Independent Component Analysis (ICA) (Hyvärinen and Oja, 2000) technique.

ICA aims at decomposing a linear mixture of measured EEG signals into the contributing sources, with the assumption that the sources are statistically independent. Since artifacts and signals of physiological sources are expected to be independent, the ICA algorithm can be used to separate them. If  $\mathbf{X}$  is a set of  $n$  measured EEG signals,

and element  $a_{ij}$  in matrix  $\mathbf{A}$  specifies the contribution of source  $s_j$  in matrix  $\mathbf{S}$  to the signal  $x_i$ , one can write:

$$\mathbf{X} = \mathbf{AS}. \quad (1)$$

To retrieve the source signals, the algorithm looks for maximum independency and estimates the unmixing matrix  $\mathbf{W}$ , where  $\mathbf{W} = \mathbf{A}^{-1}$ . As a result, each signal source,  $s_i$ , can be defined as:

$$s_{ij} = w_{i1}x_1 + w_{i2}x_2 + \dots + w_{in}x_n, \quad (2)$$

where  $w_{ij}$  specifies the weighted contribution of  $x_i$ . To identify which of the estimated independent components are in fact the artifacts, an activity map localizing the contribution of each channel ( $w_{ij}$  coefficients) was plotted for each source. For example, for the components corresponding to eye blinks, channels placed closer to the eye presented strong contributions. After identifying the artifacts' components, they were removed, and the signal matrix was reconstructed. Signal preprocessing, including data visualization, filtering, and ICA analysis were performed in Matlab using the EEGLAB toolbox (Delorme and Makeig, 2004).

### 3.2.3 ERP Segmentation

Both oddball tasks involved target and non-target stimuli. For this study, only epochs corresponding to the target stimuli were extracted and averaged. Epoch length

was 1000 ms intervals (100 ms prestimulus and 900 ms poststimulus). To track possible changes in the functionally connected regions during the execution of each task, the ERP signals were segmented to a number of shorter temporal windows. Segments were obtained by extracting portions of the ERP signals where a number of well-studied ERP components were expected to be evoked. Selected temporal windows for the visual task were P100, N100, N200, and P300, with the expected latency windows of [50-190], [50-190], [150-300], [250-500] ms, respectively. For the auditory task, the same temporal windows were used except for the P100 and N100 intervals, which were shortened to [80-190] and [85-190] ms, respectively. All the above mentioned intervals were selected based on the previously reported time windows for the corresponding ERP components (Alexander et al., 1995; Brown et al., 2007; Folstein and Van Petten, 2008; Itagaki et al., 2011; Kayser and Tenke, 2006; Kayser et al., 1998).

### 3.2.4 Employing DTW and QT clustering

To capture functional connectivity during the execution of both oddball tasks, for every segment of the 128 recorded EEG signals, DTW algorithm was applied and a  $128 \times 128$  similarity matrix was constructed.

Automatic identification of the most similar-behaving channels during various ERP components was carried out by the QT algorithm (see chapter 2). This algorithm was initially developed for the analysis of gene expression data (Heyer et al., 1999). As explained in chapter 2, for every segmented signal, a similarity matrix was computed through the DTW process. The QT algorithm begins with considering each of the 128 channels as a single cluster. In the next step, each cluster is expanded by adding channels

with distance from the given cluster (taken from the similarity matrix) below a certain threshold set by the user. Once this is done for all clusters, the most populated cluster is retained and others are discarded. The same procedure is repeated for the discarded channels until either all channels are clustered, or the largest cluster does not pass the user-defined “minimum number of points” criteria.

For each participant, applying the QT clustering algorithm on the segmented EEG signals resulted in the identification of the channels (brain regions) that, based on the DTW criteria, were functioning similarly during the corresponding time interval.

Figure 3-2-a illustrates the color-coded clustering results (on a 2D 128-sensor map) applied to the EEG signal within the time window [50-190] ms for one of the subjects. The representative temporal signals for each cluster are plotted in Figure 3-2-b. For each cluster, the solid line corresponds to the average value of the signals of all the channels in that cluster, and the dash lines represent the standard deviation of the signals. It can be seen that in this temporal window, the electrodes placed over the posterior region show a similar positive-going ERP component (shown in green), whereas the electrodes located at other regions exhibit different behavior (shown in red and black).

As mentioned in the previous section, to cluster the data, QT clustering requires a user defined threshold value, which corresponds to the similarity level between the signals in each cluster. Setting a threshold value, which results in clusters with the most analogous activity pattern, can be a challenging task: a low threshold value may result in large clusters containing channels with distinct neuronal activities, while a high threshold value might result in a large number of smaller clusters. Several threshold values for each

subject were considered, and those values that resulted in clusters with a high intra-cluster similarity (a small standard variation for the cluster-average signal) and a low inter-cluster similarity (distinct activity patterns for cluster-average signals) were selected.

Another challenge in the group analysis was the variations in the head shape and size across subjects, as these variations resulted in slightly different electrode positions across subjects. To avoid inter-subject variations in the spatial distribution of brain activity, only the activation regions, which were common in all the subjects were considered.

For each EEG segment, the group analysis involved finding the clusters that were spatially common across all the subjects. The clusters were selected if their corresponding ERP signals were consistent with the expected activity for the selected temporal window. As a result, the region identified as functionally connected was a subset of the corresponding ERP activity map for the given temporal window.

Figure 3-3 presents the group analysis results showing the 3D activation maps of functionally connected regions for multiple segments of both the auditory and the modified visual oddball tasks. The averaged and the standard deviation of the corresponding ERP waveforms (for one of the subjects as an example) are also plotted for each component. The red area on the scalp demonstrates the identified functionally connected regions whereas the yellow strip around this area determines the boundary of that region. Using the proposed technique for the auditory task, functionally connected regions corresponding to all the four designated time intervals were identified. For the

visual task, the functionally connected regions were identified for three of four designated time intervals.

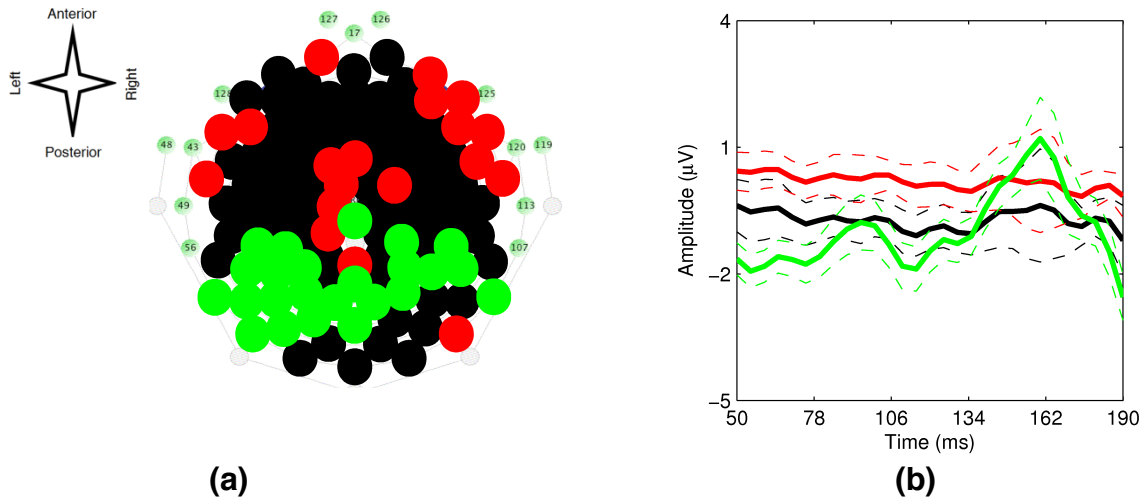


**Figure 3-2 (a) 2D map for functionally connected regions over the time interval of [50-190] ms shown by green, black, and red colors, (b) for each cluster, a cluster-representative signal obtained by averaging ERPs over all the channels (solid line), and its corresponding standard deviations (dash lines) are plotted.**

### 3.3 Clustering Performance Evaluation

In this section, the performance of the QT clustering algorithm is evaluated. Since there was no external information regarding the potential clustering structure, an unsupervised approach for measuring the performance of the clustering is being used. The performance of the clustering algorithm was determined by measuring the compactness of the clusters (cluster cohesion), as well as cluster separation (isolation). Cluster cohesion suggests how closely the ERP signals in a single cluster are, whereas cluster separation determines how well separated a cluster is from other clusters.

A commonly used method that takes into consideration both cluster cohesion and cluster separation is called silhouette coefficient (Tan et al., 2006b). To calculate this coefficient, first the average DTW distance of the  $i^{\text{th}}$  ERP signal to all other ERP signals in its own cluster ( $w_i$ ) is computed. Then, for the  $i^{\text{th}}$  ERP signal, the distance to the closest cluster ( $r_i$ ) is determined. The silhouette coefficient for the  $i^{\text{th}}$  ERP signal is then computed by the following equation:

$$\text{silhouette}_i = (r_i - w_i) / \max(r_i, w_i). \quad (4)$$

The silhouette coefficient value for every ERP signal would vary between -1 and 1. Overall, a nonnegative value for the silhouette coefficient is desirable. This may be verified from (4), where the negative value corresponds to a case where the average distance of an ERP signal in a cluster from other members of the cluster is larger than its distance from members of other clusters. Furthermore, a positive silhouette coefficient value ( $r_i > w_i$ ) suggests that the ERP signal is more similar to the members of its own cluster as opposed to the members of other clusters. In particular, values closer to 1 ( $r_i \gg w_i$ ), relate to improved performance for the clustering task.

The average silhouette coefficient of a single cluster (representing the functionally connected regions) for each subject was determined by averaging over silhouette values of all the cluster members. Next, computed silhouette coefficient values for the selected cluster across subjects

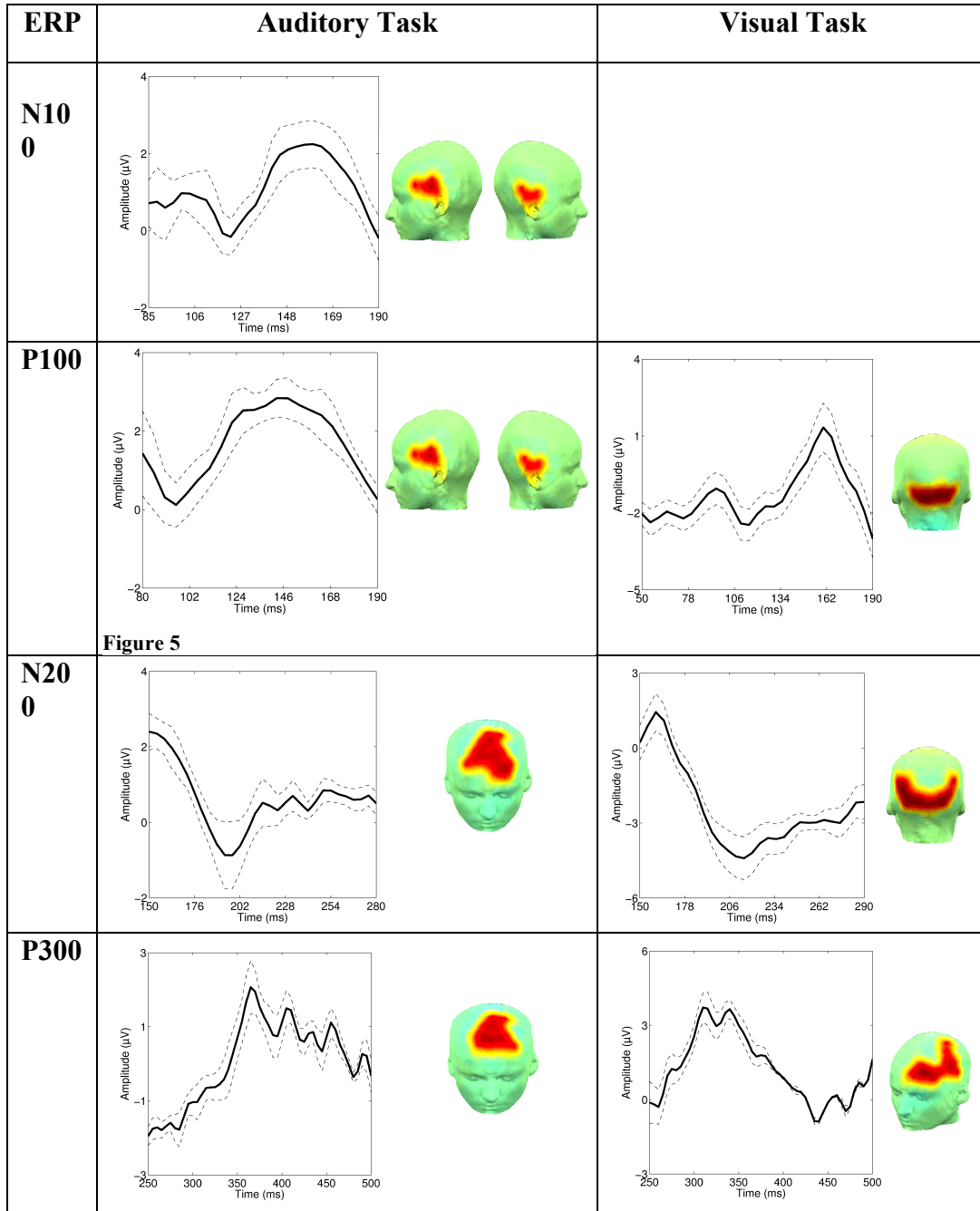


**Figure 3-3** ERP signal and its corresponding 3D map of the functionally connected regions distributed over the scalp for both auditory (left column) and visual (right column) tasks. The red region over the scalp demonstrates the identified functionally connected regions across all subjects whereas the surrounding yellow strip determines the boundary of the region.

**Table 3-1 Average silhouette coefficient value corresponding to functionally connected regions of figure 3-3. Silhouette coefficient value varies between -1 and 1 whereas a positive silhouette coefficient value suggests that the ERP signal is more similar to its own cluster members as opposed to members of other clusters. Values closer to 1 correspond to improved performance for the clustering task.**

| <b>Component</b> | <b>Silhouette coefficient/Auditory task</b> | <b>Silhouette coefficient/Visual task</b> |
|------------------|---|---|
| N100             | 0.87  |   |
| P100             | 0.90  | 0.92                                      |
| N200             | 0.86  | 0.90                                      |
| P300             | 0.91  | 0.89                                      |

were determined by averaging the cluster's silhouette coefficient of all subjects. The results are summarized in Table 3-1.

It has been found in (Rousseeuw and Kaufman, 1990), that an average silhouette coefficient greater than 0.5 indicates reasonable partitioning of data whereas values less than 0.2 suggest poor partitioning of the data. As can be seen in Table 3-1, the silhouette coefficient for each cluster suggests that a precise partitioning of the data has been performed. In other words, the ERP signals corresponding to a functionally connected region have shown a pattern of activity that are strongly similar to each other, and are well distinct from the ERP signals belonging to other regions.

### 3.4 Investigating the Identified Functionally Connected Regions

The early evoked potentials, such as the P100 and N100 components, are dependent on the stimulus type (auditory or visual), and are assumed to be generated in the primary auditory or visual cortices, respectively (Herrmann and Knight, 2001) . In contrast, the later ERP components, such as P300, are independent of the stimuli type and

their sources are localized outside the primary sensory cortices (Katayama and Polich, 1999; Polich, 2007) .

The scalp topography of the functionally connected regions obtained by the proposed technique (Figure 3-3) in reference to the well-established ERP components complies with the aforementioned expected scalp distribution of brain activation. For the auditory task, the scalp topography of the functionally connected regions during N100 and P100 components within the bilateral temporal lobes suggests the involvement of the primary auditory cortex. The region of increased connectivity during the N200 component appeared to be within the frontocentral part of the scalp. This result is consistent with the previous reports for the N200 scalp topography (Alho, 1995; Folstein and Van Petten, 2008; Patel and Azzam, 2005). The frontocentral contributed in forming the functionally connected regions during the P300 temporal window, which is in line with the previous studies (Bledowski et al., 2004; Brown et al., 2007; Katayama and Polich, 1999; Patel and Azzam, 2005).

For the visual task, during the early P100 component ([50-190] ms), functionally connected bilateral regions were revealed over the visual cortex. The area of increased functional connectivity did not change significantly for the temporal window of the N200 component ([150-280] ms). Significant connectivity was observed over the occipital lobe along with a partial involvement of the parietal lobe. This is consistent with the previous reports, which have identified sources of the N200 component within the parietal and more posterior areas (Folstein and Van Petten, 2008; Ogura et al., 1991). The scalp map

of the functionally connected regions during the P300 component [250-500] ms shows a change from the posterior to the frontocentral distribution.

The captured spatio-temporal dynamic changes in the functionally connected regions during the execution of the oddball tasks provide evidence that the task-related functional connectivity follows a dynamic pattern, and is not bounded to a static set of brain regions. This temporal dynamic in the functional connectivity pattern at time intervals of 100 ms duration was captured. Naturally, the method can work at shorter time intervals if it is of interest.

To compare the proposed technique with the commonly used correlation technique, functionally connected regions for the auditory tasks using both the DTW and the cross-correlation methods are compared by applying the techniques on the full-length signal. Then QT clustering was applied, functionally connected regions that were common across all subjects were identified.

Figure 3-4-a shows the functionally connected regions captured by DTW when applied to the full-length signal. As it can be seen, the functionally connected regions corresponding to the N100 and P100 components (which were revealed by the proposed segmentation approach as seen in Figure 3-3) were not detected with this approach. Full-length signal analysis only identified the frontocentral part of the brain as the functionally connected region. Note that the analysis on the segmented signal for the P300 component had identified a comparable region (with a broader spatial distribution). Results for the cross-correlation analysis on the full length signal are shown in Figure 3-4-b. Similar to the DTW method, the cross-correlation technique also revealed the frontocentral part as

the region of connectivity (slightly smaller in size compared to the DTW) and also was not able to capture the functionally connected regions corresponding to the P100 and N100 as was obtained when considering segmentation.

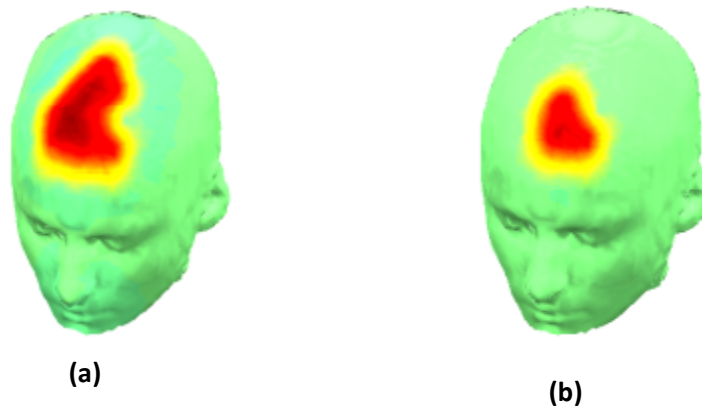


**Figure 3-2 3D maps of functionally connected regions obtained by two similarity techniques over the full length signal: (a) DTW and (b) cross-correlation.**

As seen in Figure 3-4, compared to cross-correlation, DTW has identified a larger area for functionally connected regions. This can be explained by the fact that unlike cross-correlation, DTW also considers the nonlinear alignment of the signals. Therefore, the larger frontocentral area (revealed by the DTW) could be an indication of the brain regions with nonlinear similarity behavior.

### 3.5 Summary of Chapter 3

The proposed approach of segmenting the EEG signals into multiple temporal windows, followed by identifying the functionally connected regions (by employing DTW and clustering techniques), enabled tracing the brain interactions during the execution of both oddball tasks. Four temporal windows, ranged from early stages of the ERP (50-190 ms for visual and 80-190 ms for auditory tasks) to later intervals (250-500 ms) were considered for this study.

The functionally connected regions during the execution of the auditory task were revealed in two major areas: the temporal lobe (during the early ERP component) and the frontal-parietal observed with the involvement of occipital (during the early ERP component) and occipital-parietal and frontal lobes (the later ERP component). Overall, it seems that the functionally connected regions during the early poststimulus periods tend to vary systematically with the physical modality of the stimulus, whereas the later ERP components vary in relation to the higher-order processing mechanisms of the brain that become activated later in response to the stimulus.

It should be emphasized that in this study, when looking for functionally connected regions, only identifying the regions that were similarly “*activated*” (showing similar positive/negative ERP components) were of interest. However, the technique is not bounded to activation signals, and can be used to reveal the functionally similar “*behaving*” regions in the broader sense. For example, the technique can be used to trace the regions of the brain where there are no activations during the execution of the task.

The proposed approach enables tracing the task-based functional connectivity over the scalp, and has the potential to become a useful tool for research in the field of cognitive neuroscience. It was shown that the proposed technique can identify functional connectivity in a more accurate way compared to other existing techniques. It is expected that in healthy individuals, every task can have a unique dynamic functional connectivity pattern which might differ from that of patient population. Comparing such dynamic patterns between the two groups could further help clinical investigators to identify the underlying impairments of brain functional connections in the patient groups.

## **4. Relative Brain Signature (RBS):**

In this chapter, a novel neuroimaging time series feature extraction technique, relative brain signature (RBS) is developed. This technique uses orthogonal subspace projection to transform a set of time series associated to data point (e.g. set of EEG time series corresponding to a subject) into a new coordinate system. The proposed technique provides effective dimensionality reduction, which is crucial for neuroimaging data such as EEG with high temporal resolution. The proposed technique was named relative brain signature as the values in the transformed space quantify the relative association of every single time series to a class. Another unique characteristics of this technique is that it relies on the a priori information corresponding to a class, therefore, is feasible for clinical studies where databases corresponding to a class of certain disorder are available.

### **4.1 RBS a Multichannel and Reference-based Feature Extraction Technique**

It was discussed in chapter 1 that the commonly used multichannel feature extraction techniques for neuroimaging time series obtain discriminative information from individuals' signals by treating every signal corresponding to a single channel independently and do not to consider the potential correlation among the channels (single-channel analysis). Furthermore, traditional neuroimaging time series feature extractions are not capable of incorporating individuals' class information into the analysis (blind analysis). I proposed a time series feature extraction technique that treats

neuroimaging time series collected from a multichannel modality, jointly (multichannel analysis) and takes the class association of the individuals into the feature extraction procedure (reference-based).

## 4.2 Relative Brain Signature (RBS)

Suppose that there are  $n$  individuals from  $r$  populations (or classes). Then, the neural response collected from a single site for every subject is a  $d$ -dimensional time series. Also, suppose the neural response is collected from  $m$  different sites. The aim of the proposed method is to map every time series to  $r$  scalar values whereas each scalar value determines the relative association of the subject's  $i^{th}$  channel's time series to the population  $j$ . For  $1 \leq l \leq n$ ,  $1 \leq j \leq r$ , and  $1 \leq i \leq m$ , let

- $s_l$  denote the  $l^{th}$  individual,
- $P_j = \{l: s_l \text{ belong to } j^{th} \text{ population}\}$
- $l^{th}$  denote the  $\}, n_j = |P_j|$ ,
- $e_i^l = (e_{i1}^l, e_{i2}^l, \dots, e_{id}^l)^T \in \mathbb{R}^d$  be the  $i^{th}$  time series of  $s_l$

### 4.2.1 Population-Specific-Dataset (PSD)

The first step of the proposed methodological approach is to construct the Population-Specific-Dataset (PSD). PSD is the set of time series where every element is a representation for a certain channel site. This representation can be obtained in two way: a) from the available data (e.g. by averaging the corresponding time series from the subjects for the given population) or b) from a reference data collected in the laboratory a

priori. Using the averaging for representing a channel site, the time series representation,  $f_{ij}$ , and the PSD can be expressed as follows, respectively:

$$\text{For } 1 \leq i \leq m \text{ and } 1 \leq j \leq r, f_{ij} = \frac{1}{n_j} \sum_{l \in P_j} e_i^l$$

$$PSD_j = \{f_{1j}, f_{2j}, \dots, f_{mj}\}$$

#### 4.2.2 Population-Specific-Subspace (PSS)

The subspace spanned by the elements of the PSD provides generic brain functionality for the corresponding population over certain areas of the brain. The set of these subspaces generated by every element of the PSD is referred to as Population-Specific-Subspace (PSS).

Consider the subspace (Halmos, 1947) spanned by a channel site representation,  $f_{ij}$ ,

$$S_{ij} = \text{span}(f_{ij}) = \{cf_{ij} : c \in \mathbb{R}, f_{ij} \in PSD_j\}$$

then the set of all of these subspaces for the population  $j$  is defined as:

$$PSS_j = \{S_{ij} : 1 \leq i \leq m\}$$

The subspace  $S_{ij}$  is paired with another subspace called orthogonal complement subspace (Halmos, 1947)

$$S_{ij}^\perp = \{g : f \cdot g = 0 \text{ and } f, g \in \mathbb{R}^d \text{ and } f \in S_{ij}\}. \quad (3)$$

This subspace encompasses elements that are orthogonal and dissimilar to the elements of  $S_{ij}$ . Thus,  $S_{ij}^\perp$  can be utilized to provide a generic representation for elements that belong to class  $j'$  ( $1 \leq j \leq r$  and  $j' \neq j$ ) with the maximum dissimilarity to the current elements of  $PSS_j$ .

### 4.2.3 Orthogonal Complement Projection

To assess the dissimilarity of the individual's time series to a class, every time series of the subject is projected onto its corresponding PSS element's orthogonal complement subspace. Hence, the second step of the proposed approach for the subject's  $i^{th}$  channel time series, and population  $j$  is to project the time series onto the  $S_{ij}^\perp$ .

Suppose that  $\{u_1, u_2, \dots, u_k\}$  linearly independent set of vectors in  $\mathbb{R}^d$  and let  $W =$

$\text{span}(\{u_1, u_2, \dots, u_k\})$ . Let  $A = \begin{bmatrix} | & | & | \\ u_1 & u_2 & \dots & u_k \\ | & | & | \end{bmatrix}$ . It is well known that the projection matrix

$P_W$  onto  $W$  is given by

$$P_W = A(A^T A)^T A^{-1}.$$

In particular,

$$P_{\square_{ij}} = \frac{f_{ij} f_{ij}^T}{\|f_{ij}\|^2} \text{ and } P_{S_{ij}^\perp} = I - \frac{f_{ij} f_{ij}^T}{\|f_{ij}\|^2},$$

where  $I$  is the  $d$ -dimensional identity matrix and  $\|\cdot\|$  corresponds to the norm-2 of the vectors. The projection of the  $i^{th}$  channel time series,  $e_i^l$ , onto  $S_{ij}^\perp$  is obtained by

$$(e_i^l)^\perp = P_{S_{ij}^\perp} e_i^l.$$

### 4.2.4 Quantifying the Relative Association to Classes

The quantify the similarity of the  $e_i^l$  to the population  $j'$  ( $j' \neq j$ ), the cosine similarity between the  $(e_i^l)^\perp$  and  $f_{ij'}$  is computed as

$$o_{ij'} = \frac{\mathbf{f}_{ij'}^T}{\|\mathbf{f}_{ij'}\|} \times \frac{(e_i^l)^\perp}{\|(e_i^l)^\perp\|}.$$

Value of  $o_{ij'}$  that varies between -1 and 1, quantifies the similarity of the individual's  $i^{th}$  time series to the generic representation of the  $i^{th}$  element of the  $PSD_{j'}$ .

An RBS vector with respect to the population  $\mathbf{j}'$  is composed of  $m$   $o_{ij'}$  ( $i = 1, 2, \dots, m$ ) components.

### 4.3 Summary of Chapter 4

A novel population-based feature extraction technique, RBS, for neuroimaging time series data captured from subjects within populations (classes) with functionally distinctive neuronal activity is developed. This technique attempts to generate a feature vector for subjects to quantify their relationship to the given populations. Unlike the common feature extraction techniques that are not designed to consider the potential intra- and inter-population relationship among the subjects, RBS takes into analysis such information. Considering such relationships among subjects enables obtaining biomarkers from brain activity associated to a certain population. These biomarkers are the features that are shared among all the subjects from a certain population.

The proposed technique is designed to perform a multichannel time series analysis in the settings where the individual data sample includes a set of time series. Unlike traditional time series feature extraction techniques, RBS does not analyze every time series without considering the reference (class association) of the time series. Given a neuroimaging dataset collected from different sites of the brain and formatted as multi-

time series for every individual, RBS can be utilized to perform feature extraction and efficient dimensionality reduction. RBS is developed based on the hypothesis that there are generic subspace representations for the collected time series from the distinct brain sites of the individuals of a specific population.

Figure 4-1, illustrates the general scheme of the RBS feature extraction technique. For given neuroimaging time series from the two population of subject, first the two PSD are computed for each group of subjects (figure 4-1 a). For every channel site of a population, its subspace and its orthogonal complement subspace is constructed. Then, subject's time series is projected onto the orthogonal complement subspace of the population (Figure 4-1 b). Finally, subject's RBS feature vectors that reveal the level of association of a subject to a specific population are computed within the projected subspaces (Figure 4-1 c).

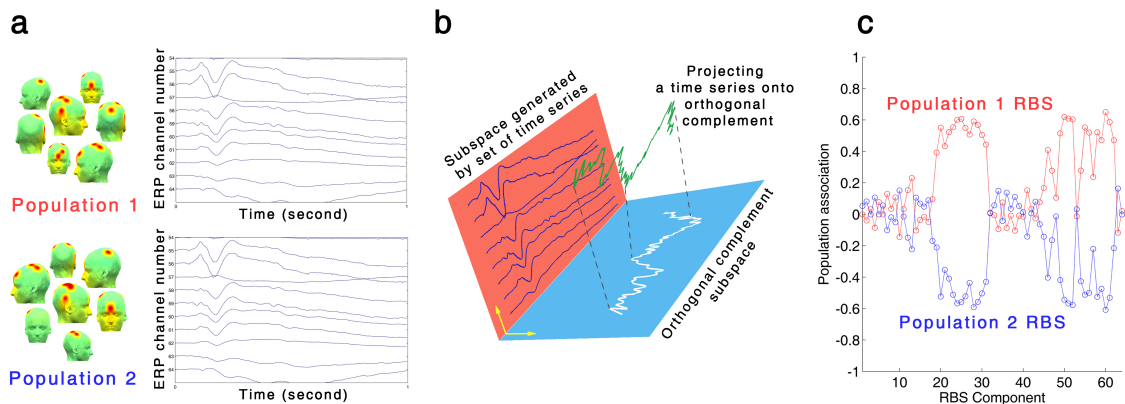


Figure 4-1 For the given neuroimaging time series from the two population of subject, first the two PSD are computed for each group of subjects (a). For every single time series of a subject is projected onto the orthogonal complement subspace of the population (Figure 4-1-b). Finally, subject's RBS feature vectors that reveal the level of association of a subject to a specific population are computed within the projected subspaces (Figure 4-1-c).

## **5. Functional Biomarker Identification Using RBS**

In this chapter, RBS is applied on an EEG data set of 77 abstinent alcoholics and 43 control subjects. To characterize subjects' relationship to the alcoholic and control populations, one RBS vector with respect to the alcoholic and one with respect to the control population is constructed. The applicability of the extracted RBS vectors in identifying functional biomarkers over the brain of alcoholics is evaluated. To achieve this goal, a classification algorithm is used to categorize subjects into alcoholics and controls classes using the RBS feature extraction technique.

### **5.1 EEG and Alcoholic Studies**

To capture brain potential impacts of long term alcohol consumption, analysis of ERP signals has been bounded to the certain temporal windows of the signals (such as P300 that occurs 300-500 ms after the stimulus onset)(Begleiter and Porjesz, 1999) or transforming signals to the frequency domain to explore specific frequency ranges(Rangaswamy et al., 2002). These studies attempt to investigate characteristics of ERP's amplitude fluctuations (Bostanov, 2004) , power spectral density(Musha et al., 1997), or time-frequency analysis(Wang et al., 2004), to extract informative and discriminative features. A major challenge in all the aforementioned EEG data analysis is the high dimensionality of the dataset. The high dimensionality of the EEG data adds more complexity, increases the computational time, and complicates the data analysis due

to the phenomenon called “curse of dimensionality” (Lotte et al., 2007b). Although the aforementioned feature extraction techniques reduce the dimensionality of the EEG signals, yet the feature space corresponding to a single subject is relatively high due to the large number of signals recorded from the subject’s brain. Therefore, EEG feature extraction is typically followed by a channel selection procedure (Ansari Asl et al., 2007) that selectively discards signals corresponding to certain channels of the subjects’ EEG signals. Furthermore, the common EEG feature extraction techniques are not designed to include attributes regarding the subject’s population association into their process of feature extraction and also cannot perform multichannel data analysis.

In this work, the RBS neuroimaging time series feature extraction technique that was introduced in chapter 4 is utilized as a features extraction technique to provide an effective dimensionality reduction for EEG signals. RBS does not require the typical EEG channel selection procedure and accounts for all the ERP signals. Furthermore, unlike common feature extraction techniques that do not consider subject’s population association in the procedure of feature extraction, RBS technique obtains information from subjects’ ERPs by investigating their relationship to the given populations of the study. RBS combines vector space analysis and orthogonal subspace projection to generate the feature vector that describes the relationship between a subject and populations. The effectiveness of utilizing RBS in identifying functional biomarkers related to alcoholics is also investigated. The identified spatially localized biomarkers will be illustrated as a topographic map over the scalp.

## 5.2 Experimental Paradigms and Data Acquisition

RBS was assessed using an EEG dataset collected from two populations of alcoholic and control subjects. This data was collected by the Neurodynamics Laboratory, SUNY Downstate Medical Center, (supported by NIH grants AA05524 and AA026686) from a group of alcoholics and control subjects and was first published in (Zhang et al., 1995). The control group consisted of 43 right-handed male (the dataset originally contained 45 subjects of which two subject data were excluded due to file errors and empty trials) subjects with an age range of 19.4-38.6 years. The alcoholic group consisted of 77 males with an age range of 22.3-49.8 years. Alcoholic subjects were initially diagnosed with alcohol abuse or dependence by the intake psychiatrist according to the Diagnostic and Statistical Manual of Mental Disorders-III (DSM-III)(Angold and Costello, 1993) criteria as well as more advanced diagnosis tools. Also a mini mental status examination (Bertolucci et al., 1994) was conducted on all subjects and no memory deficit was observed. The alcoholic subjects had a history of heavily drinking for a minimum of 15 years. At least 30 days before the start of the experiment alcoholic subjects were hospitalized and fully detoxified.

Subjects were shown a series of object pictures chosen from the 1980 Snodgrass and Vanderwart picture set (Snodgrass and Vanderwart, 1980), Figure 5-1. Two picture stimuli appeared in succession with a 1.6 s fixed interstimulus interval. The duration for the first (S1) and second (S2) picture stimulus in each test trial was 300 ms where the

interval between each trial was fixed to 3.2 s. All the pictures were paired either as matching or non-matching conditions. For the matching condition, subjects were presented identical stimuli (similar S1 and S2) and in the non-matched condition S2 was different from S1. Subjects were required to press a mouse key in one hand for the matching condition and press the mouse key in another hand for the non-matching condition. The data was captured by an EEG device with 64 electrodes of which two were mounted for Electrooculography (EOG) and one nose electrode. These three channels were excluded as well as one more channel that had been used for grounding the subjects and only used data from 60 electrodes. More information regarding the data collection procedure can be found in reference (Zhang et al., 1995).

### 5.3 ERP Feature Extraction Using RBS

As explained in chapter 4, PSD is composed of the elements that are computed by averaging the corresponding ERPs from the subjects within the population. The subspace spanned by the elements of the PSD provides generic brain functionality for the corresponding population over certain areas of the brain.

For every subject, an ERP dataset is constructed by averaging the EEG signals corresponding to every channel across all different trials of the experiment. Then for every population, a PSD, namely Alcoholic-PSD and Control-PSD, is constructed. Every element of the PSDs, Alcoholic-PSD and Control-PSD, are computed by averaging the corresponding ERPs from the subjects in the alcoholic and control populations, respectively. The Alcoholic-PSD and Control-PSD is composed of 60 elements. The

subspace spanned by an element of PSD (see chapter 4) is considered. This subspace provides a generic brain functionality for a specific region of the brain. The subspaces generated by Alcoholic- and Control-PSDs are referred to as Alcoholic-PSSs and Control-PSSs, respectively.

The proposed RBS feature extraction technique obtains information from subjects' ERPs by considering their relationship to both alcoholic and control populations. First, the subject's ERP is projected onto the orthogonal complement subspace (see Methods section) associated to the Alcoholic- and Control-PSS. The orthogonal complement subspace of the Alcoholic-PSS (Control-PSS) is a subspace in which elements illustrate distinctive functionality from the elements of the Alcoholic-PSS (Control-PSS). Hence, projection of subject's ERP onto the orthogonal complement subspace related to Alcoholic-PSS or Control-PSS contains transformed ERP components that signify subject's ERP association to the alcoholic or control populations. Each ERP is projected onto the orthogonal complement of the Alcoholic-PSS and onto the orthogonal complement subspace of the Control-PSS. To quantify the similarity of the projected ERP to the opposite population, the cosine similarity (see Methods section) between the projected ERP and the corresponding element from alcoholic and control population's PSS element is computed. These two resulting scalars explain the association of an ERP to the alcoholic and control populations. Therefore, by applying this procedure to all of the 60 ERPs two vectors of dimension 60 corresponding to the alcoholic and control population, namely Alcoholic-RBS and Control-RBS are generated. These vectors are an ordered collection of 60 elements, which are called components. A component of the

RBS vector depicts the similarity of an ERP associated to an area of the brain to the alcoholic or control population.

RBS vectors for an alcoholic and a control subject are illustrated in Figure 5-2 by the dashed line that connects the computed RBS vector components for an alcoholic (Figure 5-2-a) and a control subject (Figure 5-2-b). The component values, which quantify the connection between an ERP and the alcoholic or control populations, are shown in blue and red, respectively. The RBS component value closer to 1 indicates a stronger association to a certain population whereas smaller positive values and negative values suggest that the corresponding ERP of the subject is weakly associated to a population. It is worth noting that the largest similarity values for the Alcoholic-RBS of an alcoholic subject are expected to be observed among the ERPs originating from the regions with the foremost distinctive functionality due to prolonged alcohol effects.

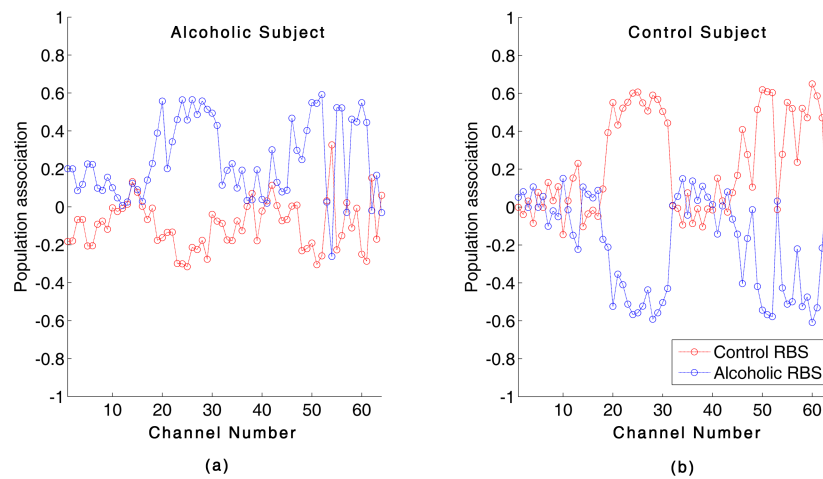


**Figure 5-1 RBS vectors for an alcoholic and a control subject are illustrated. Two RBS vectors for an alcoholic subject and a control subject are shown. The components of the RBS vectors, quantify the association of an ERP waveform and the alcoholic population (shown in blue) or to the control population (shown in red). A positive value closer to 1, for a component of the RBS vectors indicates a stronger association to a certain population whereas smaller positive values and the negative values suggest the corresponding ERP data is weakly associated to a population. In a, majority of Alcoholic-RBS component values are significantly associated to the alcoholic population while for the Control-RBS component values, majority of the ERPs were weakly associated to the control population. In b, Control-RBS component values illustrate a strong relation to the control population while Alcoholic-RBS demonstrates weak association to the alcoholic population.**

#### 5.4 Identifying Functionally Distinct Brain Regions of Alcoholic Subjects

In this section, the areas of the alcoholics' brain with distinct functional activity are identified using the RBS vectors. These areas are detected by exploring the corresponding brain regions associated with the RBS components. Considering that larger component values for the alcoholics' Alcoholic-RBS components are expected to be observed among the ERPs originated from the regions with distinct functional activity. Identifying these components is of particular interest. A set of components for which large association value to the alcoholic population (i.e. large Alcoholic-RBS value) and small association value to the control population (i.e. small Control-RBS values) across alcoholic subjects is obtained. This set of component is associated with a set of electrode

positioned on the areas of the brain with highest contribution in distinguishing between the alcoholic and control subjects. In an attempt to determine these components, a classification procedure is considered.

The classification procedure is composed of 60 classification experiments. For every classification experiment, feature vectors with a certain size are constructed from a set of RBS vector components. Classification accuracy for every classification experiment is computed. The details of the  $i^{th}$  ( $i = 1, 2, \dots, 60$ ) classification experiment are explained in the following paragraphs.

For a classification experiment, 2/3 of the alcoholic and 2/3 of control subjects are randomly selected for training purposes and the rest of the subjects are selected for the testing purposes.

### 5.5 RBS Component Selection

To construct the feature vectors, a feature selection approach is considered. Feature selection algorithms in general have two components: a selection algorithm that generates proposed subsets of features and attempts to find an optimal subset; and an evaluation algorithm that determines the performance of a proposed feature subset by returning some measure of goodness to the selection algorithm.

In this work, features are weighted and sorted by using the RBS vector of the alcoholic subjects within the training set, using equation (9),

$$\text{Component}_j = \max_j \left\{ \left( \sum_{k=1}^l \left| \frac{(\text{Alcoholic RBS})_k}{(\text{Control RBS})_k} \right| \right) \right\}, j = 1, 2, \dots, 60, l = 51 \quad (9)$$

where “ $|\cdot|$ ” is the absolute value, and  $l$  is the number of alcoholic subjects from the training set ( i.e. since 2/3 of the alcoholics are used for training the classifier,  $l = 51$  ).

For every subject, the RBS vectors are resampled by keeping their first  $i$  ranked components and discarding the rest of the components' data (i.e. the sampled vectors contain  $i$  elements). Then, feature vectors for every subject are extracted by subtracting the resampled Control-RBS from the resampled Alcoholic-RBS. It is worth emphasizing that the components are ranked and selected according to the RBS vectors of the alcoholic subjects within the training set to avoid the double dipping phenomenon (Kriegeskorte et al., 2009).

To classify the subjects using the constructed feature vectors, Linear Discriminant Analysis (LDA) (Welling, 2005) classification algorithm is employed. The generalization performance of every classification experiment is assessed by random subsampling in which the process of randomly partitioning subjects into training and testing sets is repeated many times (1000 in this study). For every classification experiment, accuracy, specificity, and sensitivity (Pang-Ning et al., 2006) are reported. The overall accuracy, specificity, and sensitivity values for every classification experiment are determined by averaging the accuracy, specificity, and sensitivity values computed for every run of the random subsampling procedure.

In Figure 5-2, performance of the LDA classification algorithm is illustrated where different number of significant components is used to generate feature vectors. A dot in the dot-line of Figure 5-2-a corresponds to the average classification accuracy for a feature vector constructed from certain number of significant components. The dash lines in Figure 5-2-a represent the standard deviation for the computed accuracy. Dots in the red and blue dot-lines in Figure 5-2-b denote the average specificity and average

sensitivity (respectively) for the corresponding significant components used to construct the feature vector. Starting with the first significant component, an accuracy of  $0.67 \pm 0.06$ , specificity of 0.65 and sensitivity of 0.69 are obtained. As it can be seen in Figure 5-3, when the top 11 significant components of the RBS vectors are used to generate the feature vectors, the average accuracy, specificity, and sensitivity increase to their maximum values where the graphs' knee is formed. The highest classification accuracy value when the feature vector is constructed using the first 11 significant components is  $0.78 \pm 0.06$  whereas the highest specificity and sensitivity for the first 11 significant components are 0.74 and 0.79, respectively.

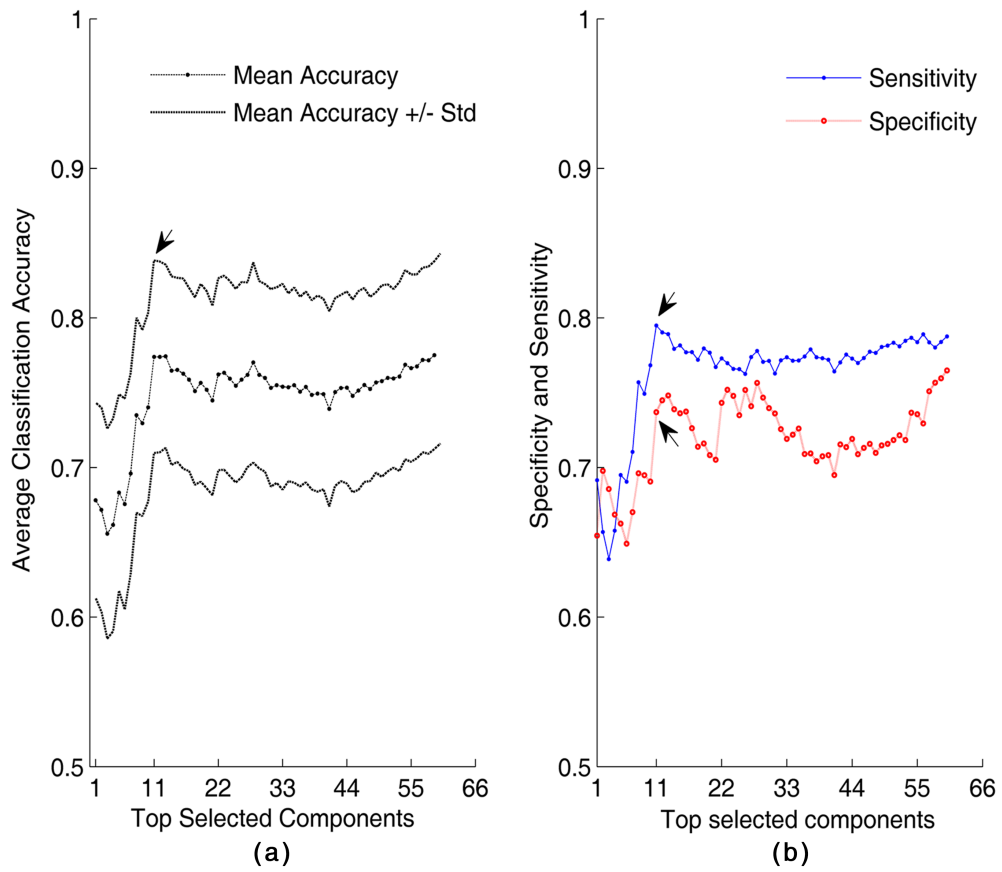


**Figure 5-2 Performance evaluation for LDA classification between alcoholics and control subjects. (a) The x-axis corresponds to different number of significant components used to generate the feature vectors and the y-axis denotes the accuracy. The dot-line corresponds to the average classification accuracy and the dash-lines represent the standard deviation for the computed accuracy. (b) The x-axis corresponds to different number of significant components used to generate the feature vectors. The red and blue dot-lines denote the average specificity and average sensitivity (respectively) for a certain number of significant components used to construct the feature vector**

In Figure 5-3, spatial distribution of the first 11 significant components over the scalp is illustrated using EEGLAB (Delorme and Makeig, 2004). The red area corresponds to the most significant component and the yellow strip around the red determines the boundary of that region.

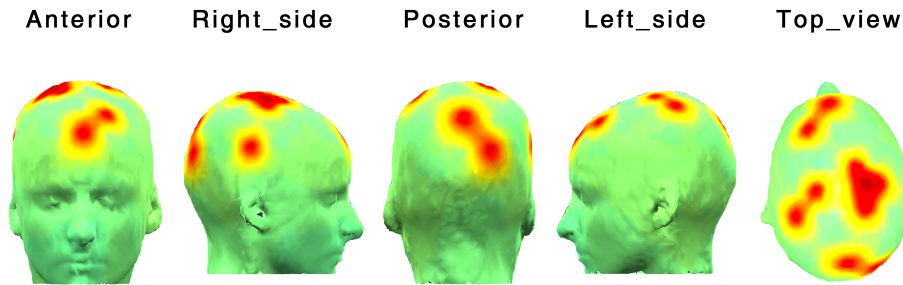


**Figure 5- 3 Different views for the top 11 functionally distinct brain areas between alcoholic and control subject. The red area corresponds to the most significant component and the yellow strip around the red determines the boundary of that region. These areas, with respect to their spatial extent are frontal and anterior frontal, centro-parietal, parieto-occipital and occipital lobes.**

To investigate the consistency of the feature sets that are employed for the classification experiments across the sampling iterations, Sets of components with which feature vectors for the first 11 classification experiments are constructed, are tabulated in. Due to a slight variability in the feature set across the 1000 iterations, the fraction of times that a feature set has been used for a classification experiment is denoted by a percentage value. As it is show in table 5-1, the feature sets selected for every classification experiment across the 1000 iterations are consistent (i.e. majority of the classifications have been performed with the similar set of features) for all the reported classification experiments.

Table 5-1 Sets of EEG channels (RBS components) selected for the first 11 classification experiments across their 1000 sampling iterations.

| <b>Number of components used to construct the feature set</b> | <b>Selected components (EEG channel ID#)</b> | <b>Fraction of selection (in percentage)</b> |
|---|--|--|
| <b>1</b>  | [17]   | 100%   |
| <b>2</b>  | [17,21]                                      | 94%  |
| <b>3</b>  | [17,21,45]                                   | 90%  |
| <b>4</b>  | [17,21,45,48]                                | 90%  |
| <b>5</b>  | [17,21,45,48,38]                             | 90%  |
| <b>6</b>  | [17,21,45,48,38,57]                          | 89%  |
| <b>7</b>  | [17,21,45,48,38,57,5]                        | 89%  |
| <b>8</b>  | [17,21,45,48,38,57,5,52]                     | 88%  |
| <b>9</b>  | [17,21,45,48,38,57,5,52,53]                  | 89%  |
| <b>10</b>   | [17,21,45,48,38,57,5,52,53,29]               | 88%  |
| <b>11</b>   | [17,21,45,48,38,57,5,52,53,29,12]            | 89%  |

## 5.6 Summary of Chapter 5

The proposed feature extraction approach of projecting the ERPs onto the orthogonal subspaces of the control and alcoholic populations has provided accurate details regarding the subjects' original population association. Two 60-dimensional RBS vectors for every subject to characterize the relationship of the subject to the two populations of alcoholic and control were extracted. As Figure 5-2-a illustrates, the Alcoholic-RBS component values for an alcoholic subject signify a strong association with the alcoholic population while majority of the Control-RBS component values of the ERPs, demonstrate a weak association to the control population. In Figure 5-2-b, the

Control-RBS component values for a control subject illustrate a strong link to the control population while Alcoholic-RBS demonstrates a weak association to the alcoholic population. It suggests that the RBS vectors can potentially explain and distinguish the association of the subject to different populations of a study. The RBS vectors were successfully utilized to detect and visualize the functionally distinct regions over brain of alcoholics. Features related to the EEG activity from these regions enabled classification between alcoholic and control subjects gains its maximum accuracy (Figure 5-3-a). In other words, these regions represent the functionally impaired regions of the alcoholics' brain and can be used as biomarkers to distinguish between alcoholic and control subjects. Figure 5-3 provides scalp topography for these regions, which correspond to the first 11 significant components. These areas, with respect to their spatial extent are frontal and anterior frontal, centro-parietal, parieto-occipital and occipital lobes. The distribution of these regions over the scalp indicates that the impact of the alcohol in the cerebral cortex of the alcoholics is spatially diffuse. The largest identified area (the centro-parietal area), engages more regions of the frontal lobe and right hemisphere relative to the left hemisphere that complies with the findings in other studies (Ellis and Oscar-Berman, 1989; Harris et al., 2008; Moselhy et al., 2001; Zhang et al., 1997). The identified regions encompass a set of smaller areas that are known to be affected by ingesting one or two drinks of alcohol by social drinkers(Luchtman et al., 2013). In other words, it seems that impairments caused by one or two (alcoholic) drink consumption by social drinkers targets the same regions of the brain that have are affected in the abstinent alcoholics.

The efficacy of the RBS techniques was evaluated by repeating the process of computing the RBS vector, without projecting ERPs onto the orthogonal subspaces and only quantified similarity of the subject's ERP to the alcoholic and control subspaces. Figure 5.4 shows the vectors composed of these values for an alcoholic subject. For computing similarity vectors, in Figure 5-4-a, ERPs are not projected onto the orthogonal subspaces and only the similarity between a given ERP and its corresponding ERP from Control- and Alcoholic-ERP is computed. As demonstrated in Figure 5-4--a, similar values of association to the populations are obtained across all of the components of the alcoholic- and control- similarity vectors. In Figure 5-4-b, the RBS vectors for the same subject are constructed by projecting the ERPs onto the orthogonal subspaces of the populations and then the similarity is computed. The computed similarity vectors (Figure 5-4-a) are not able to characterize subjects with respect to its original population association in comparison to the RBS vectors illustrated in (Figure 5-4-b).

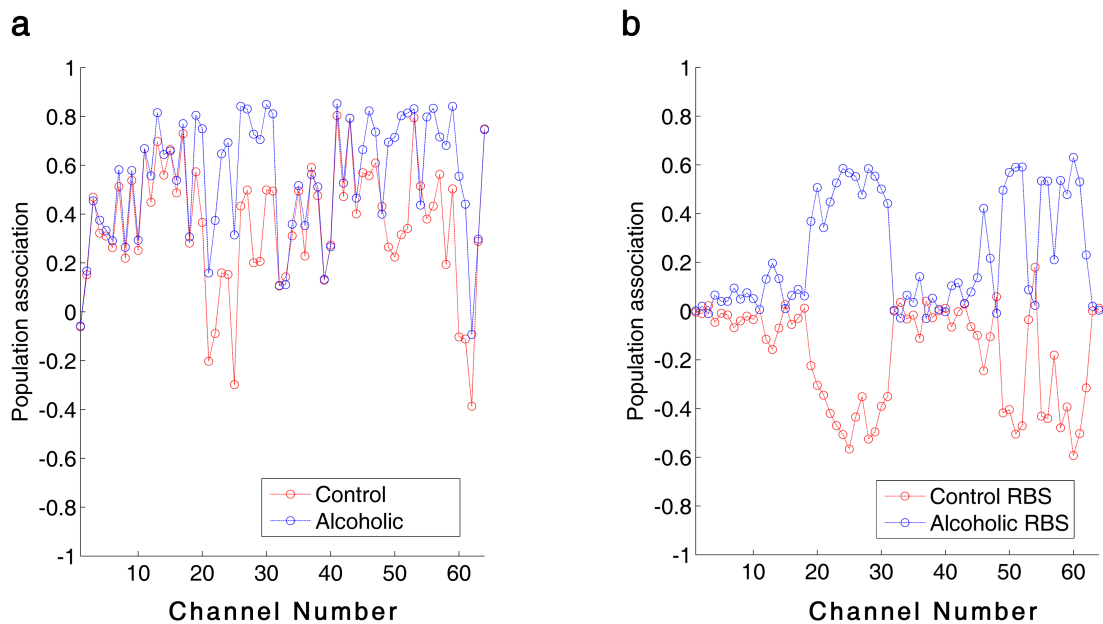


**Figure 5-4 Process of computing RBS vectors without projecting signal onto the orthogonal subspaces and vs. the proposed approach, for an alcoholic subject. (a) Subject's ERPs were not projected to the orthogonal subspaces and only similarity between subject's ERP and its corresponding ERP from Control-PSD and Alcoholic-PSD was computed. As demonstrated in a, very similar values of association to the alcoholic and control populations were obtained across all of the components of the Alcoholic- and Control-RBS. (b) The RBS vectors for the same subject were constructed by projecting the ERPs onto the orthogonal subspaces of the populations and then the similarity was computed. The computed similarity vectors in a were not able to characterize subjects with respect to its original population association in comparison to the RBS vectors illustrated in b.**

This finding verifies that the underlying assumption that the orthogonal complement subspaces of a PSS element provides a generic domain to represent distinctive brain functionality for populations other than the population of PSS. It should be emphasized that in this work, when evaluating population association of a subject, similarities and dissimilarities for the entire period of the experiment were considered and exploring the similarities (or dissimilarities) in the smaller temporal windows were disregarded. However, the proposed technique is not bounded to analysis of the ERPs for a long

period of time and can be used to reveal the potential dynamic pattern of an alcoholic's distinctive areas.

Finally, it is worth mentioning that the approach enables distinguishing between any numbers of populations and is not limited only to two populations. It may also be used for intra-population classification given enough meta-information regarding subjects within a population. In future studies, this issue can be addressed by collecting more information regarding alcoholic subjects' mental and physical health to perform an intra-alcoholics classification experiment.

## **6. Identifying Functional Biomarkers in Human Prefrontal Cortex for Individuals with Traumatic Brain Injury (TBI) Using Functional Near-Infrared Spectroscopy (fNIRS)**

In chapter 6, an approach for 6 is explained. To achieve this goal, a task-related hemodynamic response detection followed by a heuristic search for optimum set of hemodynamic features is introduced. To identify the hemodynamic signals that show task-related hemodynamic activity, trials with negatively correlated oxygenated hemoglobin (HbO) and deoxygenated hemoglobin (HbR) and HbO larger than HbR were considered for analysis. For identifying the optimum hemodynamic features, unlike common single feature analysis for studying TBI and healthy subjects, all the possible combinations of multiple hemodynamic features to compare the TBI and healthy populations were evaluated. Eleven hemodynamic features were extracted from HbO to determine the optimum set of biomarkers. I investigated the effectiveness of the extracted features in separating TBI and healthy subjects by utilizing a machine learning classification algorithm to score all the possible combinations of features according to their predictive power. The identified optimum feature elements resulted in classification accuracy, sensitivity, and specificity of 85%, 85%, and 84%, respectively. The sensitivity value of 85% suggests that TBI subjects have been successfully characterized for the identified biomarkers with reasonable accuracy. A spatio-temporal classification was conducted to identify regions within the PFC that contribute in distinguishing between

TBI and healthy subjects. As expected, Brodmann areas (BA) 10 within the PFC was isolated as the region that healthy subjects (unlike subjects with TBI), showed major hemodynamic activity in response to the High Complexity task. Overall, results indicate that the identified temporal and spatio-temporal features from PFC's hemodynamic activity are promising biomarkers in classifying subjects with TBI.

## 6.1 TBI and PFC

Executive function (EF) involves various complex cognitive processes, such as solving novel problems, generating strategies or sequencing complex actions (Elliott, 2003). Executive dysfunction in subjects with TBI has been reported in (Gioia and Isquith, 2004; McDonald et al., 2002) and is believed to be related to a dysfunctional PFC or disruption in the connection of the frontal lobes and other parts of the brain (McDonald et al., 2002). Poor performance within the PFC of TBI patients, independent of frontal parenchymal lesions, has been reported by researchers (Cazalis et al., 2006; Langfitt et al., 1986; Levin, 1982; Vilkki, 1992).

## 6.2 Functional Near infrared Spectroscopy and Traumatic Brain Injury

Advancement made in functional neuroimaging provide tools needed for the sensitive assessment of functional abnormalities following TBI in various brain regions including the PFC. In particular, functional magnetic resonance imaging (fMRI) of the blood-oxygen-level-dependent (BOLD) signal (Heeger and Ress, 2002), which depicts blood oxygenation changes followed by localized neuronal activity, has been widely used

to characterize the spatio-temporal pattern of brain regional activity in individuals with TBI (McAllister et al., 1999) (McAllister et al., 2001) (Cazalis et al., 2006; Scheibel et al., 2003).

Although fMRI has traditionally been the modality of choice to study brain function of individuals with TBI, but it is relatively expensive, requires specialized and is permanently sited (Amyot et al., 2012). Less expensive and more portable functional neuroimaging modalities such as functional near infrared spectroscopy (fNIRS) (Villringer and Chance 1997; Amyot et al. 2012; Bunce et al. 2013) have been utilized less to study brain function of individuals with TBI. Similar to its fMRI counterpart, fNIRS is capable of capturing local hemodynamic changes over the execution of a functional task. However, compared to fMRI, fNIRS offers lower spatial resolution but provides higher temporal resolution. fNIRS measures continuous change of chromophores in the blood, by sending near-infrared-range light (usually of 700~1000nm wavelength) through light-emitters and detect the diffused reflecting light after interacting with brain tissue by the detectors that are placed a few centimeters away from the emitters. HbO and HbR are the targeted chromophores measured by fNIRS. HbO and HbR signals are formed through successive measurements made over a time interval of an experiment.

There are only a few studies that have utilized fNIRS to evaluate cerebral oxygenation and blood volume alterations during the execution of functional tasks in patients after TBI (Bhambhani et al., 2006; Hibino et al., 2013; Merzagora et al., 2011; Merzagora et al., 2014). These studies have employed very small sample sizes, various

cognitive stimuli, and different analytical techniques. (Bhambhani et al., 2006) used fNIRS to investigate cerebral hemodynamic alterations in the prefrontal cortex in 25 subjects with TBI and 13 healthy control subjects while they performed the handgrip contractions task. It was reported that subjects with TBI demonstrated a significantly lower increase in oxygenation in both left and right dorsolateral prefrontal cortex (DLPFC) (Bhambhani et al., 2006). (Merzagora et al., 2011) examined the differences in the prefrontal hemodynamic activity of 5 TBI subjects and 11 healthy controls and reported significant lower mean HbO values for the subjects with TBI in comparison to healthy control subjects while performing an attention-based task, and suggested that fNIRS could be used to monitor the rehabilitation procedure for the patients with TBI (Merzagora et al., 2011). (Hibino et al., 2013) conducted a study on 9 TBI and 47 healthy subjects to investigate differences between the two populations by analyzing the HbO changes captured from frontal to temporal cortices in response to 9 different cognitive rehabilitation tasks. They documented higher HbO changes for TBI compared to healthy control patients in the medial frontal region and higher left frontal HbO changes were reported for healthy controls in majority of the cognitive tasks (Hibino et al., 2013). (Merzagora et al., 2014) investigated fNIRS to understand working memory subcomponents for 6 TBI and 11 healthy controls and compared the maximum hemodynamic response between the two populations. It was reported that TBI subjects' largest hemodynamic response was significantly higher than the healthy control subjects while performing a working memory task, in particular in the left DLPFC. Nevertheless, similar experimental settings and comparison features from the hemodynamic signals for

investigating the difference between the TBI and healthy subjects has not been employed in the two studies by the same authors, this finding of observing a higher maximum hemodynamic signal for the TBI subjects compared to the healthy subjects, seems not to comply with their initial reports (Merzagora et al., 2011) of reporting lower mean HbO signal for the TBI subjects compared to the healthy subjects.

Overall, significant hemodynamic response differences between TBI and healthy control in the PFC (or its subcomponents) have been reported in all the studies discussed above. The employed methodology for comparing the hemodynamic responses between the two populations is based on univariate statistical analysis where a single feature from the hemodynamic signal is utilized to investigate the difference between the TBI and healthy subjects by conducting a statistical testing. Although this is a valid approach to study the differences between TBI and healthy control populations, but it does not fully exploit the potential hemodynamic features that may act as TBI's functional biomarkers. The approach of single hemodynamic feature analysis, while capable of signifying a difference between the TBI and healthy subjects, is incapable of providing a general model to classify a new (unseen) subject to the TBI or healthy population. A complementary approach to the current methodology is a technique that provides a measure of ranking different hemodynamic features according to their contribution in distinguishing TBI from healthy subjects and also enables classification of subjects according to their hemodynamic features. Conversely, feature combination through a machine learning classification method in which TBI and healthy subjects are characterized by multidimensional feature sets enables exploration of potential

biomarkers in combination with each other. In this approach, the goal is to identify the feature space in which TBI and healthy subjects are characterized with maximum intra-population similarity and minimum inter-population similarity. Various heuristic feature extraction techniques attempting to construct single or multi-dimensional feature spaces from the hemodynamic signal to classify brain activity for the Brain-Computer-Interface (BCI) applications have been proposed (Coyle et al., 2004; Fazli et al., 2012; Hai et al., 2013; Holper and Wolf, 2011; Luu and Chau, 2009; Naito et al., 2007; Power et al., 2010; Power et al., 2011; Sitaram et al., 2007; Stangl et al., 2013). However, few studies have attempted to identify the most efficient set of features from subjects of a population with purportedly distinctive brain activity to provide a unique characterization for the population (here TBI population). Selecting the optimum feature elements from a set of hemodynamic features is not a trivial problem. For instance, it has been shown that single features that may seem irrelevant in a single feature analysis can prove relevant in combination with other features (Domingos, 2012). Therefore, the full inherent biomarkers of the TBI subjects' hemodynamic signal may be determined by identifying the set of features that optimally characterizes the population.

### **6.3 Methodology**

The objective of this study is to identify the potential prefrontal hemodynamic biomarkers that contribute in characterizing subjects with TBI. To achieve this goal, hemodynamic response from a group of healthy and chronic TBI subjects while performing an event-related complexity task is captured. A novel procedure to identify the trials with elicited hemodynamic responses and reject the trials with artifactual

hemodynamic responses by imposing certain restrictions on the HbO and HbR signals is proposed. The average HbO and HbR signal are obtained by averaging the remaining trials. For every subject, a set of hemodynamic features from the average trials is obtained. The optimum set of functional biomarkers is obtained by employing the wrapper feature subset selection method (Guyon and Elisseeff, 2003) from the extracted features. Wrapper feature selection method utilizes machine learning classification algorithm as a black box to score different subsets of the hemodynamic features according to their predictive power. Finally, the accuracy of the identified biomarkers in characterizing the TBI population is evaluated by employing different classification techniques.

### 6.3.1 Participant

70 subjects participated in the two IRB-approved studies (NCT01797549 and NIH 07N0139) from which data from 9 subjects were not used in this analysis. Data from these subjects were excluded from the study either due to the problems in data collection or major motion or detector artifacts. Details of the procedure to identify subjects with major artifactual data are explained in the preprocessing section. Final number of subjects available for analysis was 61, 31 healthy controls (17 male and 14 female) and 30 TBI subjects (24 male and 6 female). Table 6-1 illustrates the demographic for all the TBI and healthy participant in this study.

Table 6-1 Demographic and Clinical Characteristics of the Study Population

|                                      | TBI (n=30)      | HC (n=31)       |
|--------------------------------------|-----------------|-----------------|
| Age (years), mean $\pm$ STD          | 37.8 $\pm$ 11.6 | 30.8 $\pm$ 8.06 |
| Gender, % male                       | 80.0            | 58.06           |
| Education (yrs)                      | 15,             | 17.2            |
| Time since TBI (months), median, IQR | 21.5, 13-41     |                 |
| Road traffic incident, %             | 50              |                 |
| LOC > 30 min, %                      | 40              |                 |
| Days in ICU, median $\pm$ IQR        | 3, 1-8          |                 |
| Received Rehabilitation, %           | 43              |                 |

### 6.3.2 Experimental Design

An event-related paradigm in which subjects are required to evaluate the complexity (i.e. number of events) of certain daily life activities was chosen for this study. The paradigm was originally designed and implemented in an fMRI experiment by (Krueger et al., 2009) and has been shown to engage the PFC. Therefore, this experiment seems feasible for studying patients with TBI in respect to the susceptibility of PFC in this population (see introduction).

In this paradigm, subjects were exposed to two classes of conditions: An experimental condition or the Complexity task and a control condition or the Font task. Stimulus presentation was controlled by the E-prime software package (Psychology Software Tools, Inc., <http://www.pstnet.com/eprime.cfm>). Participants were first trained with a separate set of stimuli to familiarize them with the experiment. At the beginning of each trial, instructions describing the type of task (Complexity or Font) and the name of a daily-life activity, e.g., “stirring a cup of coffee” was displayed on a computer monitor for 4 seconds. For the Complexity task, participants were asked to make a binary

decision as to whether the activity name displayed corresponded to an activity with low complexity (i.e. less number of events), e.g., “stirring a cup of coffee” or an activity with high complexity (i.e. more number of events), e.g., “planning a wedding”, using a two-button response pad. For the Font task, participants were asked to decide whether the instructions and the activity name shown represented the same or different fonts. Participants were prompted to respond as quickly and accurately as possible. Trials were separated by a randomly varied interval of 6 to 8 seconds. 33 Font and 66 Complexity trials were randomly arranged within a 15-min period of fNIRS data collection.

The hemodynamic response changes were recorded with a continuous wave fNIRS device with 4 light sources and 10 detectors (fNIR Devices LLC). The distance between each source/detector pair was 2.5 cm. The lights were emitted from each source at two different wavelengths of 730 nm and 850 nm. The light sources were activated in sequence for collecting measurements from 16 different channels that spanned the forehead at 2Hz.

### 6.3.3 Preprocessing

The raw intensity data measured at two wavelengths was normalized for all channel sites to compute the relative change by dividing each value of the intensity signal by the mean of the signal. The intensity-normalized data was then used to calculate the change in optical density (delta-optical density). Delta-optical density was computed for each wavelength as the negative logarithm of normalized intensity. For every subject, a differential pathlength factor (DPF) was calculated as the variable of age and the

wavelength following the formula obtained in (Scholkmann and Wolf, 2013). Using the DPF values, the delta-optical density was converted to changes in HbO and HbR using the modified Beer-Lambert law (Delpy et al., 1988). HbO and HbR signals were low-pass-filtered using butterworth IIR frequency filter of order 10 with a cut-off frequency 0.1 Hz. The filtered data was then detrended using the piecewise linear detrending to remove linear trends in the data. Trials corresponding to the High complexity stimulus were considered for this study. Trials were extracted by considering 11 seconds post-stimulus onset. Three seconds extra after the trial ends was considered as it has been shown that a full hemodynamic change occurs over a 10–12 s period, after the stimulus is presented (Izzetoglu et al., 2005). To decrease the effect of motion artifacts or major detector artifacts during the data collection and also increase the relevance of the hemodynamic response to the presented stimulus, certain restrictions were imposed on the extracted trials. In an elicited trial, decrease of HbR signal is expected to be accompanied by an increase in HbO signal in the activated area (Plichta et al., 2006). Therefore, corresponding to every stimulus only trials in which HbO and HbR are negatively correlated were considered. Furthermore, to guarantee that the selected trials encompass brain hemodynamic activity elicited by the presented stimulus, trials in which HbO signal was (on average) larger than HbR were considered. Finally, trials with negative HbO values were discarded from the analysis. HbO and HbR data corresponding to the High complexity trials were then block averaged across the remaining trials for every channel.

#### 6.3.4 Feature extraction

As previously stated, the majority of the TBI fNIRS studies have attempted to construct a small feature space (feature spaces with 1 or 2 elements) to investigate the difference in the TBI and healthy populations. To enable the characterization of the subjects at the individual level, 10 time- and frequency-domain features are extracted and their potential to be employed for characterizing the TBI and healthy subjects is investigated. The optimum feature space for distinguishing TBI and healthy subjects is identified by employing a features selection method that will be explained in the next section.

Typically, the average HbO signal obtained in response to an eliciting stimulus embodies a positive deflection representing the activation in the channel that I refer to as activity curve. The activity curve is the curve embodied in the HbO signal that is formed by an increase in oxygenation and its return to the same level of oxygenation. Depending on the nature of the features, they are extracted from the entire average HbO or the activity curve as follows:

- 1) Mean value of the HbO signal (HM),
- 2) Variance of the HbO signal (HV),
- 3) Left slope of the activity curve (CSL),
- 4) Right slope of the activity curve (CSR)
- 5) Kurtosis value of the HbO signal (HK),

- 6) Skewness value of the HbO signal (HS),
- 7) Area under the activity curve (CA),
- 8) Full width half maximum of the activity curve (CF),
- 9) Peak amplitude of the activity curve (CP),
- 10) Activity start time (CAS),
- 11) Discrete Fourier Transform (DFT) Coefficients of the HbO signal (HDFT)

Figure 6-1 visualizes the HbO signal and the extracted features. Two slope values for the slope features, denoting the rate at which the oxygenation consumption increases or decreases are computed. Left slope is computed between the points corresponding to the peak of the activity curve and where the activity curve starts and the right slope is computed between the points corresponding to the peak of the activity curve and where the activity ends. Furthermore, DFT provides a projection for the HbO signal with  $n$  data points in the time domain into the frequency domain by

$$c_f = \frac{1}{\sqrt{n}} \sum_{t=1}^n HbO(t) \exp\left(\frac{-2\pi i f t}{n}\right), f = 0, 1, \dots, n-1$$

where  $c_f$  coefficients are a sequence of complex numbers that represents the amplitudes and shifts of a decomposition of the signal into sinusoid functions.  $HbO(t)$  is the value of the HbO time series at time  $t$ . Keeping a few coefficients and discarding the rest that provides a rough sketch for the original HbO signal is a common time series feature extraction technique (Mörchen, 2003). For this study, 4 coefficients corresponding to the

very low frequency oscillations (VFLO) and low-frequency oscillations (LFOs) ranging from 0.01-0.1 Hz were kept. The VFLO and LFOs from the cerebral hemodynamics are shown to be associated to the brain spontaneous response and functional stimulation, respectively (Obrig et al., 2000). Furthermore, this range of frequency is known to be related to the cerebral autoregulation (Liu et al., 2015) which is the specific intrinsic ability to maintain constant cerebral blood flow over a range of blood pressure and is known to be disturbed or absent in 49-87% of patients with TBI (Rangel-Castilla et al., 2008). All the other features result in one single value and are as follows:

Mean (HM): average signal value.

Variance (HV): measure of signal spread.

Skewness (HS): measure of the asymmetry of signal values around its mean relative to a normal distribution. If the HbO signal is symmetrically distributed, then HS will be 0.

Kurtosis (HK): measure of the degree of peakedness of a distribution of signal values relative to a normal distribution.

Activity start time (CAS): represents the time instant after stimulus onset when the oxygenation value in the HbO starts to increase toward its peak's amplitude

Full Width at Half Maximum (FWHM): is commonly used to measure the width of a peak on a curve. As it is illustrated in Figure 6-1, the FWHM ("CF" in this study) value is obtained by computing the distance between points on the curve at which the values is half of the activity curve's amplitude.

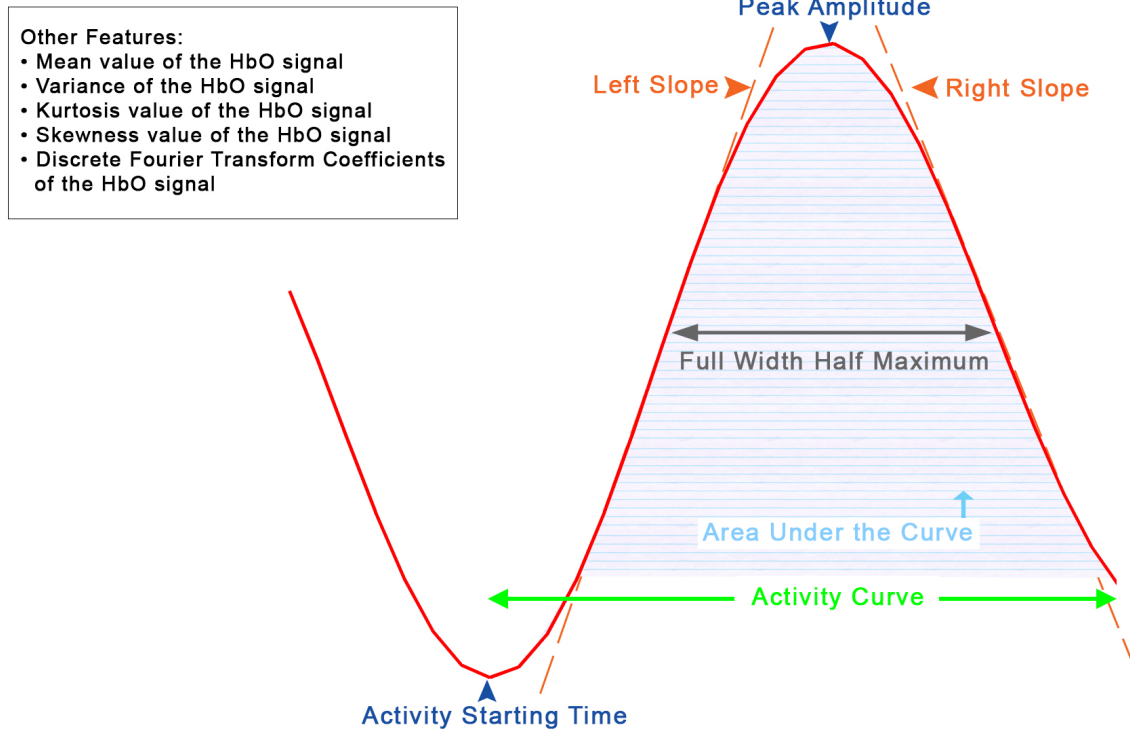


**Figure 6-1 Visualizing the HbO signal (in red), activity curve and a number of hemodynamic features extracted in this study. The activity curve is a positive deflection representing the activation embodied in the HbO signal. The activity curve is formed by oxygenation's increase and its returns to same level of oxygenation.**

### 6.3.5 Feature selection and pattern classification

To determine the optimal feature set (optimal combination of the aforementioned hemodynamic features) that enables distinguishing TBI subjects from the healthy subjects with the highest accuracy, I employed the wrapper feature selection method (Guyon and Elisseeff, 2003). Wrapper utilizes the machine learning classifier (popular predictors include decision trees, linear discriminant analysis, support vector machines, etc.) as a black box to rank different subsets of the features according to their predictive power.

Wrapper addresses the problem of variable selection effectively in comparison to other techniques, as it is independent from the selected predictor and it can search the space of all feature combinations. To employ the wrapper method, one needs to define the classifier, a method of evaluating the performance of the predictor, and method of searching the feature space (Guyon and Elisseeff, 2003). In wrapper method, a feature set is fed to the classifier and its performance is scored and the feature set with the highest rank, is selected as the optimal feature set.

In this study, due to the relatively small size of the feature space, an exhaustive search in the set of all the feature combinations was performed and for every possible combination of the feature sets a classification experiment was run. Decision Tree (Breiman et al., 1984) was utilized as the classifiers to evaluate different feature sets. 70% of the subjects (from TBI and health populations) were randomly selected for training purposes and the rest are considered for the testing purposes.

### 6.3.6 Classification evaluation

The TBI group was labeled as the positive class and the healthy group as the negative class. Generally, to assess the classification performance, evaluation indices are developed based on the counting the number of TP, TN, FP, FN where,

- True Positive (TP) – A subject belongs to the TBI population and is classified correctly as a TBI subject.
- True Negative (TN) – A subject that belongs to the healthy population and is classified correctly as a healthy subject

- False Positive (FP) – A subject that belongs to the healthy population and is classified incorrectly as a TBI subject.
- False Negative (FN) – A subject that belongs to the TBI population and is classified incorrectly as a healthy subject.

Since the number of TBI and healthy subjects are comparable (33 TBI and 34 healthy subjects), the common metric of accuracy that weights TP and TN equally is appropriate for this classification problem (Satyasree and Murthy, 2013). The generalization performance of every classification experiment is assessed by random subsampling in which the process of randomly partitioning subjects into training and testing sets and executing the classification is repeated several times (1000 times in this study) and the average accuracy value of the 1000 classifications is considered as the overall classification evaluation index. For every classification experiment, I report average accuracy, specificity, and sensitivity (Tan et al., 2006a). The overall accuracy, specificity, and sensitivity values are determined by averaging the accuracy, specificity, and sensitivity values computed for every run of the random subsampling procedure.

Accuracy, specificity, and sensitivity are computed as follows:

$$Accuracy = \frac{TP + TN}{TP + TN + FP + FN}$$

$$Sensitivity = \frac{TP}{TP + FN}$$

$$Specificity = \frac{TN}{TN + FP}$$

Sensitivity and specificity suggest how accurate the TBI and healthy subjects are detected through the classification procedure, respectively. In addition, once the optimum feature set is determined, two more classification algorithms namely, Linear Discriminant Analysis (LDA) (Welling, 2005), and Support Vector Machines (SVM) (Suykens and Vandewalle, 1999) were employed to classify the subjects.

## 6.4 Results

### 6.4.1 Trial/Channel removal

The three criteria discussed in the preprocessing section were applied on every single trial. A channel for which more than 80% or more of the trials were discarded was not considered for analysis. Subjects for which all the channel data were rejected, were also discarded from the study. 6 subjects (3 TBI and 3 healthy subjects) were discarded from the analysis by applying the trial-removal preprocessing step. The remaining channels for every subject contained only trials that were the most representative for hemodynamic activation in response to the High complexity task. Figure 6-2, illustrates the distribution of the retained channels across all the subjects after the trial/channel removal step. As it can be seen, the difference in the distribution of the retained channels between the two populations is clear. For the TBI subjects, a smaller number of subjects shared a common channel and the channel sites with elicited activity data were diffusely distributed. However, the majority of the healthy subjects shared similar channels. In particular, in the TBI population, more than half of the subjects shared only channel 16

and the rest of the channels were distributed among different subsets of subjects. However, in the healthy population except for channel 16, all other channels were shared among more than half of the subjects. The feature extraction and classification procedures in the sections below are performed merely on the channels for which the hemodynamic signal is kept

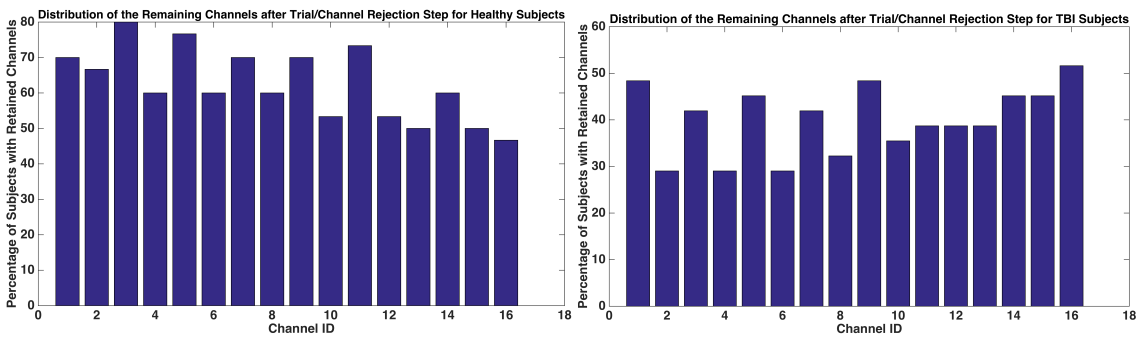


**Figure 6-2 Channel distribution for the healthy and TBI populations after the channel/trial removal step is illustrated. For the TBI subjects, less number of subjects shares a common channel whereas for majority of the healthy subjects share similar channels are kept. In the TBI population, more than half of the subjects share only channel 16. However, in healthy population except for channel 16, all the other channels are shared among more than half of the subjects.**

#### 6.4.2 Temporal Feature Extraction/Classification

Temporal features were extracted from every channel of the subjects. For every subject, these features were averaged across all the channels to obtain the subjects' representative feature set. All the possible combinations of the generated features were considered for distinguishing the TBI from the healthy subjects using the Decision Tree classification algorithm. Table 6-2 illustrates the accuracy, specificity (accuracy of

classifying healthy subjects correctly), and sensitivity (accuracy of classifying TBI subjects correctly) of the classification experiments for the feature space constructed single features. As it can be observed in table 6-2, the largest accuracy is obtained for the feature space constructed by the left slope of the activity curve (CSL) variable with the accuracy of 65%. Poor classification performance was obtained for the remaining features. Although these variables seem to be irrelevant to the task of classifying TBI from the healthy subjects once used for single variable classification, they were not discarded in search for the optimal feature set. Findings in (Domingos, 2012) indicate that an irrelevant single variable in two class classification may be relevant once used in combination with other features. Therefore, classification performance among all the possible combinations of the generated features of different sizes (2047 potential feature sets for 11 features) are computed and compared. Table 6-3 shows the classification performance for the optimum feature sets of different sizes. The optimum classification performance is obtained for the feature space constructed by the triple feature set of [CA, HDFT, CF] with the average classification accuracy of 85%. Sensitivity and specificity values computed for the corresponding classification suggest that TBI and healthy subjects are classified with accuracies of 85% and 84%, respectively. This finding suggests that on average, 26 TBI subjects (out of 30) and 26 healthy subjects (out of 31) are correctly identified for the feature space constructed by [CA, HDFT, CF]. It can also be observed in table 6-3 that comparable classification performance is obtained for the optimum feature sets of size 4 and 5. Hence, it seems safe to conclude that the feature space constructed by these 5 hemodynamic elements (CA, HDFT, CF, CSL, and CSR)

provide the most accurate distinction between the TBI and healthy subjects. Furthermore, a comparison between the sensitivity and specificity for the classifications with optimum feature sets (feature sets of size 3, 4, and 5) indicates that the TBI subjects are identified with marginally higher accuracy. The high sensitivity values signify the potential relevance of these 5 hemodynamic features to be used as biomarkers for subjects with TBI.

In Figure 6-3, Receiver Operating Characteristics (ROC) curve for the Decision Tree classifier in the feature space constructed by the optimum feature set is illustrated. An ROC curve illustrates the performance of the obtained classification model for the optimum feature set by visualizing the tradeoff between the sensitivity and the specificity. An ideal classifier would result in high sensitivity value whereas specificity value is reasonably low. The area under the curve (AUC) quantifies the overall ability of the classifier to distinguish between the TBI and the healthy subjects. An ideal classifier has an AUC of 1 and a random classifier has an AUC of 0.5. Therefore, the larger the AUC, the better the performance of the classifier in separating the TBI subjects from the healthy subjects. Specificity and sensitivity values at each point of the graph are obtained by averaging the corresponding values across the 1000 run of the random subsampling procedure. The AUC of 0.85 obtained for the constructed model in the optimum feature space signifies the high accuracy for the classification model.

**Table 6-2 Accuracy, specificity (accuracy of classifying healthy subjects correctly), and sensitivity (accuracy of classifying TBI subject correctly) of the classification experiments for the feature space constructed using one feature element. The largest accuracy value is obtained for the feature space constructed by the left slope of the activity curve (CSL) variable. Overall, the accuracy of correctly identifying the TBI subjects (sensitivity) is larger than the accuracy of correctly detecting the healthy subjects for feature set of any size.**

|                 | Feature |       |       |       |       |       |       |       |       |       |       |
|-----------------|---------|-------|-------|-------|-------|-------|-------|-------|-------|-------|-------|
|                 | HM      | HV    | HK    | HS    | CSL   | CSR   | CA    | CF    | CP    | CAS   | HDFT  |
| Accuracy (%)    | 38±9    | 57±9  | 55±9  | 55±10 | 65±10 | 57±10 | 39±10 | 57±10 | 45±10 | 58±9  | 59±10 |
| Specificity (%) | 38±19   | 61±18 | 56±19 | 55±19 | 61±18 | 61±19 | 39±18 | 58±18 | 42±20 | 57±16 | 58±18 |
| Sensitivity (%) | 42±19   | 55±17 | 56±17 | 60±19 | 71±18 | 54±18 | 42±18 | 55±19 | 49±19 | 62±18 | 61±18 |

**Table 6-3 Classification performance obtained by using the optimum feature sets of sizes 2 to 11 is presented. The optimum feature sets are selected from all the potential feature combinations of a certain size. Among all the combinations of features for a certain size, the one with the highest accuracy value is selected as the optimum feature set. The optimum classification performance is obtained for the feature space constructed by the triple of 3 features of “activity curve slopes (CS)”, “HbO kurtosis (HK)“, and “activity starting time (CAS)” resulted in the best separation between the TBI and healthy subjects. Comparison between the specificity and sensitivity indicates that in all the cases, sensitivity has been superior to the specificity meaning TBI subjects have been classified with higher accuracy.**

| Size of the feature set combinations | Feature set with the optimum performance | Accuracy (%) | Specificity (%) | Sensitivity (%) |
|--------------------------------------|--|--------------|-----------------|-----------------|
| 2                                    | [CA,HDFT]                                | 81±9         | 79±15           | 82±14           |
| 3                                    | [CA,HDFT,CF]                             | 85±13        | 84±16           | 85±17           |
| 4                                    | [CA,HDFT,CSL,CSR]                        | 83±14        | 83±18           | 84±18           |
| 5                                    | [CA,HDFT,CSL,CSR,CF]                     | 83±14        | 83±17           | 84±18           |
| 6                                    | [CA,HDFT,CSL,CSR,CF,CP]                  | 78±13        | 77±18           | 80±18           |
| 7                                    | [HV,HS,HK,CA, CAS,CF,HDFT]               | 70±13        | 67±19           | 75±18           |
| 8                                    | [HV,HS,HK,CA, CAS,CF,HDFT,CSL]           | 70±14        | 67±20           | 74±19           |
| 9                                    | [HV,HS,HK,CA, CAS,CF,HDFT,CSL,CP]        | 67±11        | 64±19           | 70±19           |
| 10                                   | [HV,HS,HK,CA, CAS,CF,HDFT,CSL,CP,CSR]    | 67±13        | 64±19           | 71±19           |
| 11                                   | [HV,HS,HK,CA,CAS,CF,HDFT,CSL,CP,CSR,HM]  | 63±11        | 60±19           | 67±17           |

It is worth noting that the classification performance for the features of the optimal set: CA, HDFT, CF, CSL, and CSR in table 6-2 suggests that 65% of accuracy (accuracy value obtained for CSL) is the optimal obtained performance if these features

are used for the single variable classification. However, the feature space formed by combining these features improved the classification performance. In particular, presence of the variable “CA” in the optimal feature set verifies that variables with poor performance in separating the subjects for single feature classification can improve the classification if used in combination with other features. On the contrary, a few variables with relatively larger accuracy values (e.g. HV) for single feature classification are not improving the classification performance in combination with other features. These observations verify the significance of performing multi-feature analysis.

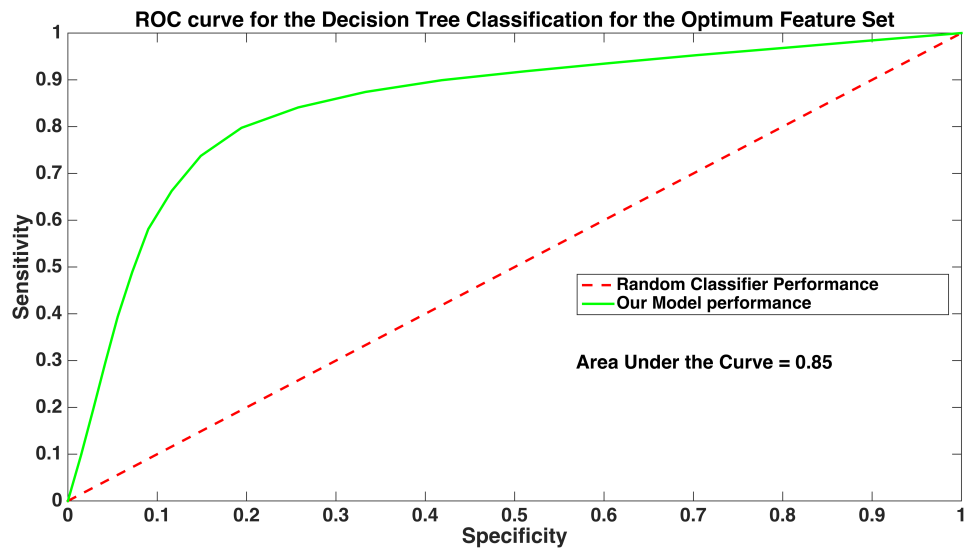


**Figure 6-3** ROC curve for the classifying subjects into TBI and healthy groups, in the feature space constructed by the optimum feature set [CA, HDFT, CF]. Specificity and sensitivity values at each point of the graph are obtained by averaging the corresponding values across the 1000 run of the random subsampling procedure. Area under the curve of 0.85 is obtained for the constructed model, which signifies the high accuracy of the constructed classification model.

For the optimal features set of [CA, HDFT, CF], I attempted to evaluate the performance of other commonly used classifiers and provide a comparison with the Decision Tree performance. In table 6-4, result of classifying TBI and healthy subjects in the feature space constructed by [CA, HDFT, CF] using the LDA and SVM (using the polynomial kernel) is illustrated. As results in table 6-3 indicates, classification of TBI and healthy subjects using the Decision Tree algorithm outperforms the two other techniques.

**Table 6-4 Classifying TBI and healthy subjects by characterizing subjects in the features space defined by the identified optimal feature set [CA,HDFT,CF] using 3 different classifiers. Decision Tree classifier outperformed LDA and SVM classifiers.**

| Classifier    | Accuracy (%) | Specificity (%) | Sensitivity (%) |
|---------------|--------------|-----------------|-----------------|
| Decision Tree | 85±13        | 84±16           | 85±17           |
| LDA           | 64±10        | 61±17           | 72±17           |
| SVM           | 65±9         | 55±16           | 76±14           |

#### 6.4.3 Temporal feature extraction/classification without rejecting trials/channels

In this section, the efficacy of the proposed preprocessing step of imposing constraints on the selected trials is evaluated. As discussed in the Methods section, trial/channel rejection step is proposed to identify the trials with meaningful HbO and HbR. Therefore, to evaluate the efficacy of the proposed technique, The entire classification procedure was repeated without imposing any of the constraints that were introduced (see Methods section). This was done to reject artifactual trials and provide a

comparison between the results of this process, which are shown in table 6-2. However, to be able to provide a fair comparison, the 6 subjects that were discarded through the trial/channel rejection in the previous section, were not considered for the current classification experiments. Table 6-5, illustrates the optimal feature sets identified through the wrapper method (see Methodology section) and the corresponding classification performance measures.

**Table 6-5 Feature sets with the largest accuracy values were selected from all the potential feature combinations of different sizes. HbO and HbR signals have been averaged across all the trials without applying the trial/channel rejection procedure on the signals.**

| Size of the feature set combinations | Feature set with highest accuracy value | Accuracy (%) | Specificity (%) | Sensitivity (%) |
|--------------------------------------|---|--------------|-----------------|-----------------|
| 1                                    | [CSR]                                   | 57±10        | 51±19           | 62±20           |
| 2                                    | [CSR,HS]                                | 62±11        | 58±19           | 58±19           |
| 3                                    | [HM,HV,CA]                              | 58±13        | 52±22           | 64±20           |
| 4                                    | [CP,HM,CSL,CF]                          | 57±11        | 54±21           | 62±18           |
| 5                                    | [CP,HM,CSR,HK,CAS]                      | 57±12        | 57±20           | 57±19           |
| 6                                    | [CP,HM,HV,CSL,CA,CF]                    | 59±14        | 57±21           | 61±19           |
| 7                                    | [CP,HM,CSL,CSR,CAS,CA,CF]               | 58±12        | 56±18           | 61±19           |
| 8                                    | [CP,HM,CSL,CSR, HK,CAS,CA,CF]           | 55±13        | 55±19           | 57±20           |
| 9                                    | [CP,HM,HV,CSL,CSR,HK,CAS,CA,CF]         | 54±12        | 54±19           | 56±11           |
| 10                                   | [CP,HM,HV,CSL,CSR,HS,HK,CAS,CA,CF]      | 51±10        | 49±19           | 53±19           |
| 11                                   | [CP,HM,HV,CSL,CSR,HK,CAS,CA,CF,HDFT]    | 46±10        | 44±18           | 49±19           |

Comparing classification performance in tables 6-3 and 6-5 suggests that the trial/channel rejection has significantly improved the classification performance. This difference in the classification performance implies that trials in which HbO and HbR and negatively

correlated and average HbO is higher than average HbR contains hemodynamic response related to brain activation elicited by the stimulus.

#### 6.4.4 Spatio-temporal feature extraction

In addition to the temporal classification, a spatio-temporal feature extraction and classification procedure was also considered to identify the features that enable distinguishing TBI subjects from healthy. In the spatio-temporal classification, unlike the temporal classification approach, the extracted features for a subject were not averaged across all the channels. Therefore, for a single feature there were at most 16 different feature values (some of the channels may have been discarded from the study, see Methods section) associated to the different channels. The DT algorithm was employed to classify the subjects in this spatio-temporal feature space. DT seemed feasible for this classification task as the spatio-temporal feature sets for the subjects contained missing values (for the discarded channels) and DT is known to be capable of handling the missing values (Safavian and Landgrebe, 1991). Table 6-6, tabulates the result of this approach, for all the extracted features.

**Table 6-6 Accuracy, specificity (accuracy of classifying healthy subjects correctly), and sensitivity (accuracy of classifying TBI subject correctly) for the spatio-temporal classification. Similar to the single feature temporal classification, HbO variance (HV) and activity curve’s left slope (CSL) resulted in relatively larger classification accuracy. However, single variable spatio-temporal classification outperformed single variable temporal classification. Similar to temporal classification, the accuracy of correctly identifying the TBI subjects (sensitivity) is consistently larger than the accuracy of correctly detecting the healthy subjects.**

|                 | Feature |       |       |       |        |       |       |       |       |       |
|-----------------|---------|-------|-------|-------|--------|-------|-------|-------|-------|-------|
|                 | HM      | HV    | HK    | HS    | CSL    | CSR   | CA    | CF    | CP    | CAS   |
| Accuracy (%)    | 68±11   | 70±9  | 65±13 | 72±11 | 71±10  | 68±10 | 70±10 | 65±12 | 72±10 | 65±11 |
| Specificity (%) | 66±18   | 68±18 | 58±21 | 71±20 | 74±117 | 67±17 | 67±18 | 65±20 | 68±17 | 61±17 |
| Sensitivity (%) | 72±18   | 73±17 | 74±18 | 75±14 | 74±18  | 70±17 | 75±17 | 66±17 | 77±16 | 72±17 |

As it can be observed in table 6-6, the largest spatio-temporal classification performances were obtained for the HS, CP, CSL, CA, and HV variables. Although, these classification experiments for the spatio-temporal features do not provide significant distinction between TBI and healthy subjects, they outperform the obtained accuracy values for the corresponding single feature temporal classification (shown in table 6-2). In Figure 6-4, the average activity maps for the CSL, and HV for the healthy and TBI subjects are illustrated. The activity map for a spatio-temporal feature associated to a population is obtained by averaging every subject's (from the corresponding population) spatio-temporal feature set.

Distinctive spatial distribution for the HV feature is observed between the two populations. For the TBI population, the larger HV values are located at multiple locations with the largest in the right hemisphere whereas for the healthy population the largest HV is concentrated in the left hemisphere within the Brodmann area 10 (BA 10)(Ramnani and Owen, 2004). Furthermore, healthy subjects on average show a larger HV value for the HbO signal that indicates that the oxygenation signal has shown higher variation in the healthy subjects. Since, HbO signals are obtained from trials that indicate hemodynamic activation (see Methods section), it is safe to conclude that the HbO signal in response to the High Complexity task for the healthy subjects shows a larger variation and is spatially less diffuse than for the TBI subjects.

The left slope of the HbO signal's activity curve (defined as CSL in the Methods section) at a certain location describes the rate by which HbO's activity curve has started to increase toward its peak. Hence, larger CSL values correspond to a faster rate of oxygenation consumption. As it can be seen in Figure 6-4, the largest CSL values for the healthy subjects cover the left frontopolar area of BA 10. A comparison of healthy and TBI subjects' CSL activity map reveals that healthy subjects have shown higher oxygenation consumption rate in response to the High complexity task at all the sites of fNIRS data collection.

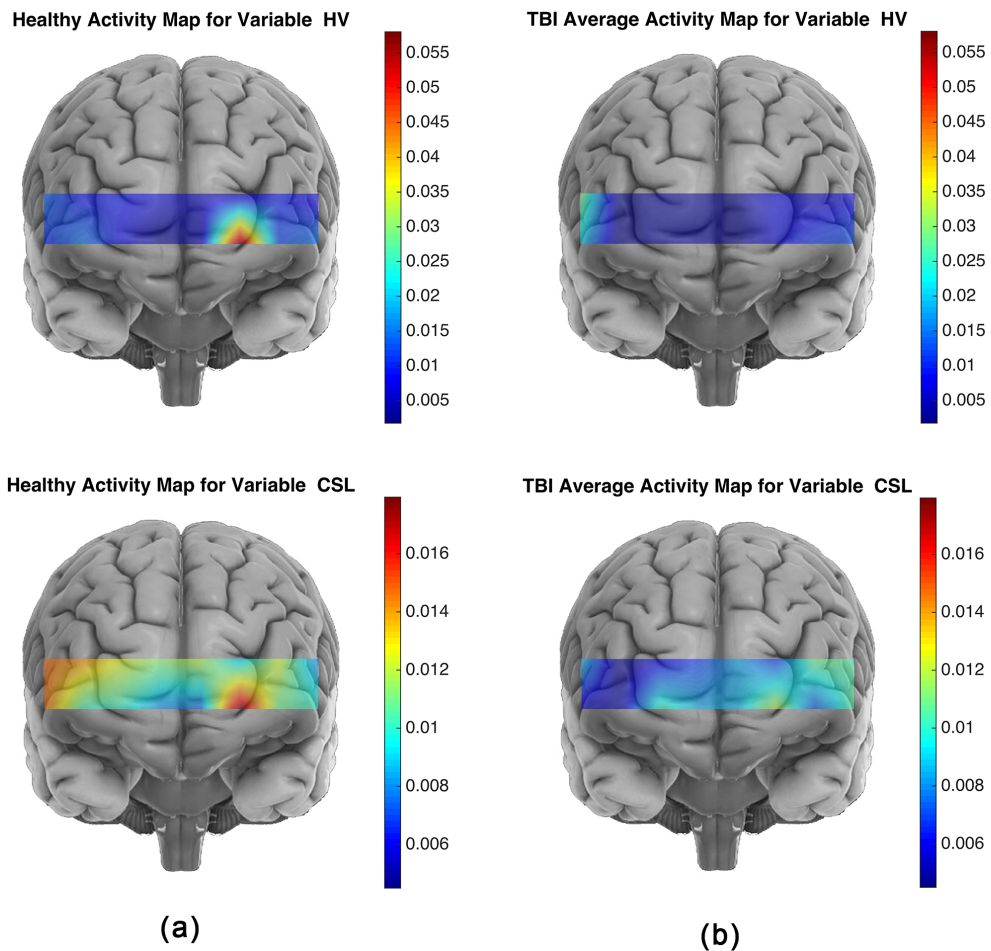


Figure 6-4 The average activity maps for the CSL and HV features for the healthy (a) and TBI (b) subjects are illustrated. The activity map for a spatio-temporal feature associated to a population is obtained by averaging every subjects' (from the corresponding population) spatio-temporal feature set. For the TBI population, the larger HV values are located at multiple locations with largest on the right hemisphere whereas for the healthy population the largest HV is concentrated on the left hemisphere of the Brodmann area 10 (BA 10). Furthermore, healthy subjects on average show larger HV values for the HbO signal that indicates oxygenation signal has shown higher variation in the healthy subjects. The HbO signal in response to the High Complexity task for the healthy subjects shows larger variation and is spatially less diffuse than for the TBI subjects. Larger CSL values correspond to faster rate of oxygenation consumption. Considering the activity map for healthy subjects, largest CSL values cover the left frontopolar of the BA 10. A comparison of healthy and TBI subjects' CSL activity map reveals that healthy subjects have shown higher oxygenation consumption rate in response to the High complexity task at all the sites of fNIRS data collection.

#### 6.4.5 Task load effects (i.e. parametric effects) in distinguishing TBI from healthy population

As discussed in the Methods section, subjects in this study performed 3 loads of complexity task, Font, Low Complexity and High Complexity. In this section, I attempt to explore the parametric effects on the performance of the population classification procedure. To this end, the feature space from the identified optimal features was constructed for the Font and Low complexity tasks in a similar way it was constructed for the High complexity task and the Decision Tree algorithm was employed for classifying subjects into TBI and healthy classes. Table 6-7, illustrates the classification performance obtained for each task load. The results in table 6-7 suggest that the as the task complexity decreases the classification performance also decreases. In other words, the difference between TBI and healthy subjects hemodynamic response is more prominent while performing the task with higher loads.

**Table 6-7 Comparison of the classification performance across tasks with different loads of complexity for the identified optimal feature set [CS, HK, CAS] using the Decision Tree classification**

| Task            | Accuracy (%) | Specificity (%) | Sensitivity (%) |
|-----------------|--------------|-----------------|-----------------|
| Font            | 52±11        | 52±18           | 53±19           |
| Low complexity  | 59±10        | 58±17           | 61±18           |
| High complexity | 79±13        | 74±18           | 84±16           |

## 6.5 Discussion

Employing temporal and spatio-temporal classification approaches, I attempted to identify the prefrontal hemodynamic biomarkers that provide the optimum distinction between the TBI and healthy subjects. To this end, I presented a novel approach for identifying single trial hemodynamic responses that encompass task-related hemodynamic activity by imposing certain restrictions on a signal's statistical characteristic followed by a hemodynamic feature extraction procedure. To determine the optimum biomarkers from the extracted hemodynamic features, the effectiveness of the 11 extracted features from subjects' prefrontal hemodynamic response in separating TBI and healthy subjects were investigated. The extracted features were employed for two types of classification, namely, temporal and spatio-temporal classification. In the temporal classification, the performance of 2047 classification experiments for every possible combination of features was evaluated. In every classification experiment, a distinct combination of the features was used to represent the subject's hemodynamic data. Optimum feature elements resulted in classification accuracy, sensitivity, and specificity of 85%, 85%, and 84%, respectively (table 6-3). The sensitivity value of 85% obtained for the optimal classification experiment suggests that TBI subjects have been successfully characterized for the optimum feature set. For the spatio-temporal classification, the performance of every single feature in distinguishing between the TBI and healthy subjects by incorporating the spatial characteristics to the feature set was evaluated. Optimum accuracy, sensitivity, and specificity of 72%, 75%, and 71%, respectively, were obtained for the spatio-temporal classification (table 6-6). The spatio-

temporal classification performance in comparison to the temporal classification was less significant. Less accurate performance of the spatio-temporal classification may be explained by the fact that for every subject a number of channels may have been rejected and it causes the spatio-temporal feature set to contain several missing values. However, for the temporal classification the average characteristics of the hemodynamic feature across the existing sites is considered and the missing data does not contribute in the classification procedure.

The selected optimum hemodynamic features set that effectively characterized TBI subjects with respect to their PFC hemodynamic response using the temporal classification are HbO's area under the curve (CA), HbO's, DFT coefficients of the HbO signal (HDFT), activity curve's full width half maximum (CF), activity curve's left slope (CSL), and activity curve's right slope (CSR). As discussed in the Methods section, HDFT is composed of 4 components of which 2 correspond to the magnitude of the very low frequencies that are associated to the spontaneous oscillations in cerebral oxygenation and the other 2 are the magnitude of low frequency between 0.07-0.1 Hz. The relationship of the magnitudes of these frequencies to the functional stimulus for the hemodynamic signal collected from the visual cortex has been investigated in (Obrig et al., 2000) and they are shown to be altered by the stimulation. The significance of these frequency magnitudes in the results, which are obtained in response to the High Complexity task is in line with findings in (Obrig et al., 2000) that suggests the relationship between these frequency magnitudes and functional stimulus and also claims that this functional response is observed over the PFC and is not bounded to the visual

cortex. Furthermore, as discussed in the Methods section, the selected components of the HDFT feature are related to the cerebral autoregulation. The contribution of the HDFT components in separating TBI from healthy subjects is consistent with previous findings in which disturbance in the cerebral autoregulation in any degree of TBI has been reported (Rangel-Castilla et al., 2008).

For the spatio-temporal classification, HbO's skewness (HS), activity curve peak value (CP), activity curve's left slope (CSL), activity curve's area under the curve (CA), and HbO signal's variance HV were identified as the optimum feature elements. In Figure 6-4, the spatial distribution of the HV and CSL variables for the healthy and TBI populations are visualized. The spatial distribution for HV and CSL signified the contribution of the left hemisphere of the BA 10 in separating the healthy subjects from the TBI for the spatio-temporal classification. Healthy subjects showed a consistent pattern of engaging this region in response to the High Complexity task. This finding complies with the reports by (Amyot et al., 2012; Krueger et al., 2009a) that BA 10 in healthy subjects is majorly activated in response to the High Complexity task. The HV's spatial distribution map for the TBI subject suggests that the TBI population have very low activation values across the entire PFC in comparison to the healthy subjects. This finding is in line with the previous study of (Sánchez-Carrión et al., 2008) that reported patients with TBI show a pattern of cerebral hypoactivation in the right middle and superior frontal regions during working memory tasks.

I investigated the parametric effects of the task complexity in distinguishing the TBI and healthy subjects by employing the optimum feature set of the temporal

classification for task with different loads. As it is shown in table 6-7, the higher the task complexity, a greater distinction was obtained between the TBI and healthy subjects. This finding complies with a previous report for this specific functional task (Krueger et al., 2009b) in which distinct activation in the BA 10 for the High Complexity task was observed.

Overall, a set of hemodynamic biomarkers that enabled identifying and characterizing subjects with TBI from healthy subjects with a significant accuracy (85% of sensitivity was reported in table 6-3) were successfully identified through constructing a feature space that maximized the difference between TBI and healthy subjects. The reported accuracy value for the classification performance is the generalized accuracy that describes the likelihood of identifying a subject with TBI correctly, given its hemodynamic signals are characterized in the similar feature space.

Finally, it is worth mentioning that the proposed approach of identifying TBI functional biomarkers using the fNIRS's hemodynamic signal has the potential to become a common approach in characterization of subjects with neurodegenerative, neurodevelopment disorders to further help clinical investigators to identify the underlying impairments of brain in the patient groups.

## 6.6 Summary of Chapter 6

In chapter 6, a methodology to explore and identify potential hemodynamic biomarkers that can be utilized for classifying subjects with TBI is devised. The proposed approach searches a large set of hemodynamic feature combinations and identifies a set of features that provides the optimum classification between the TBI and healthy

populations. The identified features from the PFC in subjects with TBI shows significant accuracy in characterizing subjects with TBI and are potentially promising PFC biomarkers for characterizing subjects with TBI. The proposed methodology of identifying hemodynamic biomarkers from PFC in subjects with TBI extends the current state of art in hemodynamic feature selection and TBI subject characterization.

## **7. Summary and Future Work**

### 7.1 Summary

It was discussed throughout this dissertation that literatures about functional neuroimaging studies with the purpose of identifying biomarkers that characterize certain brain disorders suffer from a few limitations that restrict their clinical translations. Firstly, majority of the related studies are focused on group studies that attempt to signify differences between the groups of subjects and do not provide description at the individual level. Secondly, the common techniques for characterizing functional neuroimaging response at the individual level are traditional single-channel time series feature extraction techniques that do not necessarily fit into the neuroimaging multichannel time series frameworks. Finally, for the more recently developed modalities such as fNIRS very few studies have attempted to identify biomarkers in brain disorders through the data mining and machine learning approaches. Therefore, in this dissertation emphasis was placed on improving, developing, and extracting clinically adaptable neuroimaging features to enable translating the laboratory work into clinical environments. In particular, machine learning algorithms and data mining techniques were utilized to generate spatio-temporal features from the neuroimaging time series and were evaluated for diagnosis of certain brain activity disorders.

In chapter 2 and 3, an approach to improve the current state of art of detecting the functionally connected regions in the brain is proposed and evaluated for 5 healthy subjects. The proposed approach targets certain limitations of the traditional approaches in identifying the functionally connected regions. Traditional approaches for identifying functionally connected regions failed to capture the last-shorting variations in the pattern of functional connectivity. This issue was tackled by using a cluster analysis technique, QT, for the short temporal windows. Advantages of employing QT to identify functionally connected regions are twofold. Firstly, it enables exploring all the possible clusters that indicate similar neural activity. Secondly, the algorithm determines the number of functionally connected regions and it should not be specified a priori. The second novelty of the proposed framework corresponds to utilizing the DTW dissimilarity measure that unlike the commonly used methods considers the potential misalignment of the EEG signals through a non-linear compression and extension of the time axes. The most significant insight from this study is that the proposed approach captures the dynamic patterns of brain's functional connectivity. Furthermore, it enables us to trace the brain interactions during the execution of a task.

In chapter 4, a novel neuroimaging time series feature extraction technique, RBS, was introduced. Unlike the traditional neuroimaging time series feature extraction technique, RBS treats neuroimaging time series collected from a multichannel modality, jointly (multichannel analysis) and takes the class association of the individuals into the feature extraction procedure (reference-based). RBS provided effective dimensionality reduction, which is crucial for neuroimaging data such as EEG with high temporal

resolution. Since RBS is uniquely designed to utilize the a priori information corresponding to a class (a group of subjects with brain disorder), therefore, is feasible for clinical studies where databases corresponding to a class of certain disorder are available. In chapter 5, the applicability of RBS to identify biomarkers was evaluated for an EEG data set collected from 60 distinct brain sites of the abstinent alcoholics and control subjects. Two 60-dimensional RBS vectors for every subject characterized the relationship of the subject to the two alcoholic and control classes suggesting that the RBS vectors can potentially explain and distinguish the association of the subject to different classes of a study. The RBS vectors were successfully utilized to detect and visualize the functionally distinct regions over brain of alcoholics. These regions represent the functionally impaired regions of the alcoholics' brain and can be potentially used as biomarkers to distinguish between alcoholic and control subjects.

In chapter 6, hemodynamic biomarkers that can be potentially utilized for classifying subjects with Traumatic Brain Injury (TBI) are explored. The proposed approach searches a large set of hemodynamic feature combinations and identifies a set of features that provides the optimum classification between the TBI and healthy populations. In this work, a novel approach for identifying single trial hemodynamic responses that encompass task-related hemodynamic activity by imposing certain restrictions on a signal's statistical characteristic followed by a hemodynamic feature extraction procedure was introduced. For the temporal classification, optimum feature elements resulted in classification accuracy, sensitivity, and specificity of 85%, 85%, and 84%, respectively. The sensitivity value of 85% obtained for the optimal classification

experiment suggested that TBI subjects have been successfully characterized for the optimum feature set. For the spatio-temporal classification, the performance of every single feature in distinguishing between the TBI and healthy subjects by incorporating the spatial characteristics to the feature set was evaluated. Optimum accuracy, sensitivity, and specificity of 72%, 75%, and 71%, respectively, were obtained for the spatio-temporal classification. The spatial classification signified the contribution of the left hemisphere of the BA 10 in separating the healthy subjects from the TBI for the spatio-temporal classification. Healthy subjects showed a consistent pattern of engaging this region in response to the High Complexity task suggesting that BA 10 in healthy subjects is majorly activated in response to the High Complexity task. Furthermore, TBI subjects showed very low activation values across the entire PFC in comparison to the healthy subjects. Analysis of the parametric effects of the task complexity in distinguishing the TBI and healthy subjects indicated that the functional tasks with more complexity results in more accurate distinction between the TBI and healthy subjects. Overall, a set of hemodynamic biomarkers that enabled identifying and characterizing subjects with TBI from healthy subjects with a significant accuracy (85% of sensitivity was reported in table 6-3) were successfully identified.

The overall contributions of this dissertation is summarized as follows:

- Improving, developing, and extracting clinically adaptable neuroimaging features to enable translating the laboratory work into clinical environments
- Utilizing ML algorithms to characterize brain functional activity at the individual level as opposed to the common approach of group analysis

- Developing domain-specific feature extraction techniques for neuroimaging time series
- Improving the current state of art of detecting the functionally connected regions in the brain
- Capturing the last-shorting variations in the pattern of functional connectivity (dynamicity of FC)
- Utilizing an unsupervised approach to determining the number of functionally connected regions of the brain
- Visualizing the trace of the brain's neuronal interactions during the execution of a functional task
- Devising a multichannel and reference-based neuroimaging time series feature extraction, RBS, for spatio-temporal biomarker detection applications
- Successfully evaluating the proposed biomarker detection technique through performing an accurate classification between the alcoholic and control classes
- Detecting and visualizing the functionally distinct regions over brain of alcoholics
- Exploring hemodynamic features that can be potentially utilized for classifying subjects with TBI
- Introducing a novel approach for identifying single trial hemodynamic responses that encompass task-related hemodynamic activity
- Determining the spatio-temporal hemodynamic biomarkers that characterize subjects with TBI through a supervised classification approach

- Detecting and visualizing regions within the PFC area of the TBI subjects that function distinctly
- Investigating the contribution of the loads of the complexity of the functional task loads in separating subjects with TBI from healthy subjects

## 7.2 Future work

The proposed approach to trace FC in the short temporal window has the potential to become a useful tool for research in the field of cognitive neuroscience. It was shown that the proposed technique could identify functional connectivity in a more accurate way compared to other existing techniques. It is expected that in healthy individuals, every task can have a unique dynamic functional connectivity pattern, which might differ from that of patient population. Comparing such dynamic patterns between the two groups could further help clinical investigators to identify the underlying impairments of brain functional connections in the patient groups.

The proposed RBS method is capable of distinguishing between any numbers of populations and is not limited only to two populations classification. For multi-class classifications, the orthogonally assumption may be relaxed by seeking the difference in the subspaces of different angle orientations. The complementary approaches in evaluating RBS as an efficient feature extraction and classification are as follows. For certain group of subjects with brain disorders, library of neural response for different sites of the brain is constructed and the RBS would classify the subjects by using these references for constructing the subspaces. Furthermore, RBS may also be used for intra-population classification studies, given enough meta-information regarding subjects

within a population. It can be addressed by collecting more information regarding subjects' mental and physical health to perform an intra-population classification experiment.

In this dissertation, the hemodynamic functional biomarker search was focused on the TBI group. Overall, the research community requires similar attempts to explore, identify, and localize the disorder's corresponding hemodynamic biomarkers. The similar approach proposed in this dissertation for the TBI subjects has the potential to become a common approach in characterization of subjects with neurodegenerative, neurodevelopment disorders to further help clinical investigators to identify the underlying impairments of brain in the patient groups.

## References

- Adeli, H., Zhou, Z., Dadmehr, N., 2003. Analysis of EEG records in an epileptic patient using wavelet transform. *Journal of neuroscience methods* 123, 69-87.
- Ahmadlou, M., Adeli, H., Adeli, A., 2010. New diagnostic EEG markers of the Alzheimer's disease using visibility graph. *Journal of neural transmission* 117, 1099-1109.
- Alexander, J.E., Porjesz, B., Bauer, L.O., Kuperman, S., Morzorati, S., O'CONNOR, S.J., Rohrbaugh, J., Begleiter, H., Polich, J., 1995. P300 hemispheric amplitude asymmetries from a visual oddball task. *Psychophysiology* 32, 467-475.
- Alho, K., 1995. Cerebral generators of mismatch negativity (MMN) and its magnetic counterpart (MMNm) elicited by sound changes. *Ear and hearing* 16, 38.
- Amyot, F., Zimmermann, T., Riley, J., Kainerstorfer, J.M., Chernomordik, V., Mooshagian, E., Najafizadeh, L., Krueger, F., Gandjbakhche, A.H., Wassermann, E.M., 2012. Normative database of judgment of complexity task with functional near infrared spectroscopy--application for TBI. *Neuroimage* 60, 879-883.
- Angold, A., Costello, E.J., 1993. Depressive comorbidity in children and adolescents: empirical, theoretical, and methodological issues. *Am J Psychiatry*.
- Ansari Asl, K., Chanel, G., Pun, T., 2007. A channel selection method for EEG classification in emotion assessment based on synchronization likelihood.
- Basar, E., Basar-Eroglu, C., Güntekin, B., Yener, G.G., 2012. Brain's alpha, beta, gamma, delta and theta oscillations in neuropsychiatric diseases: proposal for biomarker strategies. *Supplements to Clinical neurophysiology* 62, 287-324.
- Başar, E., Başar-Eroğlu, C., Karakaş, S., Schürmann, M., 1999. Are cognitive processes manifested in event-related gamma, alpha, theta and delta oscillations in the EEG? *Neuroscience letters* 259, 165-168.
- Begleiter, H., Porjesz, B., 1999. What is inherited in the predisposition toward alcoholism? A proposed model. *Alcoholism: Clinical and Experimental Research* 23, 1125-1135.
- Bennett, R.H., Bolling, D.Z., Anderson, L.C., Pelphrey, K.A., Kaiser, M.D., 2014. fNIRS detects temporal lobe response to affective touch. *Social cognitive and affective neuroscience* 9, 470-476.
- Bertolucci, P., Brucki, S., Campacci, S., Juliano, Y., 1994. [The Mini-Mental State Examination in a general population: impact of educational status]. *Arq Neuropsiquiatr* 52, 1-7.
- Bhambhani, Y., Maikala, R., Farag, M., Rowland, G., 2006. Reliability of near-infrared spectroscopy measures of cerebral oxygenation and blood volume during handgrip

exercise in nondisabled and traumatic brain-injured subjects. *Journal of rehabilitation research and development* 43, 845.

Bhattacharya, J., Petsche, H., 2005. Phase synchrony analysis of EEG during music perception reveals changes in functional connectivity due to musical expertise. *Signal processing* 85, 2161-2177.

Bishop, C.M., 2006. *Pattern recognition and machine learning*. Springer.

Bledowski, C., Prvulovic, D., Hoechstetter, K., Scherg, M., Wibral, M., Goebel, R., Linden, D.E.J., 2004. Localizing P300 generators in visual target and distractor processing: a combined event-related potential and functional magnetic resonance imaging study. *The Journal of neuroscience* 24, 9353-9360.

Boley, D., Gini, M., Gross, R., Han, E.-H.S., Hastings, K., Karypis, G., Kumar, V., Mobasher, B., Moore, J., 1999. Partitioning-based clustering for web document categorization. *Decision Support Systems* 27, 329-341.

Borbély, A.A., Tobler, I., Loepfe, M., Kupfer, D.J., Ulrich, R.F., Grochocinski, V., Doman, J., Matthews, G., 1984. All-night spectral analysis of the sleep EEG in untreated depressives and normal controls. *Psychiatry research* 12, 27-33.

Bosl, W., Tierney, A., Tager-Flusberg, H., Nelson, C., 2011. EEG complexity as a biomarker for autism spectrum disorder risk. *BMC medicine* 9, 18.

Bostanov, V., 2004. BCI competition 2003-data sets Ib and IIb: feature extraction from event-related brain potentials with the continuous wavelet transform and the t-value scalogram. *Biomedical Engineering, IEEE Transactions on* 51, 1057-1061.

Bracewell, R., 1965. *The Fourier Transform and IIS Applications*. New York.

Breiman, L., Friedman, J., Stone, C.J., Olshen, R.A., 1984. *Classification and regression trees*. CRC press.

Brown, C.R., Clarke, A.R., Barry, R.J., 2007. Auditory processing in an inter-modal oddball task: Effects of a combined auditory/visual standard on auditory target ERPs. *International Journal of Psychophysiology* 65, 122-131.

Cazalis, F., Feydy, A., Valabrègue, R., Péligrini-Issac, M., Pierot, L., Azouvi, P., 2006. fMRI study of problem-solving after severe traumatic brain injury. *Brain Injury* 20, 1019-1028.

Chisci, L., Mavino, A., Perferi, G., Sciandrone, M., Anile, C., Colicchio, G., Fuggetta, F., 2010. Real-time epileptic seizure prediction using AR models and support vector machines. *Biomedical Engineering, IEEE Transactions on* 57, 1124-1132.

Coyle, S., Ward, T., Markham, C., McDarby, G., 2004. On the suitability of near-infrared (NIR) systems for next-generation brain-computer interfaces. *Physiological measurement* 25, 815.

Custo, A., Boas, D.A., Tsuzuki, D., Dan, I., Mesquita, R., Fischl, B., Grimson, W.E.L., Wells, W., 2010. Anatomical atlas-guided diffuse optical tomography of brain activation. *Neuroimage* 49, 561-567.

Dauwels, J., Vialatte, F., Musha, T., Cichocki, A., 2010. A comparative study of synchrony measures for the early diagnosis of Alzheimer's disease based on EEG. *Neuroimage* 49, 668-693.

Delorme, A., Makeig, S., 2004. EEGLAB: an open source toolbox for analysis of single-trial EEG dynamics including independent component analysis. *Journal of neuroscience methods* 134, 9-21.

Delpy, D.T., Cope, M., Van der Zee, P., Arridge, S., Wray, S., Wyatt, J., 1988. Estimation of optical pathlength through tissue from direct time of flight measurement. *Physics in medicine and biology* 33, 1433.

Doi, T., Makizako, H., Shimada, H., Park, H., Tsutsumimoto, K., Uemura, K., Suzuki, T., 2013. Brain activation during dual-task walking and executive function among older adults with mild cognitive impairment: a fNIRS study. *Aging clinical and experimental research* 25, 539-544.

Domingos, P., 2012. A few useful things to know about machine learning. *Communications of the ACM* 55, 78-87.

Duncan, C.C., 1988. Event-related brain potentials: a window on information processing in schizophrenia. *Schizophrenia Bulletin* 14, 199.

Ehlis, A.-C., Bähne, C.G., Jacob, C.P., Herrmann, M.J., Fallgatter, A.J., 2008. Reduced lateral prefrontal activation in adult patients with attention-deficit/hyperactivity disorder (ADHD) during a working memory task: a functional near-infrared spectroscopy (fNIRS) study. *Journal of Psychiatric Research* 42, 1060-1067.

Elliott, R., 2003. Executive functions and their disorders Imaging in clinical neuroscience. *British Medical Bulletin* 65, 49-59.

Ellis, R.J., Oscar-Berman, M., 1989. Alcoholism, aging, and functional cerebral asymmetries. *Psychological Bulletin* 106, 128.

Estrada, E., Nazeran, H., Nava, P., Behbehani, K., Burk, J., Lucas, E., 2004. EEG feature extraction for classification of sleep stages. *Engineering in Medicine and Biology Society, 2004. IEMBS'04. 26th Annual International Conference of the IEEE. IEEE*, pp. 196-199.

Fazli, S., Mehnert, J., Steinbrink, J., Curio, G., Villringer, A., Müller, K.-R., Blankertz, B., 2012. Enhanced performance by a hybrid NIRS-EEG brain computer interface. *Neuroimage* 59, 519-529.

Fingelkurts, A.A., Fingelkurts, A.A., Kähkönen, S., 2005. Functional connectivity in the brain—is it an elusive concept? *Neuroscience & Biobehavioral Reviews* 28, 827-836.

Flor-Henry, P., Lind, J.C., Koles, Z.J., 2004. A source-imaging (low-resolution electromagnetic tomography) study of the EEGs from unmedicated males with depression. *Psychiatry Research: Neuroimaging* 130, 191-207.

Folstein, J.R., Van Petten, C., 2008. Influence of cognitive control and mismatch on the N2 component of the ERP: a review. *Psychophysiology* 45, 152-170.

Ford, J.M., 1999. Schizophrenia: the broken P300 and beyond. *Psychophysiology* 36, 667-682.

Friedman, D., Johnson, R., 2000. Event-related potential (ERP) studies of memory encoding and retrieval: a selective review. *Microscopy research and technique* 51, 6-28.

Friedman, D., Squires-Wheeler, E., 1994. Event-related potentials (ERPs) as indicators of risk for schizophrenia. *Schizophrenia Bulletin* 20, 63-74.

Frodl, T., Hampel, H., Juckel, G., Bürger, K., Padberg, F., Engel, R.R., Möller, H.j., Hegerl, U., 2002. Value of event-related P300 subcomponents in the clinical diagnosis of mild cognitive impairment and Alzheimer's Disease. *Psychophysiology* 39, 175-181.

Germon, T., Kane, N., Manara, A., Nelson, R., 1994. Near-infrared spectroscopy in adults: effects of extracranial ischaemia and intracranial hypoxia on estimation of cerebral oxygenation. *British journal of anaesthesia* 73, 503-506.

Gersch, W., Yonemoto, J., 1977. Parametric time series models for multivariate EEG analysis. *Computers and biomedical research* 10, 113-125.

Gioia, G.A., Isquith, P.K., 2004. Ecological assessment of executive function in traumatic brain injury. *Developmental neuropsychology* 25, 135-158.

Gordon, E., Sim, M., 1967. The EEG in presenile dementia. *Journal of neurology, neurosurgery, and psychiatry* 30, 285.

Gottemukkula, V., Derakhshani, R., 2011. Classification-guided feature selection for NIRS-based BCI. *Neural Engineering (NER), 2011 5th International IEEE/EMBS Conference on. IEEE*, pp. 72-75.

Grady, C.L., Furey, M.L., Pietrini, P., Horwitz, B., Rapoport, S.I., 2001. Altered brain functional connectivity and impaired short-term memory in Alzheimer's disease. *Brain* 124, 739-756.

Greicius, M.D., Flores, B.H., Menon, V., Glover, G.H., Solvason, H.B., Kenna, H., Reiss, A.L., Schlaggar, B.L., 2007. Resting-state functional connectivity in major depression: abnormally increased contributions from subgenual cingulate cortex and thalamus. *Biological psychiatry* 62, 429-437.

Guyon, I., Elisseeff, A., 2003. An introduction to variable and feature selection. *The Journal of Machine Learning Research* 3, 1157-1182.

Guyon, I., Elisseeff, A., 2006. An introduction to feature extraction. *Feature extraction. Springer*, pp. 1-25.

Haas, L., 2003. Hans Berger (1873–1941), Richard Caton (1842–1926), and electroencephalography. *Journal of Neurology, Neurosurgery & Psychiatry* 74, 9-9.

Hagmann, P., Cammoun, L., Gigandet, X., Meuli, R., Honey, C.J., Wedeen, V.J., Sporns, O., 2008. Mapping the structural core of human cerebral cortex. *PLoS Biol* 6, e159.

Hai, N.T., Cuong, N.Q., Khoa, T.Q.D., Van Toi, V., 2013. Temporal hemodynamic classification of two hands tapping using functional near—infrared spectroscopy. *Frontiers in human neuroscience* 7.

Halmos, P.R., 1947. *Finite dimensional vector spaces*. Princeton University Press.

Hämäläinen, M., Hari, R., Ilmoniemi, R.J., Knuutila, J., Lounasmaa, O.V., 1993. Magnetoencephalography—theory, instrumentation, and applications to noninvasive studies of the working human brain. *Reviews of modern Physics* 65, 413.

Harmony, T., Fernández, T., Silva, J., Bernal, J., Díaz-Comas, L., Reyes, A., Marosi, E., Rodríguez, M., Rodríguez, M., 1996. EEG delta activity: an indicator of attention to internal processing during performance of mental tasks. *International journal of psychophysiology* 24, 161-171.

Harris, G.J., Jaffin, S.K., Hodge, S.M., Kennedy, D., Caviness, V.S., Marinkovic, K., Papadimitriou, G.M., Makris, N., Oscar-Berman, M., 2008. Frontal white matter and

cingulum diffusion tensor imaging deficits in alcoholism. *Alcoholism: Clinical and Experimental Research* 32, 1001-1013.

Hartigan, J.A., Wong, M.A., 1979. Algorithm AS 136: A k-means clustering algorithm. *Journal of the Royal Statistical Society. Series C (Applied Statistics)* 28, 100-108.

Heeger, D.J., Ress, D., 2002. What does fMRI tell us about neuronal activity? *Nature Reviews Neuroscience* 3, 142-151.

Herrmann, C.S., Knight, R.T., 2001. Mechanisms of human attention: event-related potentials and oscillations. *Neuroscience & Biobehavioral Reviews* 25, 465-476.

Heyer, L.J., Kruglyak, S., Yooseph, S., 1999. Exploring expression data: identification and analysis of coexpressed genes. *Genome research* 9, 1106-1115.

Hibino, S., Mase, M., Shirataki, T., Nagano, Y., Fukagawa, K., Abe, A., Nishide, Y., Aizawa, A., Iida, A., Ogawa, T., 2013. Oxyhemoglobin Changes During Cognitive Rehabilitation After Traumatic Brain Injury Using Near Infrared Spectroscopy. *Neurologia medico-chirurgica* 53, 299-303.

Higuchi, T., 1988. Approach to an irregular time series on the basis of the fractal theory. *Physica D: Nonlinear Phenomena* 31, 277-283.

Hillyard, S.A., Anllo-Vento, L., 1998. Event-related brain potentials in the study of visual selective attention. *Proceedings of the National Academy of Sciences* 95, 781-787.

Hogan, M.J., Swanwick, G.R., Kaiser, J., Rowan, M., Lawlor, B., 2003. Memory-related EEG power and coherence reductions in mild Alzheimer's disease. *International Journal of Psychophysiology* 49, 147-163.

Holper, L., Wolf, M., 2011. Single-trial classification of motor imagery differing in task complexity: a functional near-infrared spectroscopy study. *J Neuroeng Rehabil* 8, 34.

Hoshi, Y., Kobayashi, N., Tamura, M., 2001. Interpretation of near-infrared spectroscopy signals: a study with a newly developed perfused rat brain model. *Journal of Applied Physiology* 90, 1657-1662.

Huettel, S.A., Song, A.W., McCarthy, G., 2004. *Functional magnetic resonance imaging*. Sinauer Associates Sunderland.

Hyvärinen, A., Oja, E., 2000. Independent component analysis: algorithms and applications. *Neural networks* 13, 411-430.

Iosifescu, D.V., Greenwald, S., Devlin, P., Mischoulon, D., Denninger, J.W., Alpert, J.E., Fava, M., 2009. Frontal EEG predictors of treatment outcome in major depressive disorder. *European Neuropsychopharmacology* 19, 772-777.

IRAGUI, V.J., Kutas, M., Mitchiner, M.R., Hillyard, S.A., 1993. Effects of aging on event-related brain potentials and reaction times in an auditory oddball task. *Psychophysiology* 30, 10-22.

Itagaki, S., Yabe, H., Mori, Y., Ishikawa, H., Takanashi, Y., Niwa, S., 2011. Event-related potentials in patients with adult attention-deficit/hyperactivity disorder versus schizophrenia. *Psychiatry research*, 288-291.

Izzetoglu, M., Izzetoglu, K., Bunce, S., Ayaz, H., Devaraj, A., Onaral, B., Pourrezaei, K., 2005. Functional near-infrared neuroimaging. *Neural Systems and Rehabilitation Engineering, IEEE Transactions on* 13, 153-159.

Jalili, M., Knyazeva, M.G., 2011. EEG-based functional networks in schizophrenia. *Computers in biology and medicine* 41, 1178-1186.

- Jeon, Y.W., Polich, J., 2003. Meta-analysis of P300 and schizophrenia: Patients, paradigms, and practical implications. *Psychophysiology* 40, 684-701.
- Jodo, E., Kayama, Y., 1992. Relation of a negative ERP component to response inhibition in a Go/No-go task. *Electroencephalography and clinical neurophysiology* 82, 477-482.
- John, E.R., 1990. *Machinery of the mind: data, theory, and speculations about higher brain function: based on the First International Conference on Machinery of the Mind, February 25-March 3, 1989, Havana City, Cuba.* Birkhauser.
- John, E.R., Harmony, T., 1990. *Machinery of the mind.* Springer Science & Business Media.
- Johnson, M., Rosenfeld, J., 1992. A new ERP-based deception detector analog II: Utilization of non-selective activation of relevant knowledge. *International journal of psychophysiology* 12, 289-306.
- Kang, J., Wang, L., Yan, C., Wang, J., Liang, X., He, Y., 2011a. Characterizing dynamic functional connectivity in the resting brain using variable parameter regression and Kalman filtering approaches. *Neuroimage*, 1222-1234.
- Kang, J., Wang, L., Yan, C., Wang, J., Liang, X., He, Y., 2011b. Characterizing dynamic functional connectivity in the resting brain using variable parameter regression and Kalman filtering approaches. *Neuroimage* 56, 1222-1234.
- Kasahara, M., Menon, D., Salmond, C., Outtrim, J., Tavares, J.T., Carpenter, T., Pickard, J., Sahakian, B., Stamatakis, E., 2010. Altered functional connectivity in the motor network after traumatic brain injury. *Neurology* 75, 168-176.
- Katayama, J., Polich, J., 1999. Auditory and visual P300 topography from a 3 stimulus paradigm. *Clinical Neurophysiology* 110, 463-468.
- Kayser, J., Tenke, C.E., 2006. Principal components analysis of Laplacian waveforms as a generic method for identifying ERP generator patterns: I. Evaluation with auditory oddball tasks. *Clinical Neurophysiology* 117, 348-368.
- Kayser, J., Tenke, C.E., Bruder, G.E., 1998. Dissociation of brain ERP topographies for tonal and phonetic oddball tasks. *Psychophysiology* 35, 576-590.
- Kelly, A.C., Uddin, L.Q., Biswal, B.B., Castellanos, F.X., Milham, M.P., 2008. Competition between functional brain networks mediates behavioral variability. *Neuroimage* 39, 527-537.
- Kennedy, D.P., Courchesne, E., 2008. The intrinsic functional organization of the brain is altered in autism. *Neuroimage* 39, 1877-1885.
- Keogh, E., Ratanamahatana, C.A., 2005. Exact indexing of dynamic time warping. *Knowledge and information systems* 7, 358-386.
- Kleinhans, N.M., Richards, T., Sterling, L., Stegbauer, K.C., Mahurin, R., Johnson, L.C., Greenson, J., Dawson, G., Aylward, E., 2008. Abnormal functional connectivity in autism spectrum disorders during face processing. *Brain* 131, 1000-1012.
- Kleinschmidt, A., Obrig, H., Requardt, M., Merboldt, K.-D., Dirnagl, U., Villringer, A., Frahm, J., 1996. Simultaneous recording of cerebral blood oxygenation changes during human brain activation by magnetic resonance imaging and near-infrared spectroscopy. *Journal of cerebral blood flow & metabolism* 16, 817-826.

Klimesch, W., 1999. EEG alpha and theta oscillations reflect cognitive and memory performance: a review and analysis. *Brain research reviews* 29, 169-195.

Koenig, T., Prichep, L., Lehmann, D., Sosa, P.V., Braeker, E., Kleinlogel, H., Isenhardt, R., John, E.R., 2002. Millisecond by millisecond, year by year: normative EEG microstates and developmental stages. *Neuroimage* 16, 41-48.

Koenig, T., Studer, D., Hubl, D., Melie, L., Strik, W., 2005. Brain connectivity at different time-scales measured with EEG. *Philosophical Transactions of the Royal Society B: Biological Sciences* 360, 1015-1024.

Koh, P.H., Glaser, D.E., Flandin, G., Kiebel, S., Butterworth, B., Maki, A., Delpy, D.T., Elwell, C.E., 2007. Functional optical signal analysis: a software tool for near-infrared spectroscopy data processing incorporating statistical parametric mapping. *Journal of biomedical optics* 12, 064010-064010-064013.

Koike, S., Nishimura, Y., Takizawa, R., Yahata, N., Kasai, K., 2013. Near-infrared spectroscopy in schizophrenia: a possible biomarker for predicting clinical outcome and treatment response. *Frontiers in psychiatry* 4.

Koshino, H., Carpenter, P.A., Minshew, N.J., Cherkassky, V.L., Keller, T.A., Just, M.A., 2005. Functional connectivity in an fMRI working memory task in high-functioning autism. *Neuroimage* 24, 810-821.

Kriegeskorte, N., Simmons, W.K., Bellgowan, P.S., Baker, C.I., 2009. Circular analysis in systems neuroscience: the dangers of double dipping. *Nat Neurosci* 12, 535-540.

Krueger, F., Spampinato, M.V., Barbey, A.K., Huey, E.D., Morland, T., Grafman, J., 2009a. The frontopolar cortex mediates event knowledge complexity: a parametric functional MRI study. *Neuroreport* 20, 1093-1097.

Krueger, F., Spampinato, M.V., Barbey, A.K., Huey, E.D., Morland, T., Grafman, J., 2009b. The frontopolar cortex mediates event knowledge complexity: a parametric functional MRI study. *Neuroreport* 20, 1093.

Kurz, M.J., Wilson, T.W., Arpin, D.J., 2014. An fNIRS exploratory investigation of the cortical activity during gait in children with spastic diplegic cerebral palsy. *Brain and Development* 36, 870-877.

Langfitt, T.W., Obrist, W.D., Alavi, A., Grossman, R.I., Zimmerman, R., Jaggi, J., Uzzell, B., Reivich, M., Patton, D.R., 1986. Computerized tomography, magnetic resonance imaging, and positron emission tomography in the study of brain trauma: preliminary observations. *Journal of neurosurgery* 64, 760-767.

Lehmann, D., Faber, P.L., Galderisi, S., Herrmann, W.M., Kinoshita, T., Koukkou, M., Mucci, A., Pascual-Marqui, R.D., Saito, N., Wackermann, J., 2005. EEG microstate duration and syntax in acute, medication-naive, first-episode schizophrenia: a multi-center study. *Psychiatry Research: Neuroimaging* 138, 141-156.

Lehmann, D., Faber, P.L., Tei, S., Pascual-Marqui, R.D., Milz, P., Kochi, K., 2012. Reduced functional connectivity between cortical sources in five meditation traditions detected with lagged coherence using EEG tomography. *Neuroimage* 60, 1574-1586.

Lehmann, D., Strik, W., Henggeler, B., Koenig, T., Koukkou, M., 1998. Brain electric microstates and momentary conscious mind states as building blocks of spontaneous thinking: I. Visual imagery and abstract thoughts. *International Journal of Psychophysiology* 29, 1-11.

Letemendia, F., Pampiglione, G., 1958. Clinical and electroencephalographic observations in Alzheimer's disease. *Journal of neurology, neurosurgery, and psychiatry* 21, 167.

Levin, H.S., 1982. *Neurobehavioral consequences of closed head injury*. Oxford University Press.

Li, Y., Wee, C.-Y., Jie, B., Peng, Z., Shen, D., 2014. Sparse multivariate autoregressive modeling for mild cognitive impairment classification. *Neuroinformatics* 12, 455-469.

Liu, X., Czosnyka, M., Donnelly, J., Budohoski, K.P., Varsos, G.V., Nasr, N., Brady, K.M., Reinhard, M., Hutchinson, P.J., Smielewski, P., 2015. Comparison of frequency and time domain methods of assessment of cerebral autoregulation in traumatic brain injury. *Journal of Cerebral Blood Flow & Metabolism* 35, 248-256.

Liu, Y., Gao, J.-H., Liotti, M., Pu, Y., Fox, P.T., 1999. Temporal dissociation of parallel processing in the human subcortical outputs. *Nature* 400, 364-367.

Lotte, F., Congedo, M., Lécuyer, A., Lamarche, F., 2007a. A review of classification algorithms for EEG-based brain-computer interfaces. *Journal of neural engineering* 4.

Lotte, F., Congedo, M., Lécuyer, A., Lamarche, F., Arnaldi, B., 2007b. A review of classification algorithms for EEG-based brain-computer interfaces. *Journal of neural engineering* 4.

Luchtmann, M., Jachau, K., Adolf, D., Baecke, S., Lützkendorf, R., Müller, C., Tempelmann, C., Bernarding, J., 2013. Decreased effective connectivity in the visuomotor system after alcohol consumption. *Alcohol* 47, 195-202.

Luck, S.J., Heinze, H., Mangun, G., Hillyard, S.A., 1990. Visual event-related potentials index focused attention within bilateral stimulus arrays. II. Functional dissociation of P1 and N1 components. *Electroencephalography and clinical Neurophysiology* 75, 528-542.

Luck, S.J., Muthalal, D.H., O'Donnell, B.F., Hämäläinen, M.S., Spencer, K.M., Javitt, D.C., Uhlhaas, P.J., 2011. A roadmap for the development and validation of event-related potential biomarkers in schizophrenia research. *Biological psychiatry* 70, 28-34.

Luu, S., Chau, T., 2009. Decoding subjective preference from single-trial near-infrared spectroscopy signals. *Journal of neural engineering* 6, 016003.

Mayer, A.R., Mannell, M.V., Ling, J., Gasparovic, C., Yeo, R.A., 2011. Functional connectivity in mild traumatic brain injury. *Human brain mapping* 32, 1825-1835.

McAllister, T.W., Saykin, A., Flashman, L., Sparling, M., Johnson, S., Guerin, S., Mamourian, A., Weaver, J., Yanofsky, N., 1999. Brain activation during working memory 1 month after mild traumatic brain injury A functional MRI study. *Neurology* 53, 1300-1300.

McAllister, T.W., Sparling, M.B., Flashman, L.A., Guerin, S.J., Mamourian, A.C., Saykin, A.J., 2001. Differential working memory load effects after mild traumatic brain injury. *Neuroimage* 14, 1004-1012.

McCarley, R.W., Faux, S.F., Shenton, M.E., Nestor, P.G., Adams, J., 1991. Event-related potentials in schizophrenia: their biological and clinical correlates and new model of schizophrenic pathophysiology. *Schizophrenia research* 4, 209-231.

McDonald, B.C., Flashman, L.A., Saykin, A.J., 2002. Executive dysfunction following traumatic brain injury: neural substrates and treatment strategies. *NeuroRehabilitation* 17, 333-344.

Merica, H., Gaillard, J.-M., 1992. The EEG of the sleep onset period in insomnia: a discriminant analysis. *Physiology & behavior* 52, 199-204.

Merzagora, A.C., Schultheis, M.T., Onaral, B., Izzetoglu, M., 2011. Functional near-infrared spectroscopy-based assessment of attention impairments after traumatic brain injury. *Journal of Innovative Optical Health Sciences* 4, 251-260.

Merzagora, A.C.R., Izzetoglu, M., Onaral, B., Schultheis, M.T., 2014. Verbal working memory impairments following traumatic brain injury: an fNIRS investigation. *Brain imaging and behavior* 8, 446-459.

Mientus, S., Gallinat, J., Wuebben, Y., Pascual-Marqui, R.D., Mulert, C., Frick, K., Dorn, H., Herrmann, W.M., Winterer, G., 2002. Cortical hypoactivation during resting EEG in schizophrenics but not in depressives and schizotypal subjects as revealed by low resolution electromagnetic tomography (LORETA). *Psychiatry Research: Neuroimaging* 116, 95-111.

Minagawa-Kawai, Y., van der Lely, H., Ramus, F., Sato, Y., Mazuka, R., Dupoux, E., 2010. Optical brain imaging reveals general auditory and language-specific processing in early infant development. *Cerebral Cortex*, bhq082.

Monden, Y., Dan, I., Nagashima, M., Dan, H., Uga, M., Ikeda, T., Tsuzuki, D., Kyutoku, Y., Gunji, Y., Hirano, D., 2015. Individual classification of ADHD children by right prefrontal hemodynamic responses during a go/no-go task as assessed by fNIRS. *NeuroImage: Clinical* 9, 1-12.

Mörchen, F., 2003. Time series feature extraction for data mining using DWT and DFT. Univ.

Moretti, D.V., Babiloni, C., Binetti, G., Cassetta, E., Dal Forno, G., Ferreric, F., Ferri, R., Lanuzza, B., Miniussi, C., Nobili, F., 2004. Individual analysis of EEG frequency and band power in mild Alzheimer's disease. *Clinical Neurophysiology* 115, 299-308.

Moselhy, H.F., Georgiou, G., Kahn, A., 2001. Frontal lobe changes in alcoholism: a review of the literature. *Alcohol and Alcoholism* 36, 357-368.

Mousavi, S., Niknazar, M., Vahdat, B.V., 2008. Epileptic seizure detection using AR model on EEG signals. *Biomedical engineering conference, 2008. CIBEC 2008. Cairo International. IEEE*, pp. 1-4.

Musha, T., Terasaki, Y., Haque, H.A., Ivamitsky, G.A., 1997. Feature extraction from EEGs associated with emotions. *Artificial Life and Robotics* 1, 15-19.

Naito, M., Michioka, Y., Ozawa, K., KIGUCHI, M., KANAZAWA, T., 2007. A communication means for totally locked-in ALS patients based on changes in cerebral blood volume measured with near-infrared light. *IEICE transactions on information and systems* 90, 1028-1037.

Nazari, M., Berquin, P., Missonnier, P., Aarabi, A., Debatisse, D., De Broca, A., Wallois, F., 2010. Visual sensory processing deficit in the occipital region in children with attention-deficit/hyperactivity disorder as revealed by event-related potentials during cued continuous performance test. *Neurophysiologie Clinique/Clinical Neurophysiology* 40, 137-149.

Nicolas-Alonso, L.F., Gomez-Gil, J., 2012. Brain computer interfaces, a review. *Sensors* 12, 1211-1279.

- Niedermeyer, E., 2005. 9. The normal EEG of the waking adult. *Electroencephalography: Basic principles, clinical applications, and related fields*, 167.
- Niedermeyer, E., da Silva, F.L., 2005. *Electroencephalography: basic principles, clinical applications, and related fields*. Lippincott Williams & Wilkins.
- Obrig, H., Neufang, M., Wenzel, R., Kohl, M., Steinbrink, J., Einhäupl, K., Villringer, A., 2000. Spontaneous low frequency oscillations of cerebral hemodynamics and metabolism in human adults. *Neuroimage* 12, 623-639.
- Ogura, C., Nageishi, Y., Matsubayashi, M., Omura, F., Kishimoto, A., Shimokochi, M., 1991. Abnormalities in Event-Related Potentials, N100, P200, P300 and Slow Wave in Schizophrenia. *Psychiatry and Clinical Neurosciences* 45, 57-65.
- Okada, F., Tokumitsu, Y., Hoshi, Y., Tamura, M., 1994. Impaired interhemispheric integration in brain oxygenation and hemodynamics in schizophrenia. *European archives of psychiatry and clinical neuroscience* 244, 17-25.
- Pang-Ning, T., Steinbach, M., Kumar, V., 2006. *Introduction to data mining*. Library of Congress.
- Patel, S.H., Azzam, P.N., 2005. Characterization of N200 and P300: selected studies of the event-related potential. *International Journal of Medical Sciences* 2, 147.
- Pijnenburg, Y.A., Strijers, R.L., vd Made, Y., van der Flier, W.M., Scheltens, P., Stam, C.J., 2008. Investigation of resting-state EEG functional connectivity in frontotemporal lobar degeneration. *Clinical Neurophysiology* 119, 1732-1738.
- Plenger, P., Krishnan, K., Cloud, M., Bosworth, C., Qualls, D., de la Plata, C.M., 2015. fNIRS-based investigation of the Stroop task after TBI. *Brain imaging and behavior*, 1-10.
- Plichta, M., Herrmann, M., Baehne, C., Ehlis, A.-C., Richter, M., Pauli, P., Fallgatter, A., 2006. Event-related functional near-infrared spectroscopy (fNIRS): are the measurements reliable? *Neuroimage* 31, 116-124.
- Polich, J., 1989. P300 and Alzheimer's disease. *Biomedicine & pharmacotherapy* 43, 493-499.
- Polich, J., 2007. Updating P300: an integrative theory of P3a and P3b. *Clinical neurophysiology* 118, 2128-2148.
- Polich, J., Kok, A., 1995. Cognitive and biological determinants of P300: an integrative review. *Biological psychology* 41, 103-146.
- Polich, J., Ladish, C., Bloom, F.E., 1990. P300 assessment of early Alzheimer's disease. *Electroencephalography and Clinical Neurophysiology/Evoked Potentials Section* 77, 179-189.
- Polikar, R., Greer, M.H., Udpa, L., Keinert, F., 1997. Multiresolution wavelet analysis of ERPs for the detection of Alzheimer's disease. *Engineering in Medicine and Biology Society, 1997. Proceedings of the 19th Annual International Conference of the IEEE. IEEE*, pp. 1301-1304.
- Pollonini, L., Patidar, U., Situ, N., Rezaie, R., Papanicolaou, A.C., Zouridakis, G., 2010. Functional connectivity networks in the autistic and healthy brain assessed using Granger causality. *Engineering in Medicine and Biology Society (EMBC), 2010 Annual International Conference of the IEEE. IEEE*, pp. 1730-1733.

- Portin, R., Kovala, T., Polo-Kantola, P., Revonsuo, A., Müller, K., Matikainen, E., 2000. Does P3 reflect attentional or memory performances, or cognition more generally? *Scandinavian Journal of Psychology* 41, 31-40.
- Power, S.D., Chau, T., 2013. Automatic single-trial classification of prefrontal hemodynamic activity in an individual with Duchenne muscular dystrophy. *Developmental neurorehabilitation* 16, 67-72.
- Power, S.D., Falk, T.H., Chau, T., 2010. Classification of prefrontal activity due to mental arithmetic and music imagery using hidden Markov models and frequency domain near-infrared spectroscopy. *Journal of neural engineering* 7, 026002.
- Power, S.D., Kushki, A., Chau, T., 2011. Towards a system-paced near-infrared spectroscopy brain-computer interface: differentiating prefrontal activity due to mental arithmetic and mental singing from the no-control state. *Journal of neural engineering* 8, 066004.
- Ramnani, N., Owen, A.M., 2004. Anterior prefrontal cortex: insights into function from anatomy and neuroimaging. *Nature Reviews Neuroscience* 5, 184-194.
- Rangaswamy, M., Porjesz, B., Chorlian, D.B., Wang, K., Jones, K.A., Bauer, L.O., Rohrbaugh, J., O'Connor, S.J., Kuperman, S., Reich, T., 2002. Beta power in the EEG of alcoholics. *Biol Psychiatry* 52, 831-842.
- Rangel-Castilla, L., Gasco, J., Nauta, H.J., Okonkwo, D.O., Robertson, C.S., 2008. Cerebral pressure autoregulation in traumatic brain injury. *Neurosurgical focus* 25, E7.
- Rioul, O., Vetterli, M., 1991. Wavelets and signal processing. *IEEE signal processing magazine* 8, 14-38.
- Rizk-Jackson, A., Stoffers, D., Sheldon, S., Kuperman, J., Dale, A., Goldstein, J., Corey-Bloom, J., Poldrack, R.A., Aron, A.R., 2011. Evaluating imaging biomarkers for neurodegeneration in pre-symptomatic Huntington's disease using machine learning techniques. *Neuroimage* 56, 788-796.
- Roth, W.T., Cannon, E.H., 1972. Some features of the auditory evoked response in schizophrenics. *Archives of General Psychiatry* 27, 466-471.
- Rousseeuw, P.J., Kaufman, L., 1990. *Finding Groups in Data*. Wiley Online Library.
- Sadatnezhad, K., Boostani, R., Ghanizadeh, A., 2011. Classification of BMD and ADHD patients using their EEG signals. *Expert Systems with Applications* 38, 1956-1963.
- Safavian, S.R., Landgrebe, D., 1991. A survey of decision tree classifier methodology. *IEEE transactions on systems, man, and cybernetics* 21, 660-674.
- Sakoe, H., Chiba, S., 1978. Dynamic programming algorithm optimization for spoken word recognition. *Acoustics, Speech and Signal Processing, IEEE Transactions on* 26, 43-49.
- Sánchez-Carrión, R., Gómez, P.V., Junqué, C., Fernández-Espejo, D., Falcon, C., Bargalló, N., Roig-Rovira, T., Enseñat-Cantallops, A., Bernabeu, M., 2008. Frontal hypoactivation on functional magnetic resonance imaging in working memory after severe diffuse traumatic brain injury. *Journal of neurotrauma* 25, 479-494.
- Satyasree, K., Murthy, J., 2013. An Exhaustive Literature Review on Class Imbalance Problem. *Int. J. Emerg. Trends Technol. Comput. Sci* 2, 109-118.

- Scheibel, R., Pearson, D., Faria, L., Kotrla, K., Aylward, E., Bachevalier, J., Levin, H., 2003. An fMRI study of executive functioning after severe diffuse TBI. *Brain Injury* 17, 919-930.
- Scholkmann, F., Wolf, M., 2013. General equation for the differential pathlength factor of the frontal human head depending on wavelength and age. *Journal of biomedical optics* 18, 105004-105004.
- Schroeter, M.L., Bücheler, M.M., Müller, K., Uludağ, K., Obrig, H., Lohmann, G., Tittgemeyer, M., Villringer, A., von Cramon, D.Y., 2004. Towards a standard analysis for functional near-infrared imaging. *Neuroimage* 21, 283-290.
- Sheline, Y.I., Price, J.L., Yan, Z., Mintun, M.A., 2010. Resting-state functional MRI in depression unmasks increased connectivity between networks via the dorsal nexus. *Proceedings of the National Academy of Sciences* 107, 11020-11025.
- Shensa, M.J., 1992. The discrete wavelet transform: wedding the a trous and Mallat algorithms. *Signal Processing, IEEE Transactions on* 40, 2464-2482.
- Shimada, S., Hiraki, K., 2006. Infant's brain responses to live and televised action. *Neuroimage* 32, 930-939.
- Singh, A.K., Dan, I., 2006. Exploring the false discovery rate in multichannel NIRS. *Neuroimage* 33, 542-549.
- Sitaram, R., Zhang, H., Guan, C., Thulasidas, M., Hoshi, Y., Ishikawa, A., Shimizu, K., Birbaumer, N., 2007. Temporal classification of multichannel near-infrared spectroscopy signals of motor imagery for developing a brain-computer interface. *Neuroimage* 34, 1416-1427.
- Snodgrass, J.G., Vanderwart, M., 1980. A standardized set of 260 pictures: norms for name agreement, image agreement, familiarity, and visual complexity. *Journal of experimental psychology: Human learning and memory* 6, 174.
- Snyder, S.M., Hall, J.R., 2006. A meta-analysis of quantitative EEG power associated with attention-deficit hyperactivity disorder. *Journal of Clinical Neurophysiology* 23, 441-456.
- Stahl, D., Pickles, A., Elsabbagh, M., Johnson, M.H., Team, B., 2012. Novel machine learning methods for ERP analysis: a validation from research on infants at risk for autism. *Developmental neuropsychology* 37, 274-298.
- Stangl, M., Bauernfeind, G., Kurzmann, J., Scherer, R., Neuper, C., 2013. A haemodynamic brain-computer interface based on real-time classification of near infrared spectroscopy signals during motor imagery and mental arithmetic. *J. Near Infrared Spectrosc* 21, 157-171.
- Sutton, S., Braren, M., Zubin, J., John, E., 1965. Evoked-potential correlates of stimulus uncertainty. *Science* 150, 1187-1188.
- Suykens, J.A., Vandewalle, J., 1999. Least squares support vector machine classifiers. *Neural processing letters* 9, 293-300.
- Tak, S., Ye, J.C., 2014. Statistical analysis of fNIRS data: a comprehensive review. *Neuroimage* 85, 72-91.
- Tan, P.-N., Steinbach, M., Kumar, V., 2006a. Introduction to data mining. Pearson Addison Wesley Boston.

- Tan, P.N., Steinbach, M., Kumar, V., 2006b. Introduction to data mining. Pearson Addison Wesley Boston.
- Taylor, L.J., Maybery, M.T., Whitehouse, A.J., 2014. Moving beyond behaviour-only assessment: Incorporating biomarkers to improve the early detection and diagnosis of autism spectrum disorders. *International journal of speech-language pathology* 16, 19-22.
- Teplan, M., 2002. Fundamentals of EEG measurement. *Measurement science review* 2, 1-11.
- Tiitinen, H., Sinkkonen, J., Reinikainen, K., Alho, K., Lavikainen, J., Näätänen, R., 1993. Selective attention enhances the auditory 40-Hz transient response in humans.
- Tononi, G., Sporns, O., Edelman, G.M., 1994. A measure for brain complexity: relating functional segregation and integration in the nervous system. *Proceedings of the National Academy of Sciences* 91, 5033-5037.
- Torsvall, L., 1987. Sleepiness on the job: continuously measured EEG changes in train drivers. *Electroencephalography and clinical Neurophysiology* 66, 502-511.
- Uhlhaas, P.J., Singer, W., 2006. Neural synchrony in brain disorders: relevance for cognitive dysfunctions and pathophysiology. *Neuron* 52, 155-168.
- Van Deursen, J., Vuurman, E., Verhey, F., van Kranen-Mastenbroek, V., Riedel, W., 2008. Increased EEG gamma band activity in Alzheimer's disease and mild cognitive impairment. *Journal of neural transmission* 115, 1301-1311.
- Vilkki, J., 1992. Cognitive flexibility and mental programming after closed head injuries and anterior or posterior cerebral excisions. *Neuropsychologia* 30, 807-814.
- Villringer, A., Dirnagl, U., 1994. Coupling of brain activity and cerebral blood flow: basis of functional neuroimaging. *Cerebrovascular and brain metabolism reviews* 7, 240-276.
- Villringer, A., Planck, J., Hock, C., Schleinkofer, L., Dirnagl, U., 1993. Near infrared spectroscopy (NIRS): a new tool to study hemodynamic changes during activation of brain function in human adults. *Neuroscience letters* 154, 101-104.
- Wang, L., Kuroiwa, Y., Kamitani, T., Takahashi, T., Suzuki, Y., Hasegawa, O., 1999. Effect of interstimulus interval on visual P300 in Parkinson's disease. *Journal of Neurology, Neurosurgery & Psychiatry* 67, 497-503.
- Wang, T., Deng, J., He, B., 2004. Classifying EEG-based motor imagery tasks by means of time-frequency synthesized spatial patterns. *Clinical Neurophysiology* 115, 2744-2753.
- Welling, M., 2005. Fisher linear discriminant analysis. Department of Computer Science, University of Toronto 3.
- Woon, W., Cichocki, A., Vialatte, F., Musha, T., 2007. Techniques for early detection of Alzheimer's disease using spontaneous EEG recordings. *Physiological Measurement* 28, 335.
- Yu-Feng, Z., Yong, H., Chao-Zhe, Z., Qing-Jiu, C., Man-Qiu, S., Meng, L., Li-Xia, T., Tian-Zi, J., Yu-Feng, W., 2007. Altered baseline brain activity in children with ADHD revealed by resting-state functional MRI. *Brain and Development* 29, 83-91.
- Zhang, X.L., Begleiter, H., Porjesz, B., Litke, A., 1997. Electrophysiological evidence of memory impairment in alcoholic patients. *Biol Psychiatry* 42, 1157-1171.

Zhang, X.L., Begleiter, H., Porjesz, B., Wang, W., Litke, A., 1995. Event related potentials during object recognition tasks. *Brain Res Bull* 38, 531-538.

Zhang, Z., Liao, W., Chen, H., Mantini, D., Ding, J.-R., Xu, Q., Wang, Z., Yuan, C., Chen, G., Jiao, Q., 2011. Altered functional–structural coupling of large-scale brain networks in idiopathic generalized epilepsy. *Brain* 134, 2912-2928.

## **Biography**

Nader Shahni Karamzadeh received his Bachelor of Science in Applied Mathematics from Chamran University, Ahvaz, Iran, in 2004. He worked as graduate researcher at George Mason University for 3 years and received his Master of Science in Geoinformatics from George Mason University in 2011. He started his Ph.D. in Computation Sciences and Informatics at George Mason University in Spring 2012. During the course of his Ph.D. he was awarded a graduate fellowship through NIH Graduate Partnership Program.